UILU-ENG-80-2015

CIVIL ENGINEERING STUDIES

Structural Research Series No. 481



# EXPERIMENTAL STUDY OF SMALL-SCALE R/C COLUMNS SUBJECTED TO AXIAL AND SHEAR FORCE REVERSALS



By

NOREEN D. GILBERTSEN

and

JACK P. MOEHLE

A Report to the
NATIONAL SCIENCE FOUNDATION
Research Grant PFR 78-16318

UNIVERSITY OF ILLINOIS
at URBANA-CHAMPAIGN
URBANA, ILLINOIS
JULY 1980

| BIBLIOGRAPHIC DATA SHEET | 1. Report No. UILU-ENG-80-2015 | 2. | 3. Recipient's Accession No. |
|---|---|---|---|
| 4. Title and Subtitle<br>EXPERIMENTAL STUDY OF SMALL-SCALE R/C COLUMNS SUBJECTED TO AXIAL AND SHEAR FORCE REVERSALS | | | 5. Report Date<br>July 1980<br>6. |
| 7. Author(s)<br>N. D. Gilbertsen and J. P. Moehle | | | 8. Performing Organization Rept. No. SRS 481 |
| 9. Performing Organization Name and Address<br>University of Illinois at Urbana-Champaign<br>Urbana, Illinois 61801 | | | 10. Project/Task/Work Unit No.<br>11. Contract/Grant No.<br>NSF PF R78-16318 |
| 12. Sponsoring Organization Name and Address<br>National Science Foundation<br>Washington, D.C. 20013 | | | 13. Type of Report & Period Covered<br>14. |

15. Supplementary Notes

16. Abstracts

Small-scale reinforced concrete columns were subjected to a series of shear force or simultaneous shear and axial force reversals. The specimens were similar to the first story columns of the nine-story, three-bay frames tested dynamically on the University of Illinois Earthquake Simulator. Test variables included the reinforcement ratio, the dead load on the column, and the rate of axial load variation during shear force reversals. Behavior of the specimens is represented by measured hysteresis relations and crack patterns. The observed behavior is compared with the calculated response.

17. Key Words and Document Analysis. 17a. Descriptors

Bond, Deflection, Column, Cyclic Loads, Hysteresis, Moment, Reinforcement, Rotation, Stiffness, Strength

17b. Identifiers/Open-Ended Terms

17c. COSATI Field/Group

| 18. Availability Statement | 19. Security Class (This Report) | 21. No. of Pages |
|---|---|---|
| Release Unlimited | UNCLASSIFIED | |
| | 20. Security Class (This Page) UNCLASSIFIED | 22. Price |

UILU-ENG-80-2015

# EXPERIMENTAL STUDY OF SMALL-SCALE R/C COLUMNS SUBJECTED TO AXIAL AND SHEAR FORCE REVERSALS

by

Noreen D. Gilbertsen

and

Jack P. Moehle

University of Illinois
Urbana, Illinois

July 1980

# ACKNOWLEDGMENT

This study is part of a continuing investigation of the response of reinforced concrete structures subjected to earthquake motions. Experimental work is being conducted at the Structural Research Laboratory of the Civil Engineering Department at the University of Illinois at Urbana-Champaign. This work was sponsored by the National Science Foundation under research grant NSF PF R78-16318.

The writers wish to express their appreciation to Professor M. A. Sozen for valuable discussion and assistance. Appreciation is also due Professor V. J. McDonald and Mr. G. Lafenhagen for their advice and assistance with instrumentation and data reduction facilities. The writers express their thanks to Mr. O. H. Ray and his staff for fabrication of the testing apparatus and test specimens, and to Mrs. P. Lane for secretarial work.

Credit is due to the members of the panel of consultants for their advise and criticism. Members of the panel include M. H. Eligator, Weiskopf and Pickworth; A. E. Fiorato, Portland Cement Association; W. D. Holmes, Rutherford and Chekene; R. G. Johnston, Brandow and Johnston; J. Lefter, Veterans Administration; W. P. Moore, Jr., Walter P. Moore and Associates; and A. Walser, Sargent and Lundy Engineers.

The Cyber 175 computer system of the Department of Computer Science was used for data reduction.

TABLE OF CONTENTS

# LIST OF TABLES

# LIST OF FIGURES

# 1. OBJECT AND SCOPE

The objective of this work was to study experimentally the inelastic response of small-scale reinforced concrete column specimens. Dimensions, materials and reinforcement ratios were selected to be similar to the first story columns of the nine-story, three bay frames subjected to earthquake simulations on the University of Illinois Earthquake Simulator (Ref. 1, 2 and 4). Columns tested with constant axial load were representative of interior columns in the three bay frames. Columns tested with varying axial loads were intended to provide insight into the behavior of exterior columns.

The specimens were subjected to a series of shear force or simultaneous shear and axial force reversals. Specimen behavior was studied using measured hysteretic relations, crack patterns, and comparisons of measured and calculated response.

# 2. OUTLINE OF EXPERIMENTAL WORK

## 2.1 Introduction

Eight column specimens were fabricated identical to first story columns of the nine-story, three-bay frames (Fig. 2.1) tested on the Earthquake Simulator at the University of Illinois. Similar structures have also been tested [1,2,3,4]. The small-scale reinforced concrete specimens had a shear span of 250 mm and cross-sectional dimensions of 38 mm by 51 mm (Fig. 2.2 and 2.3). Concrete consisted of small aggregate with high early strength cement. Reinforcing steel comprised No. 13 gage (2.33 mm dia.) undeformed wire. The specimens were subjected to a series of statically applied shear force reversals in which the axial load variation was controlled.

## 2.2 Specimen Description

Column details are shown in Figures 2.2 and 2.3. Nominal cross-sectional dimensions were identical to those of the nine story framed structures (Fig. 2.1). The columns were 400 mm tall and were cast monolithically with a stiff base girder. Load reversals were applied to the column centerline at the height of 250 mm above the base. An additional 150 mm above the point of load application allowed for the development of reinforcing steel. Measured cross-sectional dimensions are listed in Table 2.1.

The concrete used in the specimens was a small aggregate type consisting of Type III cement, Wabash River sand and fine lake sand. The mix proportions by dry weight were 4.5:0.9:1.0 (coarse:fine:cement) with a water cement ratio of 0.74.

Location and amounts of reinforcing steel were identical to those used in the nine-story structures. Longitudinal reinforcement consisted of undeformed No. 13 gage wire (2.33 mm dia.) tied inside transverse reinforcement made from rectangular spirals (Fig. 2.2). All longitudinal steel was continuous over the column height without splices. Anchorage within the supporting base girder was provided by welding to a 3 mm thick steel plate (Fig. 2.2). Longitudinal reinforcing ratios, defined as the ratio of total steel to the gross concrete area, were 0.88 and 1.75 percent.

Transverse reinforcement was provided by rectangular-shaped spirals (No. 16 gage wire (1.65 mm dia.) with a pitch of 10 mm). The transverse reinforcement, which was identical for all specimens, was designed with a minimum factor of safety of three so that primary failure in shear would be unlikely.

Additional column reinforcement consisted of steel tubing and spirals located at the point of load application (Fig. 2.2). Base girder details appear in Figure 2.2.

## 2.3 Fabrication

Before constructing reinforcing cages, dirt, oil and rust were removed from all steel by first soaking it in a petroleum-based solvent and then cleaning it with acetone. Following cleaning, the longitudinal and transverse reinforcement were tied together with .912 mm dia. wire to form continuous reinforcement cages. The cages were sprayed with a 10% solution of hydrochloric acid solution and placed in a fog room for three days in order to pit and rust the steel. A wire brush and high pressure water jet were used to remove loose rust particles.

Prior to casting, the cages were placed in steel formwork. Steel plates, intended to anchor the flexural steel, were then welded to the reinforcing cages 100 mm into the base girder (Fig. 2.2).

Columns were cast in two batches with all columns having the same longitudinal reinforcement ratios cast simultaneously. The specimens were cast in a horizontal position and monolithically with the stiff base girders. The concrete was consolidated with a stud vibrator and trowelled smooth.

Columns were covered with wet burlap and plastic four hours after completion of casting. Formwork was removed after an additional four hours. All specimens were cured under wet burlap and plastic for ten days and then stored in the testing area. Control specimens (twenty 102 mm dia. by 203 mm cylinders and twelve 51 by 51 by 203 mm prisms), which had been cast with the test specimens, received identical treatment. Table 2.1 gives the specimen age at time of testing.

## 2.4 Test Variables

The test variables included the reinforcement ratio, the dead load in the column, and the rate of change in axial load with change in the lateral load. Four columns were tested with constant axial force. Dead load in those columns was chosen to represent dead loads in nine-story frames (Fig. 2.1). For the remaining four columns, axial load varied in direct proportion with column shear. Dead load and axial load variation were chosen so that columns could be subjected to a range of axial force between 1 kN tension and 11 kN compression within the size constraints of the laboratory. The load-moment interaction diagram (Fig. 2.4) illustrates the cycling pattern of the columns. The following table summarizes the relationship between specimens and test variables.

| Specimen | Reinforcement Ratio % | Dead Load | Change in Axial Load / Change in Lateral Load |
|---|---|---|---|
| 2A | .88 | 5.36 | 0 |
| 2B | .88 | 5.36 | 0 |
| 2C | .88 | 2.41 | 6.0 |
| 2D | .88 | 2.41 | 6.0 |
| 4A | 1.75 | 5.36 | 0 |
| 4B | 1.75 | 5.36 | 0 |
| 4C | 1.75 | 3.25 | 4.0 |
| 4D | 1.75 | 3.25 | 4.0 |

## 2.5 Test Procedure

All specimens were subjected statically to the displacement pattern shown in Figure 2.5. Each test was monitored by plotting lateral load versus deflection of the column on an x-y plotter throughout the test. Data readings from electrical instruments were taken frequently in order to produce a well defined hysteresis curve. In addition, concrete cracking and crushing were recorded at each displacement maximum. Location of small-width cracks was aided through the use of a flourescent fluid which, when washed over specimens, collected in cracks and reflected black light.

## 2.6 Test Setup

### a) General Description

The test setup shown in Figure 2.7 was used to subject column specimens to a series of displacement reversals. In the setup, the column base girder was prestressed to the floor of the Structural Research Laboratory so that column base fixity was attained. A loading frame used to load the specimen was designed so that simultaneous variation of lateral shear and axial force could be accomplished. The loading frame was attached to the column using

a ball bearing connection (Fig. 2.8) so that minimal rotational restraint existed at the point of load application. A roller connection (Fig. 2.9) on the loading frame was simulated near the column in order to stabilize the test setup. Stability transverse to the loading plane was provided by lubricated ball bearings (Fig. 2.10).

Initial dead load was provided by the weight of the loading frame and by attaching additional weights to the frame at the end opposite to the roller simulation (Fig. 2.6). During testing, axial force could be maintained at the initial value by applying load at the column level. Axial force could be made to vary in proportion with the lateral force by loading at various heights along the loading frame.

An eleven kilonewton capacity ram was used to provide lateral forces to the loading frame. The ram was attached to a 480 mm thick reinforced concrete foundation wall of the Structural Research Laboratory. The ram was attached to the loading frame by two methods (Fig. 2.11 and Fig. 2.12). Both methods were designed to transmit negligible vertical force. Connection A (Fig. 2.11) consists of a bearing connection attached to a steel rod with reduced sections to minimize transfer of vertical force. This connection was used when lateral force was applied at the column level. Connection B (Fig. 2.12) consists of a series of parallel bearing connections and was used for tests in which column axial load was varied.

b) Performance of Bearing Connections

Bearing connections were used in the test setup to simulate roller connections and hinges (see Sec. 2.6a). Because of the small specimen sizes and large thrusts carried by the bearings, tests were required to investigate the frictional resistance of these connections.

Figure 2.13 illustrates the procedure used to determine the frictional resistance in the bearing connections. Two bearing connections were embedded in separate steel plates. The plates were then bolted together by a steel rod through the bearing connection. A shearing force of 8.9 kN was applied to the setup. A torque was then applied to the steel rod and measured with a torque wrench.

The torque measured was 3.4 kN-mm or 1.7 kN-mm per bearing connection. These results indicate a possible lateral force resistance of 6 Newtons or approximately one percent of the lateral load resistance of the columns.

## 2.7 Instrumentation

Parameters measured in the tests included applied lateral load, deflection of the column at the location of the load application, and rotation one inch above the base of the column. Figure 2.14 shows the location of the instrumentation. Column deflections and rotations were measured relative to the base girder so that movement of the girder during the tests would not affect measured data. It should be noted that no movement was observed during the tests.

Deflections were measured by an LVDT (linear voltage differential transformer) attached to the column at the point of loading. In order to measure rotations, two LVDT's were attached to 250 mm aluminum bars connected to the column 25 mm above the base (Figure 2.13). The LVDT's measured the vertical displacement of the bars as the column displaced. Rotations were then calculated from these data. Load was measured with a nine kilonewton capacity load cell.

All electrical instruments were calibrated immediately before testing began. Electrical signals for instruments were transmitted to a VIDAR data acquisition system and recorded on paper tape. Paper tape was subsequently transferred to a disc file on the CDC-Cyber 175 system of the Department of Computer Science where recorded signals were calibrated and plotted using CALCOMP routines. Base moments were calculated using column height and deflection (for P-delta moment) as additional calibration factors.

## 2.8 Material Properties

Concrete properties were determined from tests of control specimens from each batch of concrete. Half of the control specimens were tested immediately after the first column test, and the remaining half were tested after the last column test for that batch.

Stress-strain curves for each batch were determined by loading 102 mm diameter by 203 mm long cylinders in compression and recording the strain over a 125-mm gage length. Figure 2.15 shows the mean stress-strain curves for both batches of concrete.

The concrete splitting strength was estimated by subjecting cylinders to compressive loads normal to the longitudinal axis. Modulus of rupture was determined by loading 51 x 51 x 203 mm prisms at the middle of a 150 mm simple span. Table 2.2 summarizes the results from these tests.

Twelve coupons of No. 13 gage (2.33 mm dia.) wire used as longitudinal reinforcement were loaded in tension with a strain rate of .001 mm/mm/sec. The mean stress-strain curve for steel is shown in Figure 2.16. Yield stress and strength are listed in Table 2.3.

# 3. OBSERVED BEHAVIOR

## 3.1 Introduction

The behavior of the column specimens is presented and discussed in this chapter. Hysteresis curves and crack patterns are used to describe the response of the columns. These observations are then compared in terms of reinforcement ratio and axial load variation.

## 3.2 Hysteresis Curves

Four hysteresis curves were plotted for each test: (1) lateral load versus displacement at load level, (2) lateral load versus rotation near the base, (3) moment at the base versus displacement at load level, and (4) moment at the base versus rotation near the base. Base moment included the effect of axial forces acting through lateral displacements (P-delta effect).

Test variables in the eight tests included reinforcement ratio and axial load. Axial load in four tests remained constant and in the remaining four tests varied in proportion with column shear. Parameters are summarized below.

| Specimen | Reinforcement Ratio, % | Axial Load |
|---|---|---|
| 2A | .88 | constant |
| 2B | .88 | constant |
| 2C | .88 | varying |
| 2D | .88 | varying |
| 4A | 1.75 | constant |
| 4B | 1.75 | constant |
| 4C | 1.75 | varying |
| 4D | 1.75 | varying |

Figures 3.1, 3.2, 3.5 and 3.6 illustrate the hysteretic behavior of columns with constant axial load. General features of these curves are listed below.

1. The curves are nearly symmetric about the axis of zero load.

2. Slopes observed during the first quarter-cycle decreased with increasing displacement.

3. Unloading slopes were always greater than the previous loading slope.

4. For all but the first load reversal, the unloading slope decreased at low loads.

5. Slopes after load reversal continued to decrease until displacements were near the displacement origin after which point slopes began to increase again.

6. When cycling at constant amplitudes, loading slopes of the initial cycle were higher than those in subsequent cycles. Stiffness generally did not deteriorate after the seocnd cycle unless a new displacement maximum was attained.

7. Unloading slopes generally did not degrade unless a new maximum displacement had been attained in the previous loading stage. All subsequent unloading slopes remained nearly the same as that observed during unloading from the maximum in that direction.

8. If the maximum displacement attained during the previous half-cycle had been exceeded at an earlier stage, subsequent loading slopes at a given displacement were larger than slopes observed while cycling at the maximum amplitude.

9. No loss of flexural capacity was observed if the P-delta effect on base moment was included. Because of stiffness degradation, apparent strength was reached only during cycles when displacement amplitudes exceeded the previous displacement maxima.

Figures 3.3, 3.4, 3.7 and 3.8 illustrate the hysteretic behavior of columns with varying axial loads. Cycling began in the region of increasing axial load for all specimens except 4D. The following trends were observed.

1. The curves were not symmetric about the axis of zero load. For a given displacement, the specimens were effectively stiffer in regions of increasing axial load than in regions of decreasing axial load.

2. Observations 2 through 4 for specimens with constant axial load were valid.

3. Slopes after load reversals were less than slopes in previous unloading portions. In regions of increasing axial load, the slope began to increase near the displacement origin. In regions of decreasing axial load, the slopes continued decreasing to a nearly zero slope.

4. Stiffness degradation was apparent only for regions of increasing axial load. Degradation in regions of decreasing axial load was negligible.

5. Observations 7 and 8 for specimens with constant axial load were valid.

6. Strength degradation was observed only for loading with increasing axial load.

Maximum responses of columns are listed in Table 3.1.

## 3.3 Crack Patterns

Crack patterns observed in the specimens consisted of intersecting flexural cracks near the base of the columns and spalling at the base of the columns. The first cracks that occurred were in the lower half of the column. The cracks increased in size and number for the first five cycles of load reversals. Subsequent cycles increased the size of existing cracks, especially at the base of the columns. Figure 3.9 shows the crack patterns for "lightly" and "heavily" reinforced specimens.

Crack widths at maximum displacements are summarized in Table 3.2. It was observed that the crack width on both sides of a specimen during a given cycle of loading were nearly identical for columns tested with constant axial load. For tests in which axial load varied, larger cracks were observed when the net axial loads were smallest. Spalling occurred in all specimens at the base of the column during the 9 mm cycles. Spalling occurred on both sides of the columns tested with constant axial force and on the side with high compressive stress on the columns tested with varying axial load.

## 3.4 Comparisons of Observed Behavior

### a) Behavior with Constant Axial Load

The hysteresis curves for column specimens tested with constant axial load are shown in Figures 3.1, 3.2, 3.5 and 3.6. All curves were nearly symmetric about the axis of zero load. The mean flexural strength for the columns with reinforcement ratio of 1.75 percent was 50 percent higher than the yield moment for columns with reinforcement ratio of 0.88 percent. The moment capacity did not decrease noticeably as the column was subjected to higher displacements.

The columns with larger reinforcement ratio achieved stiffer loading and unloading slopes than specimens with smaller reinforcement ratio. In addition, the hysteresis for the specimens with larger reinforcement ratio tended to be wider and exhibited less "pinching" effect.

At any deflection level, rotations were approximately 50 percent larger for specimens with reinforcement ratio of .88 percent. The cracks for these specimens tended to be wider and fewer in number. Cracks in specimens with reinforcement ratio of 1.75 percent were more numerous, slightly smaller in width, and more evenly distributed along the height of the column.

b) Behavior with Varying Axial Load

Specimens subjected to varying axial loads cannot be compared directly with one another nor with specimens with constant axial load because of different initial dead loads on the columns (Sect. 2.4). However, general trends can be qualitatively compared.

The hysteresis curves for specimens with varying axial load are shown in Figure 3.3, 3.4, 3.7 and 3.8. All curves were unsymmetric with higher moments occurring in quadrant of high axial load. The moments under high axial load were approximately three times larger than moments under the tensile loads for specimens with reinforcement ratio of .88 percent and approximately two times larger for specimens with reinforcement ratio of 1.75 percent.

The bounds of axial load in the columns ranged from approximately 0.5 kN tension to 10 kN compression so that extreme axial loads deviated approximately equally from the axial load used for specimens tested with constant axial load. The mean strengths of columns under constant axial

load were 257 kN-mm and 392 kN-mm for reinforcement ratios of 0.88 percent and 1.75 percent, respectively. The strengths under tensile and high compressive loads were averaged for specimens under varying axial load. The averages (236 kN-mm and 390 kN-mm for reinforcement ratios of 0.88 percent and 1.75 percent) compared closely with the strengths of columns under constant axial load. This is to be expected because the moment-axial load interaction relation (Fig. 2.5) is nearly linear for this range of axial loads.

Loading slopes were nearly horizontal in regions of low axial load. In regions of high axial load, the loading slopes were initially high and gradually decreased. Unloading slopes were similar to those for columns with constant axial load. Strength loss was observed under high axial load, but no strength loss was noticed under tensile loads.

# 4. COMPARISON OF CALCULATED AND OBSERVED BEHAVIOR

## 4.1 Introduction

Behavior of columns was studied to determine whether observed behavior could be understood using basic reinforced concrete principles and to verify experimental results. Moment-curvature diagrams were constructed for columns with reinforcement ratios of 0.88 percent and 1.75 percent and for several axial loads. These moment-curvature relationships were used to calculate rotations and deflections corresponding to the axial load and moment on the column. The calculated and observed behaviors are compared in this chapter.

## 4.2 Moment-Curvature Relationships of the Column Section

Moment-curvature diagrams were constructed for each column cross section subjected to several axial loads. The moment-curvature relationships were based on idealized stress-strain curves for the concrete and the steel reinforcing bars as described in this section.

Figure 4.1 shows the idealized stress-strain curve used for concrete. The idealized curve is represented by the following expressions:

$$
\begin{aligned}
f_c &= 0 && \varepsilon_c < \varepsilon_t \\
f_c &= 2f'_c\left(\frac{\varepsilon_c}{\varepsilon_o}\right) && \varepsilon_t \leq \varepsilon_c \leq 0 \\
f_c &= f'_c\left[2\left(\frac{\varepsilon_c}{\varepsilon_o}\right) - \left(\frac{\varepsilon_c}{\varepsilon_o}\right)^2\right] && 0 \leq \varepsilon_c \leq \varepsilon_o \\
f_c &= f'_c - m(\varepsilon_c - \varepsilon_o) && \varepsilon_o \leq \varepsilon_c
\end{aligned}
\qquad (4.1)
$$

where,

$\varepsilon_t$ = strain at maximum tensile strength

$\varepsilon_o$ = strain at maximum compressive strength

$f'_c$ = maximum compressive strength

m = slope of the descending portion of the concrete stress-strain curve assumed equal to 2000 in this study.

The values of stress and strain at maximum compression and tension were determined from testing of control specimens.

Figure 4.2 shows the idealized stress-strain relationship used for longitudinal steel. The idealized relationship is defined below.

$$
\begin{aligned}
f_s &= E_s\,\varepsilon_s && 0 \le \varepsilon_s \le \varepsilon_{sy} \\
f_s &= f_{sy} && \varepsilon_{sy} \le \varepsilon_s \le \varepsilon_{sh} \\
f_s &= f_{sy} + E_{sh}(\varepsilon_s - \varepsilon_{sh}) && \varepsilon_{sh} \le \varepsilon_s \le \varepsilon_{su} \\
f_s &= f_{su} && \varepsilon_s \ge \varepsilon_{su}
\end{aligned}
\qquad (4.2)
$$

where,

$\varepsilon_{sy}$ = strain at yield

$\varepsilon_{sh}$ = strain at onset of strain hardening

$\varepsilon_{su}$ = strain at ultimate stress

$E_s$ = Young's Modulus of steel

$E_{sh} = \dfrac{f_{su} - f_{sy}}{\varepsilon_{su} - \varepsilon_{sh}}$

$f_{sy}$ = yield stress of steel

and $f_{su}$ = ultimate stress of steel.

The steel is assumed to maintain its maximum stress without fracture. The values for stress and strain at yield, at the onset of strain hardening, and at ultimate were determined from measured stress-strain curves.

Moments and curvatures were computed for different values of concrete strains and axial loads using a computer program developed by Lybas (Ref. 5). Moments were computed about the plastic centroid of the section. Curvatures were determined from the following relationship,

$$\phi = \frac{\varepsilon_{cm}}{C_o} \tag{4.3}$$

where,

$\varepsilon_{cm}$ = compressive strain in concrete at the compression edge of the section

$C_o$ = distance to the neutral axis.

Moments and corresponding curvatures are plotted to give moment-curvature relationships for several axial loads (Fig. 4.3 and 4.4).

## 4.3 Comparison of Measured and Calculated Strengths

Envelopes of measured moment-deflection response were constructed from measured first-quarter cycles and extended to failure using subsequent response envelopes in the first-quarter cycle. The envelopes are compared in Figure 4.5. Also indicated in that figure are axial loads corresponding to maximum moment. The measured bounds are similar for specimens with similar reinforcement type and axial load. However, specimens with two bars per face (2C and 2D) exhibited approximately ten percent difference in flexural strength under high axial loads. Depths to the reinforcing bars and strengths of steel compared almost identically for these specimens.

Flexural strengths were calculated for the column specimens so that measured strengths could be verified. For specimens subjected to compressive axial forces at the time that flexural strengths were reached, calculated strengths were those found from the calculated moment-curvature relationships (sec. 4.2). For specimens reaching flexural strengths under tensile axial loads, it was likely that compressive reinforcement had been plastically elongated under loading in the opposite direction. Because the column was subjected to a net tension, the crack which was opened by loading in the opposite direction would not be expected to close completely. Therefore, flexural strengths were calculated considering only the couple formed by longitudinal reinforcement as shown in the following expression.

$$M = A_s' \, d \, f_{eff}$$

where

$f_{eff}$ = the effective stress in the steel defined as $(f_y - \frac{N}{A_s})$,

$f_y$ = yield stress in steel

$N$ = axial load in column

$A_s$ = total area of steel

$A_s'$ = area of steel in each face of column section

$d$ = distance between layers of steel in each face of column section.

Calculated strengths are compared with measured strengths in Figure 4.5. The strengths compared well for specimens subjected to tensile loads and for specimens with constant axial load. For specimens subjected to high compressive loads, the measured strengths exceeded the calculated strengths by approximately ten percent.

An upper bound on flexural strengths was estimated for the specimens under high axial load by assuming tensile and compressive strengths for top and bottom steel and using measured material properties and dimensions. The calculated strengths were 362 and 500 kN-mm for specimens with two and four bars per face, respectively. The measured strengths for specimens with four bars per face exceeded the calculated bound by five and eight percent, suggesting a small measurement error.

## 4.4 Moment-Rotation and Moment-Deflection Relationships

The calculated moment-curvature relations (Fig. 4.3 and 4.4) were used to calculate rotations and deflections of the column specimens on the primary curve. Estimates of bond slip effects were included. The idealized model considered the columns to be subdivided into six elements as shown in Figure 4.6. Elements one and two are located below the point where rotations were measured during tests. Smaller elements were located near the base of the column where most of the cracking occurred. Curvatures corresponding to a given base moment were determined at the centroid of each element from the calculated moment-curvature relations.

Rotations were calculated by summing the curvature areas for elements one and two. Major cracking occurred only in this area. Rotation due to bond slip was added to the rotation computed from the idealized model. Rotation due to bond slip was defined by (Ref. 6)

$$\theta = \frac{d\left(\frac{f_y}{M_y}\right)^2 M^2}{8\mu EC}$$

where,

d = diameter of reinforcing bar

$f_y$ = yield stress of steel

$M_y$ = yield moment of column specimen

M = base moment of column

$\mu$ = bond stress taken as 2 MPa in this study (Ref. 7)

E = Young's modulus of steel

C = distance between tensile steel and neutral axis.

Deflections at point of loading were calculated by summing curvature moments about that point and adding deflection due to bond slip.

Rotations and deflections were calculated for several base moments. Calculated moment-rotation and moment-deflection relationships are plotted with the observed relationships in Figures 4.7 through 4.8.

It should be emphasized that response was calculated only for the primary curve and that no attempt was made to account for response under load reversals. However, the characteristics of observed hysteresis relations were similar to those observed for other reinforced concrete members, so that response under reversed loading can probably be represented satsifactorily using existing hysteresis rules (Ref. 6, 8, and 9).

## 4.5 Comparison of Measured and Calculated Response

Primary curves of measured response are compared with calculated response in Figures 4.7 and 4.8. The primary curves were constructed from measured first-quarter cycles and extended to approximate response during subsequent cycles. The measured responses are taken from the following specimens.

| Specimen Type | Positive Moment Region | Negative Moment Region |
|---|---|---|
| Series 2 Constant | 2B | Symmetric |
| Series 2 Varying | 2C | Inferred from 3rd quarter cycle of 2C |
| Series 4 Constant | 4B | Symmetric |
| Series 4 Varying | 4C | 4C |

Comparison with other specimens was similar. As noted above, the negative moment curve for Series 2 columns with varying axial load was inferred from response of Specimen 2C in the third quadrant and thus does not represent a measured first-quarter cycle response. This was required because no Series 2 specimens were tested with first-quarter cycles in the region of decreasing axial load. The curves are discussed below.

a) Moment-Deflection Relationships

Figure 4.7 compares measured and calculated moment-deflection relationships. For Series 2 columns with constant axial load, the calculated moment-deflection curves are nearly coincident with the measured moment-deflection curves. Calculated deflections were approximately ten percent smaller than those measured for the remaining specimens except for Series 4 columns under high axial load. This consistant difference may be due to an error in one of the parameters used to calculate displacements. The similarity between the shapes of the calculated and measured curves indicates that the overall calculation procedure was adequate.

Calculated deflections for regions of high compressive loads for Series 4 columns with varying axial load are significantly smaller than those

measured. This difference is attributable to a ram malfunction which occurred during the first cycle in testing of Specimen 4C. The malfunction caused the ram to load the column before testing. The column was returned to the location of zero deflection and the test was restarted. This malfunction accounts for the smaller initial slope of the measured curve.

b) Moment-Rotation Relationships

Figure 4.8 compares measured and calculated moment-rotation relationships. Calculated rotations compared closely to measured rotations in all cases except Series 2 columns under constant axial load and Series 4 columns under high axial load. Calculated rotations for Series 2 columns with constant axial load underestimated measured rotations by approximately 30 percent. The discrepancy was observed for both Specimen 2A and 2B. Calculated rotations for Series 4 columns under high axial load were significantly smaller than those measured. This discrepancy may be due to a ram malfunction as discussed in Section 4.5a.

Errors in calculated rotations may be due to inaccuracies in the assumptions used to estimate reinforcement pullout. For instance, bond slip in regions of the column above the point at which rotations were measured may have increased the measured rotations. Bond slip in this region is normally accounted for with moment-curvature relations. However, the existance of large cracks only below the point at which rotations were measured suggests that these curvatures were concentrated in cracks near the column base. The calculated rotations include effects of reinforcement pullout and of curvatures below the level at which rotations were measured (See Sec. 4.4). In addition, large scatter in effective bond stress has been observed in previous tests using plain No. 8 gage wire (Ref. 7).

Bond stress properties of No. 13 gage wire used in the column specimens have not been studied experimentally.

# 5. SUMMARY AND CONCLUSIONS

## 5.1 Summary

Eight small-scale reinforced concrete columns were subjected to simultaneously varying axial and shear force reversals. The specimens were similar to the first story columns used in small-scale, multistory frames tested on the University of Illinois Earthquake Simulator. Test variables included the reinforcement ratio, the dead load on the column, and the rate of axial load variation during shear force reversals. Behavior of the specimens is represented by measure hysteresis relations and crack patterns. The observed behavior is compared with the response calculated using reinforced concrete principles.

## 5.2 Conclusions

The hysteresis curves for column specimens with constant axial load were symmetric about the axis of zero load. The mean flexural strength was 50 percent higher for columns with reinforcement ratio of 1.75 percent than for columns with reinforcement ratio of 0.88 percent. Moment capacities were maintained to displacements exceeding four percent of column height.

Observed damage in columns comprised flexural cracks and nominal concrete spalling. The cracks for the "lightly" reinforced columns tended to be wider and fewer in number. Cracks in "heavily" reinforced columns tended to be more numerous and more uniformly distributed along the height of the column. In addition, rotations measured near the base of columns were approximately 50 percent larger for specimens with the "lighter" reinforcement ratios.

The hysteresis curves for specimens with varying axial loads were unsymmetric with higher moments occurring under "high" axial load. Moments in regions of "high" axial load were approximately two times larger for specimens with reinforcement ratio of 1.75 percent than for specimens with reinforcement ratio of 0.88 percent. Strength loss was observed under "high" axial loads, but no strength loss was noticed under tensile loads.

The average of the bounding values of axial loads in columns with varying axial load was approximately equal to the axial load used for specimens with constant axial load. The strengths under tensile and high compressive loads were averaged for columns with varying axial load. The average strength compared closely with the strengths of columns under constant axial load. This is to be expected because the moment-axial load interaction relation is nearly linear for this range of axial load.

Calculated strengths compared well for specimens subjected to tensile loads and for specimens with constant axial load. For specimens subjected to high compressive loads, the measured strengths exceeded calculated strengths by a maximum of eight percent.

Deflections and rotations were calculated using reinforced concrete principles including the effects of bond slippage. Calculated deflections and rotations compared well with the measured response. The satisfactory comparisons between measured and calculated responses suggests that overall deformation characteristics of the small-scale columns were similar to those of full-scale reinforced concrete members.

## REFERENCES


1. Abrams, D.P., and M.A. Sozen, "Experimental Study of Frame-Wall Interaction in Reinforced Concrete Structures Subjected to Strong Earthquake Motions," Civil Engineering Studies, Structural Research Series No. 460, University of Illinois, Urbana, May 1979.

2. Healey, T.J., and M.A. Sozen, "Experimental Study of the Dynamic Response of a Ten-Story Reinforced Concrete Frame with a Tall First Story," Civil Engineering Studies, Structural Research Series No. 450, University of Illinois, Urbana, August 1978.

3. Kreger, M.E., and D.P. Abrams, "Measured Hysteresis Relationships for Small-Scale Beam-Column Joints," Civil Engineering Studies, Structural Research Series No. 453, University of Illinois, Urbana, August 1978.

4. Moehle, J.P., and M.A. Sozen, "Earthquake-Simulation Tests of a Ten-Story Reinforced Concrete Frame with a Discontinued First-Level Beam," Civil Engineering Studies, Structural Research Series No. 451, University of Illinois, Urbana, August 1978.

5. Lybas, J.M., and M.A. Sozen, "Effect of Beam Strength and Stiffness on Dynamic Behavior of Reinforced Concrete Coupled Walls," Civil Engineering Studies, Structural Research Series No. 444, University of Illinois, Urbana, July 1977.

6. Saiidi, M., and M.A. Sozen, "Simple and Complex Models for Nonlinear Seismic Response of Reinforced Concrete Structures, Civil Engineering Studies, Structural Research Series No. 465, University of Illinois, Urbana, August 1979.

7. Gavlin, N., "Bond Characteristics of Model Reinforcement," Civil Engineering Studies, Structural Research Series No. 427, University of Illinois, April 1976.

8. Otani, S., and M.A. Sozen, "Behavior of Multistory Reinforced Concrete Frames During Earthquakes," Civil Engineering Studies, Structural Research Series No. 392, University of Illinois, Urbana, November 1972.

9. Takeda, T., M.A. Sozen, and N.N. Nelsen, "Reinforced Concrete Response to Simulated Earthquakes," Journal of the Structural Division, ASCE, Vol. 96, No. ST12, Proc. Paper 7759, December 1970, pp. 2557-2573.

10. Moehle, J. P. and M. A. Sozen, "Experiments to Study Earthquake Response of R/C Structures with Stiffness Interruptions," Civil Engineering Studies, Structural Research Series No. 482, University of Illinois, Urbana, August 1980.

TABLE 2.1

Measured Cross-Sectional Dimensions
and Age at Testing of Specimens

| Specimen | Age (days) | Width at Base (mm) | Width at Joint (mm) | Depth at Base (mm) | Depth at Joint (mm) |
|---|---|---|---|---|---|
| 2A | 32 | 51.6 | 51.4 | 38.2 | 38.4 |
| 2B | 39 | 50.5 | 51.3 | 38.4 | 38.2 |
| 2C | 53 | 51.6 | 50.9 | 37.9 | 38.1 |
| 2D | 49 | 51.3 | 51.4 | 38.0 | 37.9 |
| 4A | 32 | 51.1 | 50.9 | 38.6 | 38.4 |
| 4B | 40 | 50.3 | 50.8 | 38.8 | 38.6 |
| 4C | 66 | 50.7 | 50.7 | 38.2 | 38.2 |
| 4D | 69 | 50.8 | 50.7 | 37.8 | 38.2 |

TABLE 2.2

Measured Concrete Properties

| Specimen | Age at Testing (days) | Compressive Strength (MPa) | Splitting Strength (MPa) | Modulus of Rupture (MPa) |
|---|---|---|---|---|
| Series 2 Specimens | 32 | 36.2 | 3.4 | 7.0 |
| | 49 | 34.3 | 2.9 | 10.7 |
| Series 4 Specimens | 32 | 35.8 | 2.8 | 7.2 |
| | 69 | 38.8 | 3.4 | 7.8 |

TABLE 2.3

Measured Steel Properties

| Specimen | Yield Stress (MPa) | Strength (MPa) | No. of Coupons Tested |
|---|---|---|---|
| 2A | 379.0 | 410.5 | 1 |
| 2B | 379.0 | 405.3 | 1 |
| 2C | 384.2 | 413.7 | 1 |
| 2D | 394.8 | 428.4 | 1 |
| 4A | 382.1 | 415.8 | 3 |
| 4B | 379.0 | 407.4 | 2 |
| 4C | 392.6 | 424.2 | 2 |
| 4D | 373.7 | 407.4 | 2 |

Overall Mean of Yield Stress = 383.1 MPa
Overall Standard Deviation = 8.6
Overall Mean of Strength = 414.1 MPa
Overall Standard Deviation = 10.3

TABLE 3.1

Summary of Response Maxima and Minima

| Specimen | Lateral Load KN | | Base Moment KN-mm | | Deflection mm | | Rotations rad * 100 | |
|---|---|---|---|---|---|---|---|---|
| | Max | Min | Max | Min | Max | min | Max | Min |
| 2A | .93 | -.90 | 260. | -256. | 8.6 | -9.0 | 36.7 | -35.2 |
| 2B | 1.0 | -.86 | 271. | -241. | 8.9 | -9.0 | 33.8 | -34.5 |
| 2C | 1.18 | -.46 | 339. | -116. | 9.3 | -8.8 | 33.8 | -33.6 |
| 2D | 1.34 | -.46 | 375. | -115. | 9.2 | -8.8 | 34.7 | -34.0 |
| 4A | 1.62 | -1.26 | 444. | -356. | 9.1 | -9.3 | 31.8 | -29.5 |
| 4B | 1.41 | -1.36 | 391. | -377. | 9.3 | -9.3 | 33.0 | -30.7 |
| 4C | 1.87 | -.98 | 541. | -244. | 9.4 | -9.3 | 32.7 | -30.6 |
| 4D | 1.84 | -.99 | 527. | -248. | 9.0 | -9.9 | 31.6 | -36.0 |

TABLE 3.2

Crack Widths Measured at Maximum Cycle Displacements

| Cycle Displacement | Specimen | | | | | | | |
|---|---|---|---|---|---|---|---|---|
| | 2A | 2B | 2C | 2D | 4A | 4B | 4C | 4D |
| +3 | -- | -- | -- | -- | -- | -- | -- | -- |
| -3 | .10 | .20 | .15 | .30 | .15 | -- | -- | -- |
| +3 | .10 | .15 | .15 | -- | .15 | -- | -- | -- |
| -3 | .15 | .20 | .20 | .30 | .15 | -- | .15 | .15 |
| +3 | .15 | .15 | .20 | -- | .15 | .05 | .10 | .10 |
| -3 | .15 | .20 | .20 | .30 | .15 | .10 | .15 | .30 |
| +6 | .60 | .50 | .60 | .40 | .40 | .70 | .30 | .15 |
| -6 | .60 | .60 | .60 | .60 | .35 | .50 | .50 | .60 |
| +6 | .60 | .50 | .60 | .40 | .45 | .80 | .60 | .50 |
| -6 | .60 | .60 | .80 | .60 | .35 | .60 | .90 | .80 |
| +6 | .70 | .50 | .60 | .50 | .45 | .80 | .60 | .50 |
| -6 | .70 | .60 | .80 | 1.00 | .40 | .60 | .90 | .80 |
| +3 | .20 | .20 | .30 | .15 | .15 | .30 | .30 | .70 |
| -3 | .20 | .20 | .40 | .40 | .20 | .30 | .90 | .50 |
| +9 | 1.40 | 1.00 | 1.00 | .80 | 1.00 | 1.20 | 1.10 | .20 |
| - | 1.40 | 1.10 | 1.20 | 1.40 | .90* | 1.20 | 1.40 | 1.40 |
| +9 | 1.40 | 1.20 | 1.20* | .90 | 1.00 | 1.20 | 1.20 | 1.00 |
| -9 | 1.40 | 1.30 | 1.40 | 1.40 | .90 | 1.20* | 1.20 | 1.50 |
| +9 | 1.40 | 1.20 | 1.30 | .90* | 1.10 | 1.20 | 1.40 | 1.20 |
| -9 | 1.40 | 1.30 | 1.40 | 1.40 | 1.00 | 1.20 | 1.20 | 1.60 |
| +3 | .20* | .20 | .40 | .20 | .20 | .15 | .60 | |
| -3 | .25 | .30 | .50 | .60 | .20 | .30 | .80 | |

* crushing occurs

(All Dimensions In Millimeters)

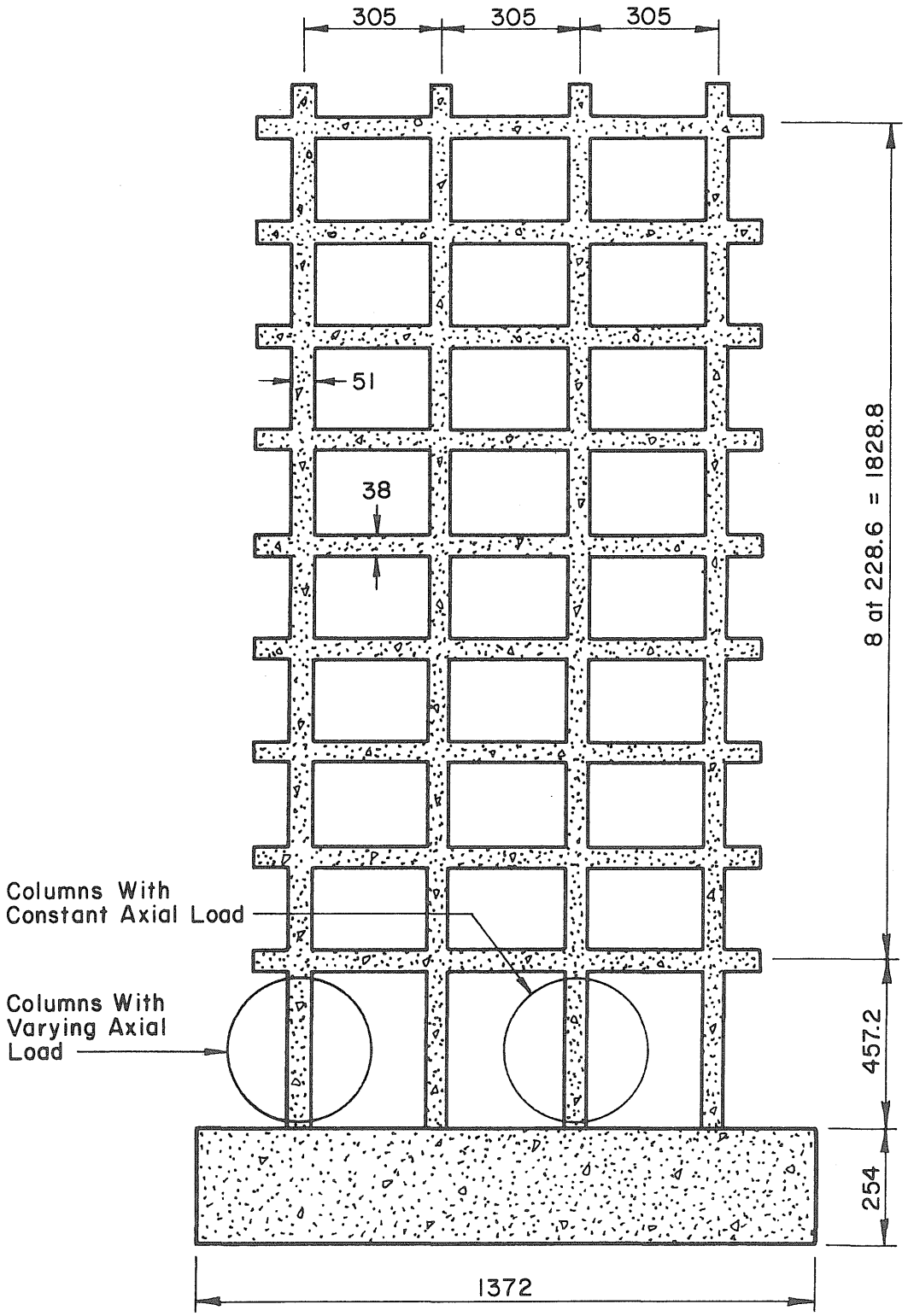


Fig. 2.1 Nine-Story, Three-Bay Frame

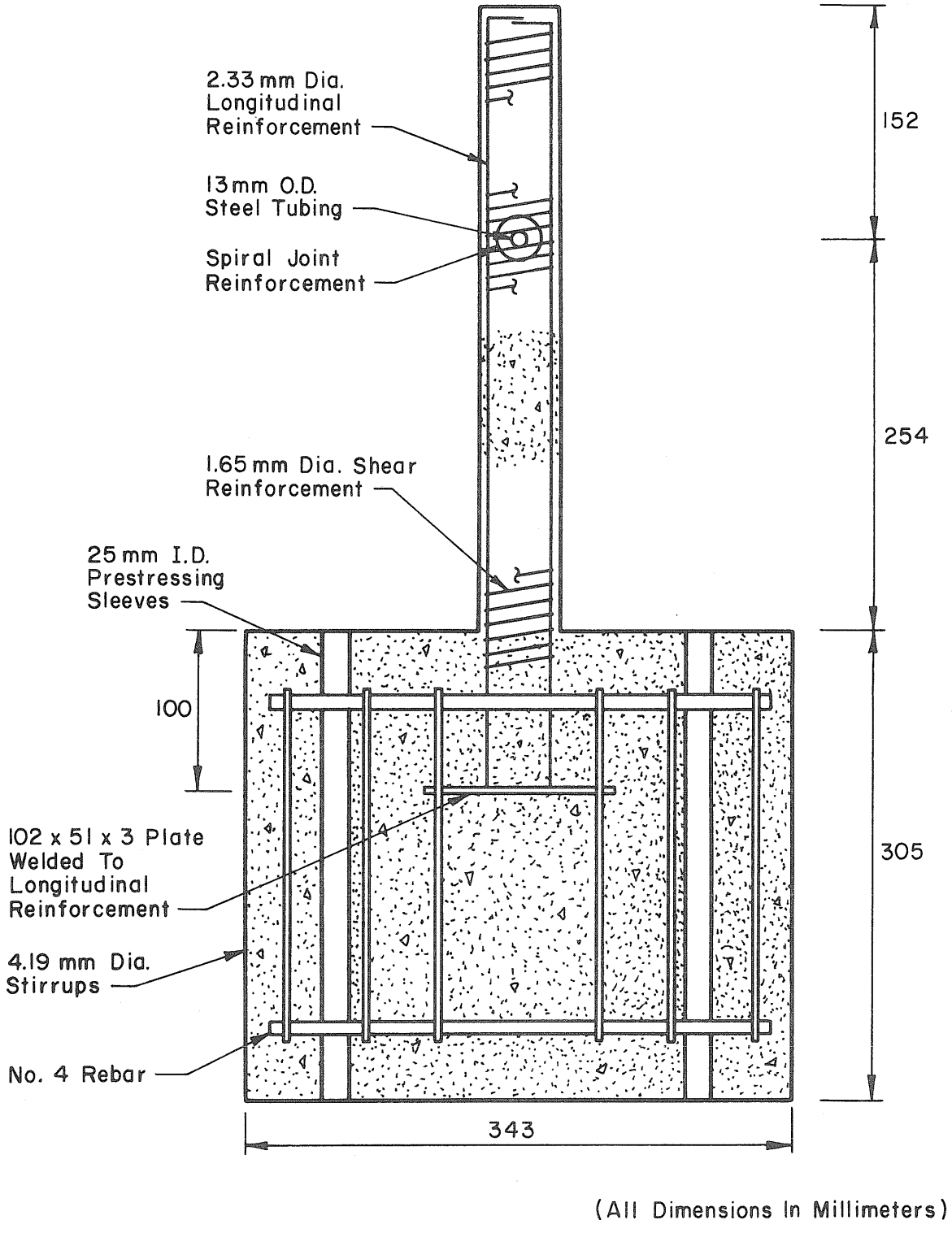


Fig. 2.2 Elevation of Column Specimen Placement of Reinforcing Steel

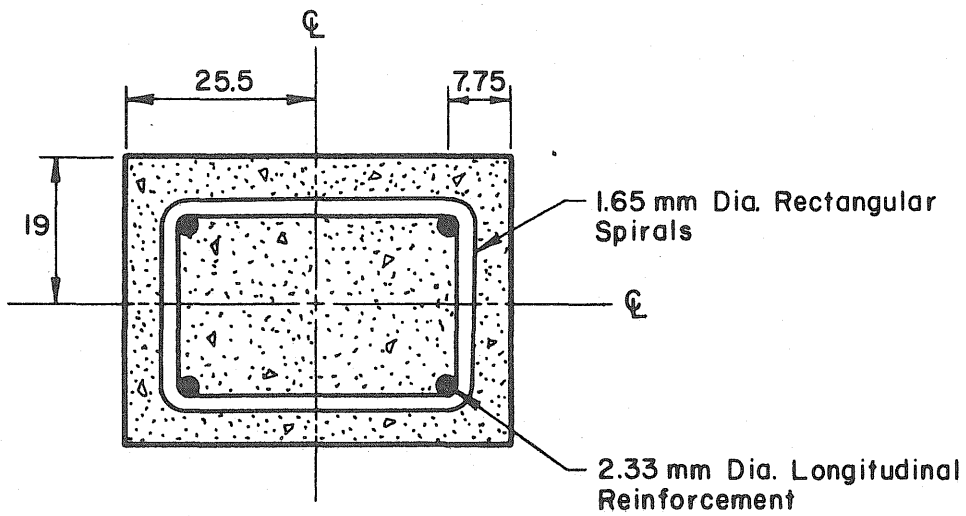


Series 2

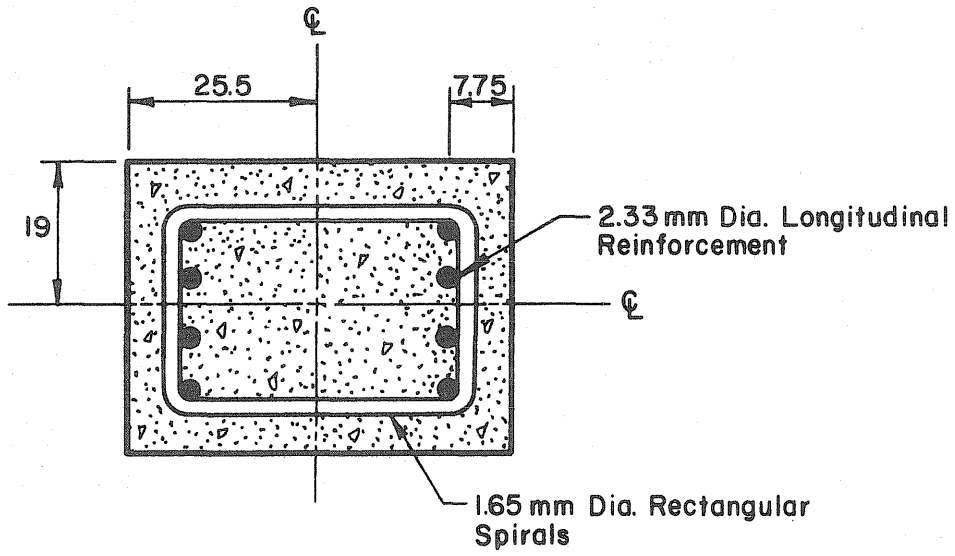


Series 4

(All Dimensions In Millimeters)

Fig. 2.3 Nominal Cross Sectional Dimensions

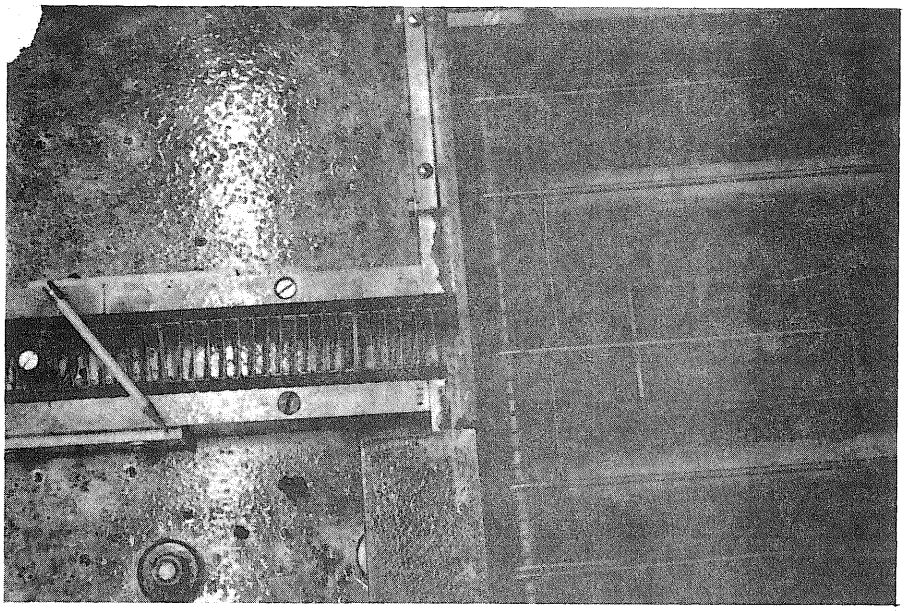

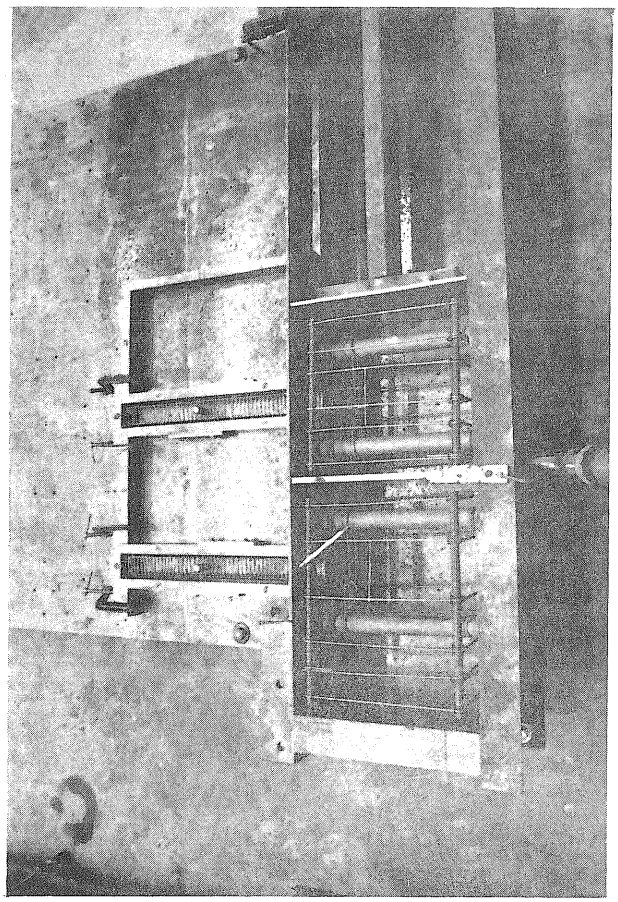

Fig. 2.4 Formwork with Reinforcing Cages

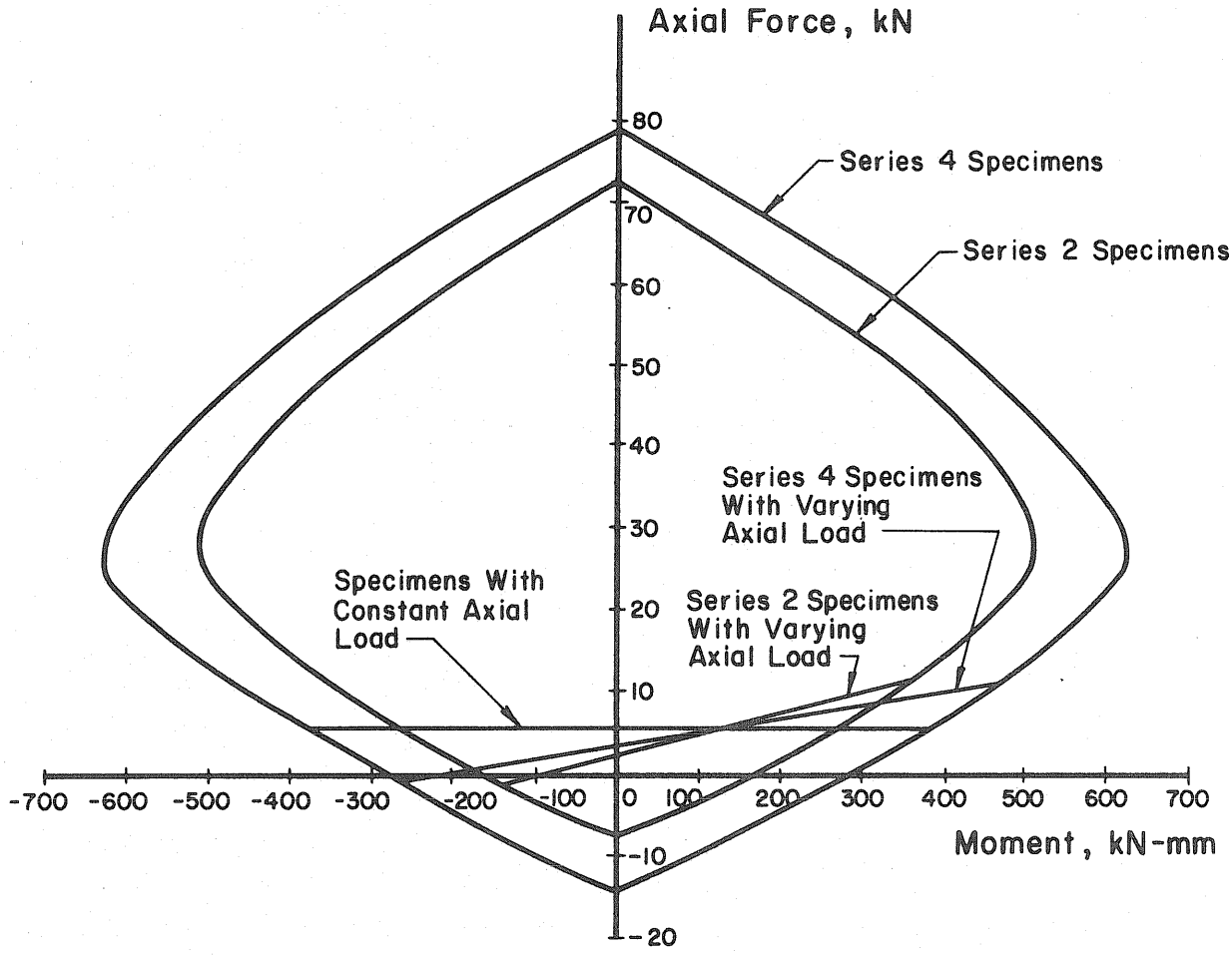


Fig. 2.5 Load-Moment Interaction Diagram

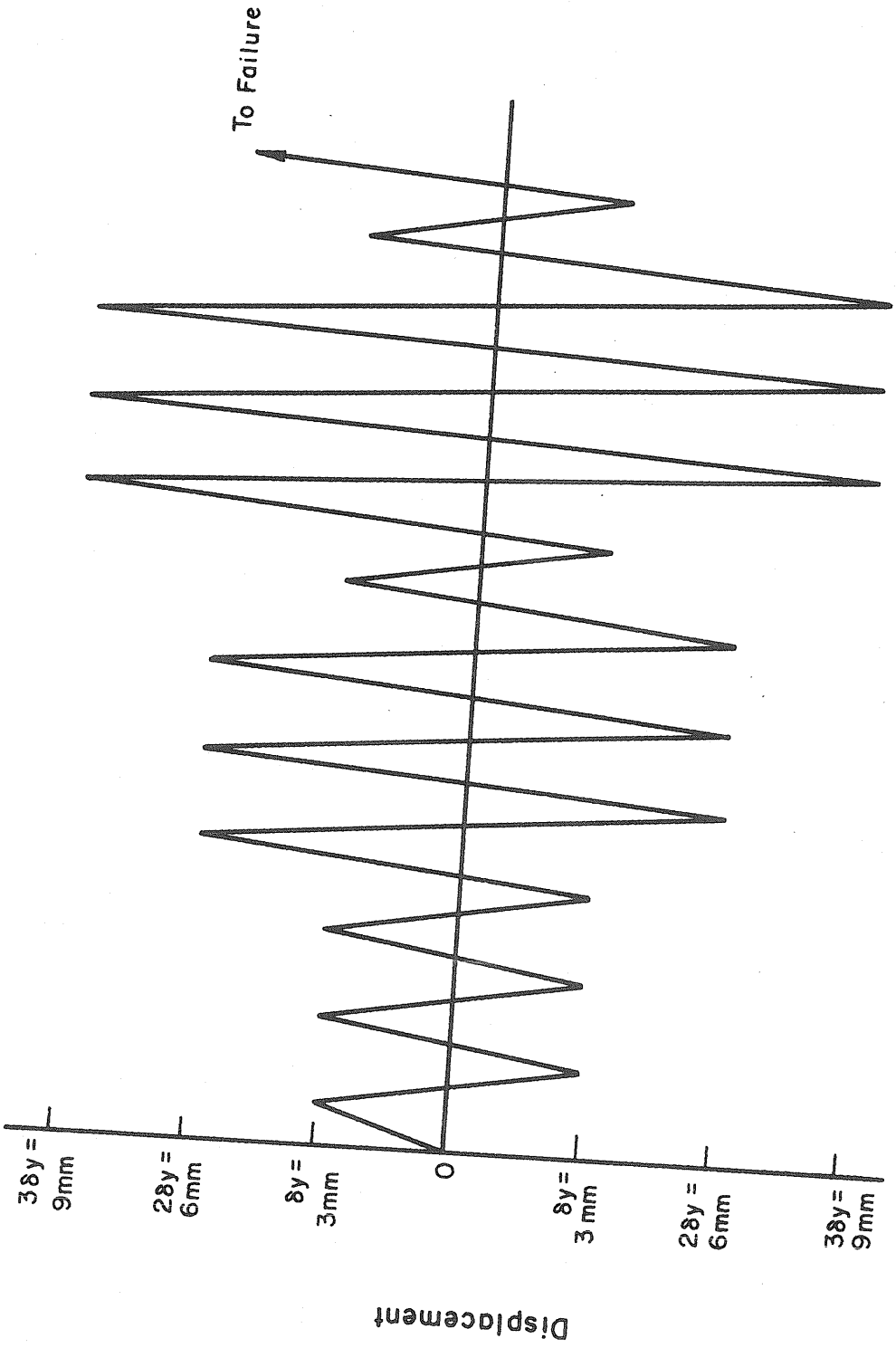


Fig. 2.6 Displacement Pattern

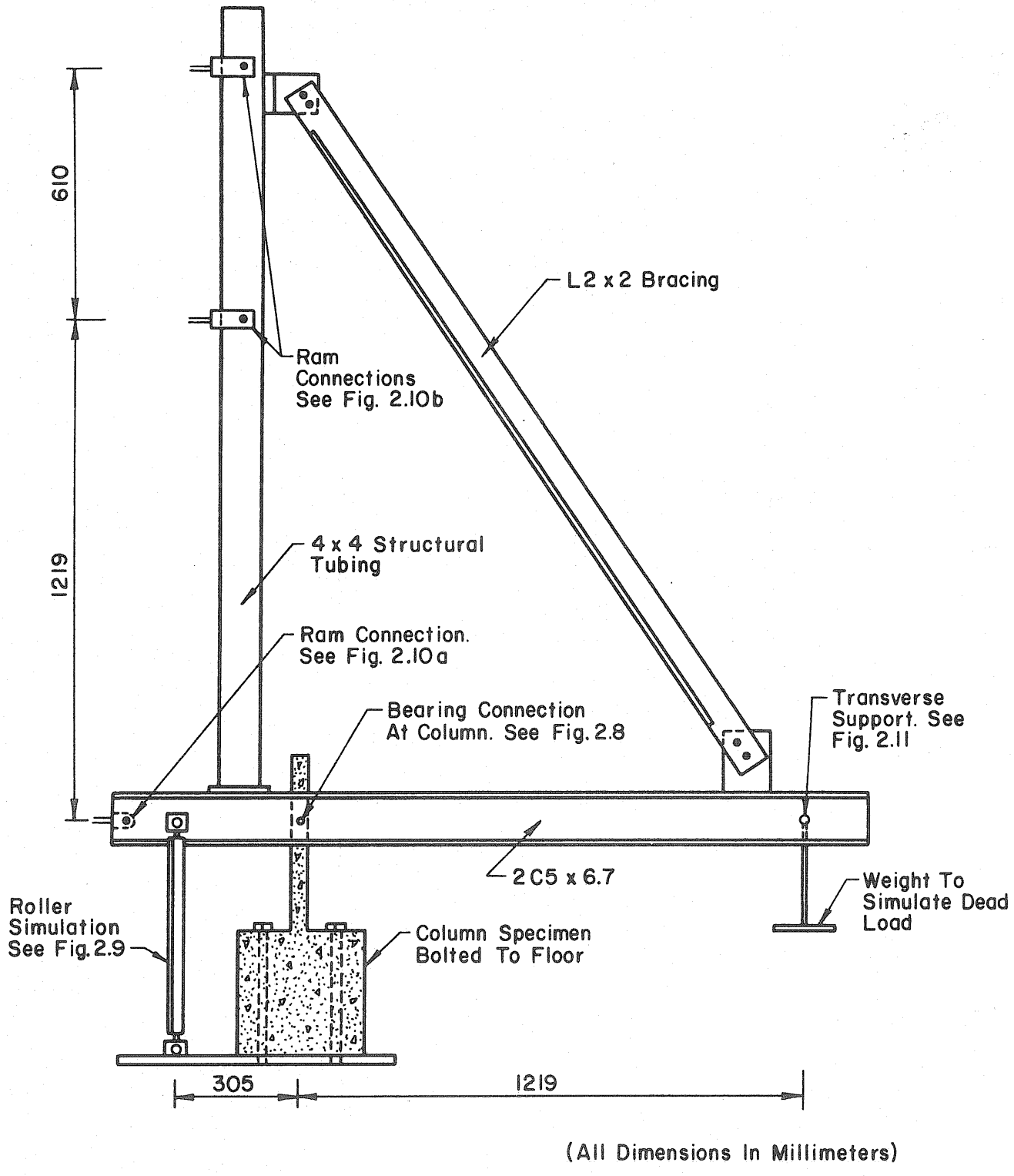


Fig. 2.7 Test Setup

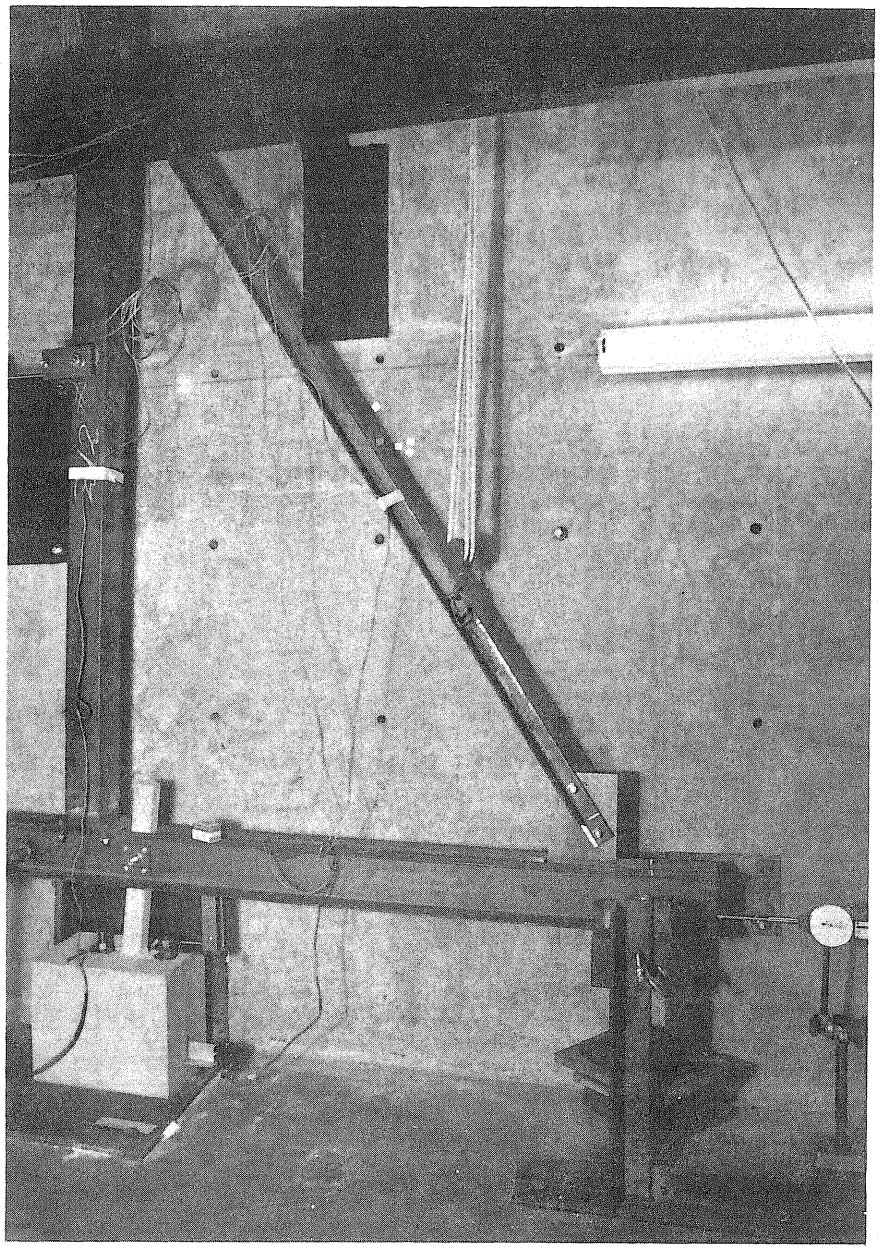

Fig. 2.7 Contd. Test Setup

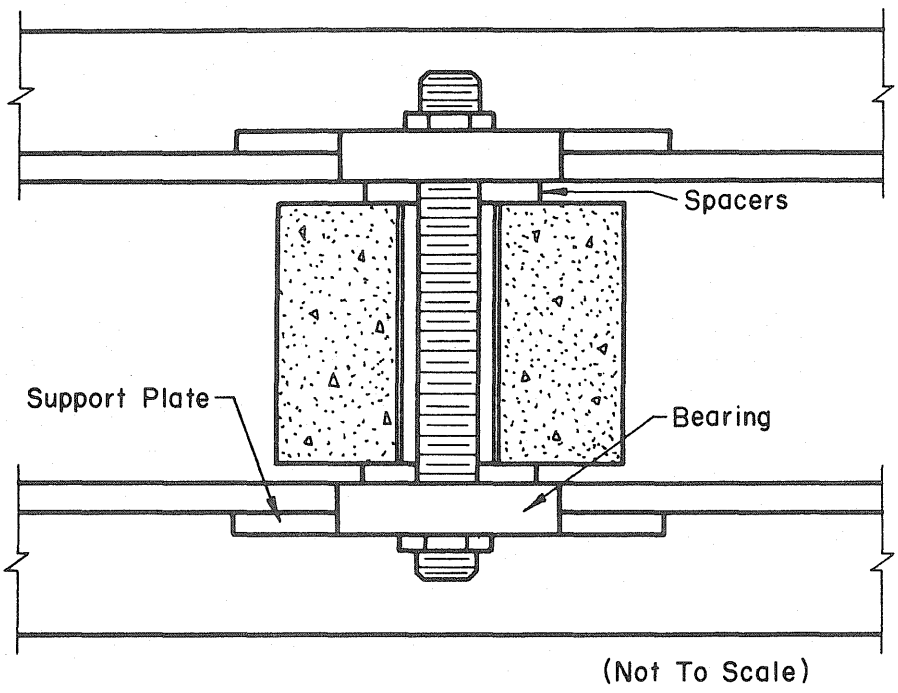


Section A-A

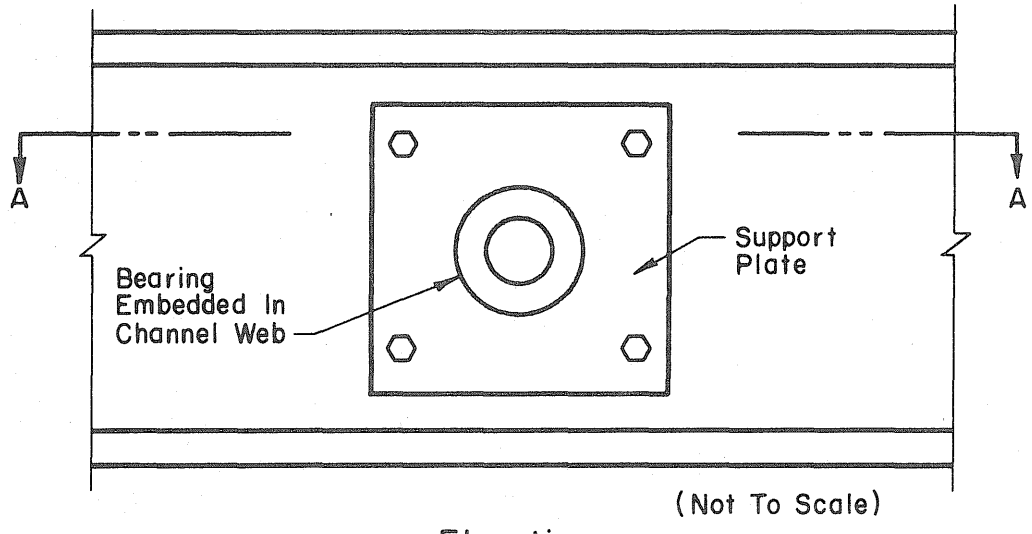


Elevation

Fig. 2.8 Loading Frame-Column Connection

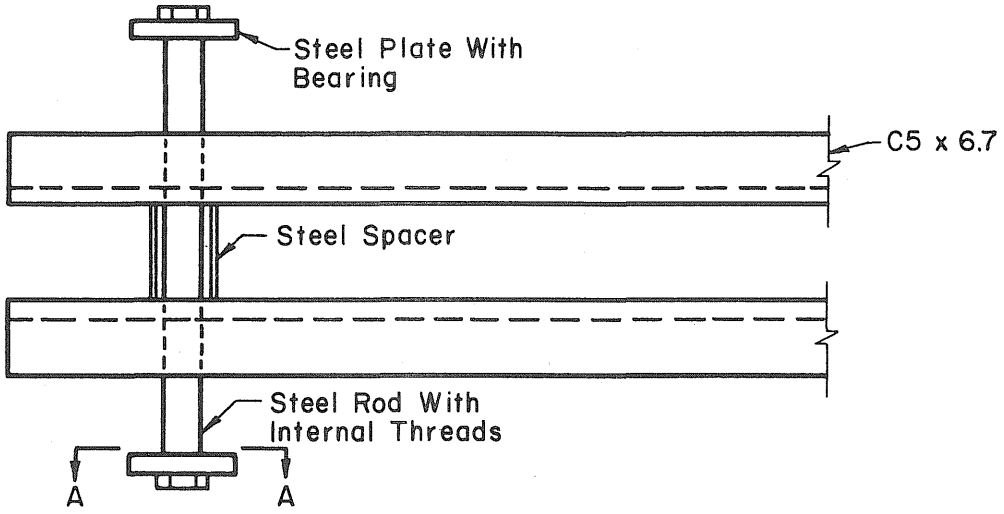


Plan View

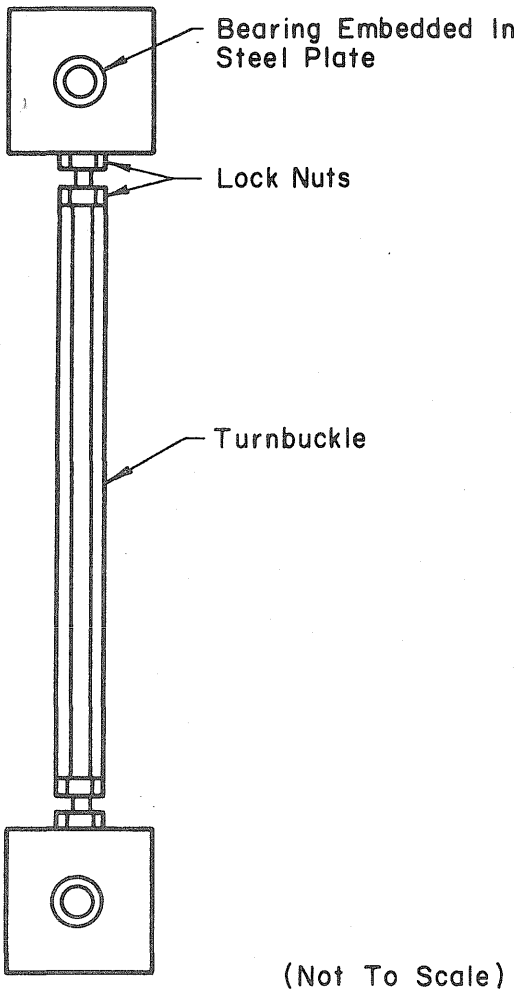


Section A-A

Fig. 2.9 Roller Simulator

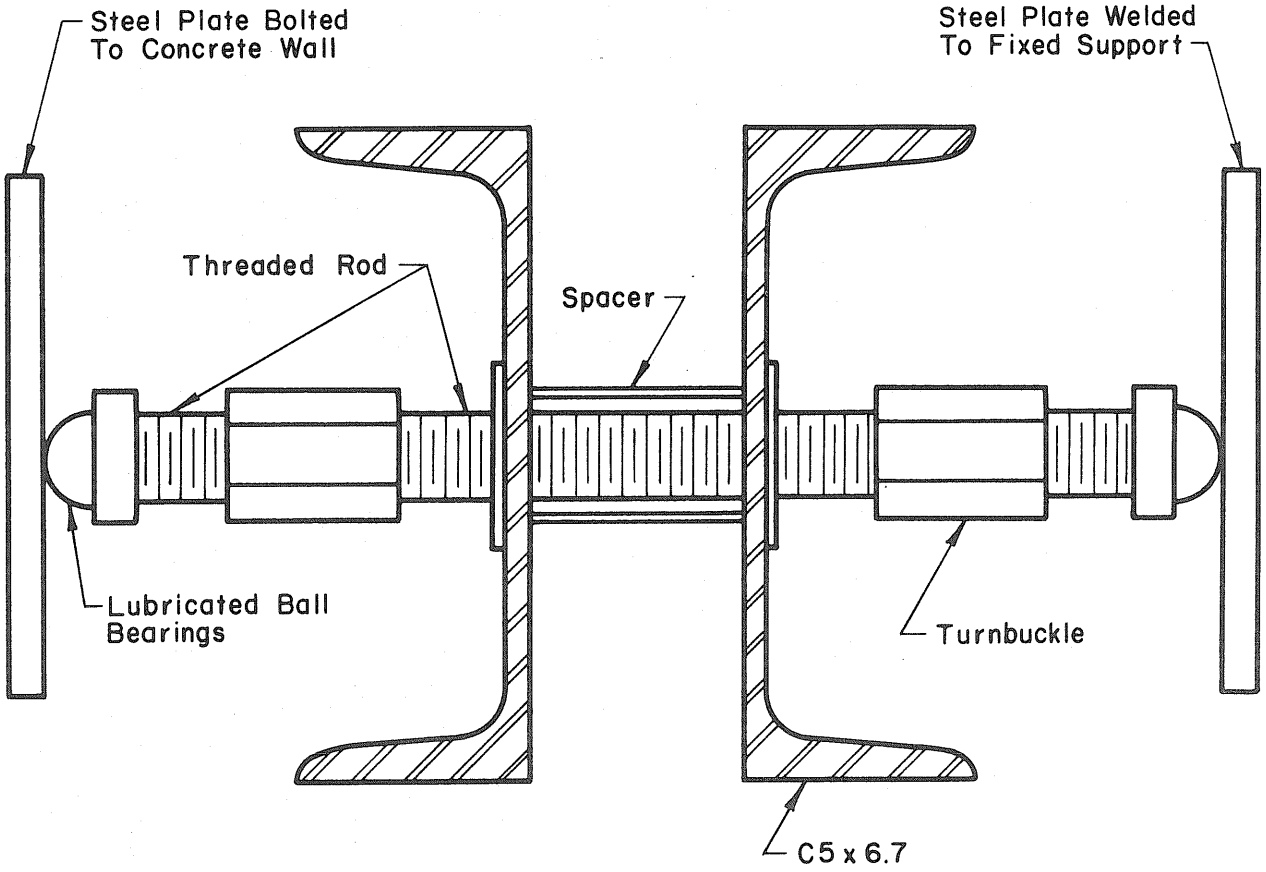


Fig. 2.10 Transverse Stability Mechanism Viewed Along Direction of Load

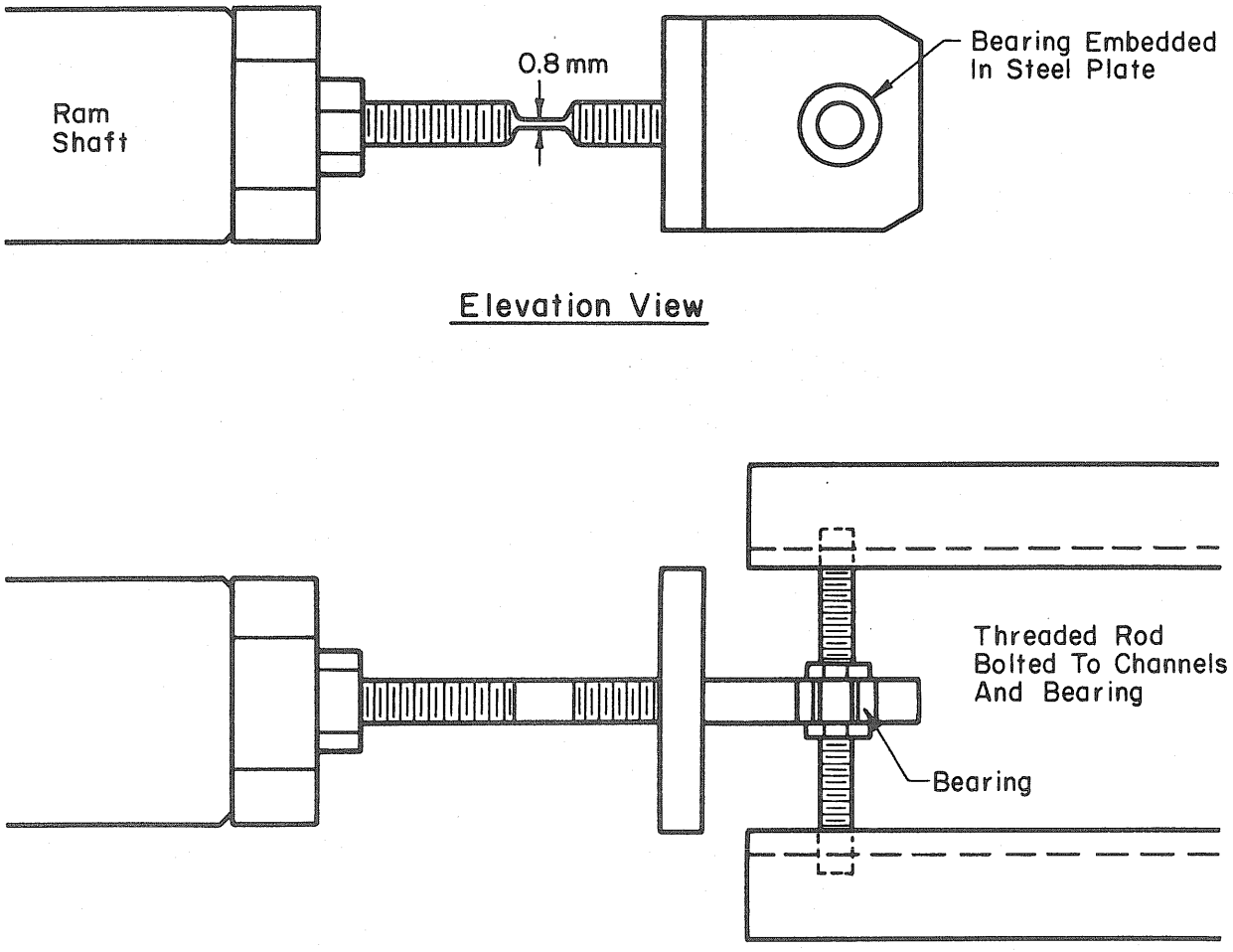


Fig. 2.11 Loading Frame-Ram Connection:
Type A

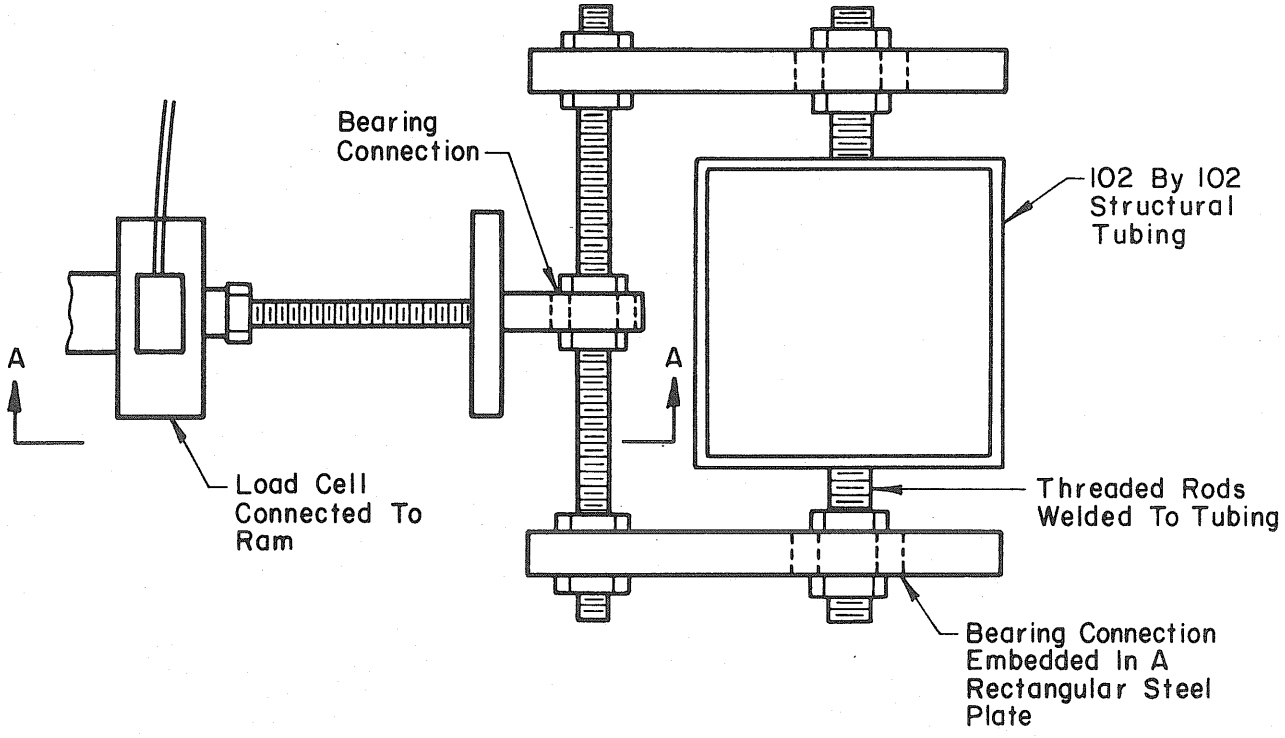


Plan View
Not To Scale

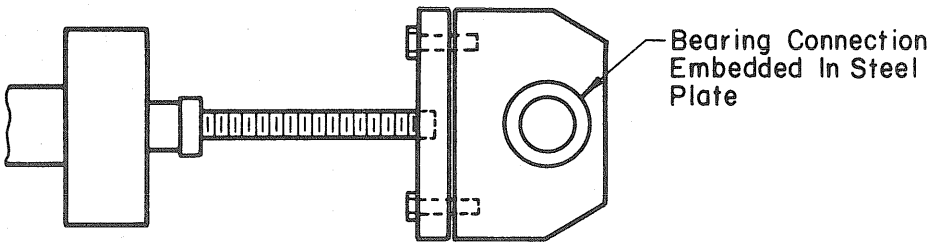


Section A-A
Not To Scale

Fig. 2.12 Loading Frame-Ram Connection:
Type B

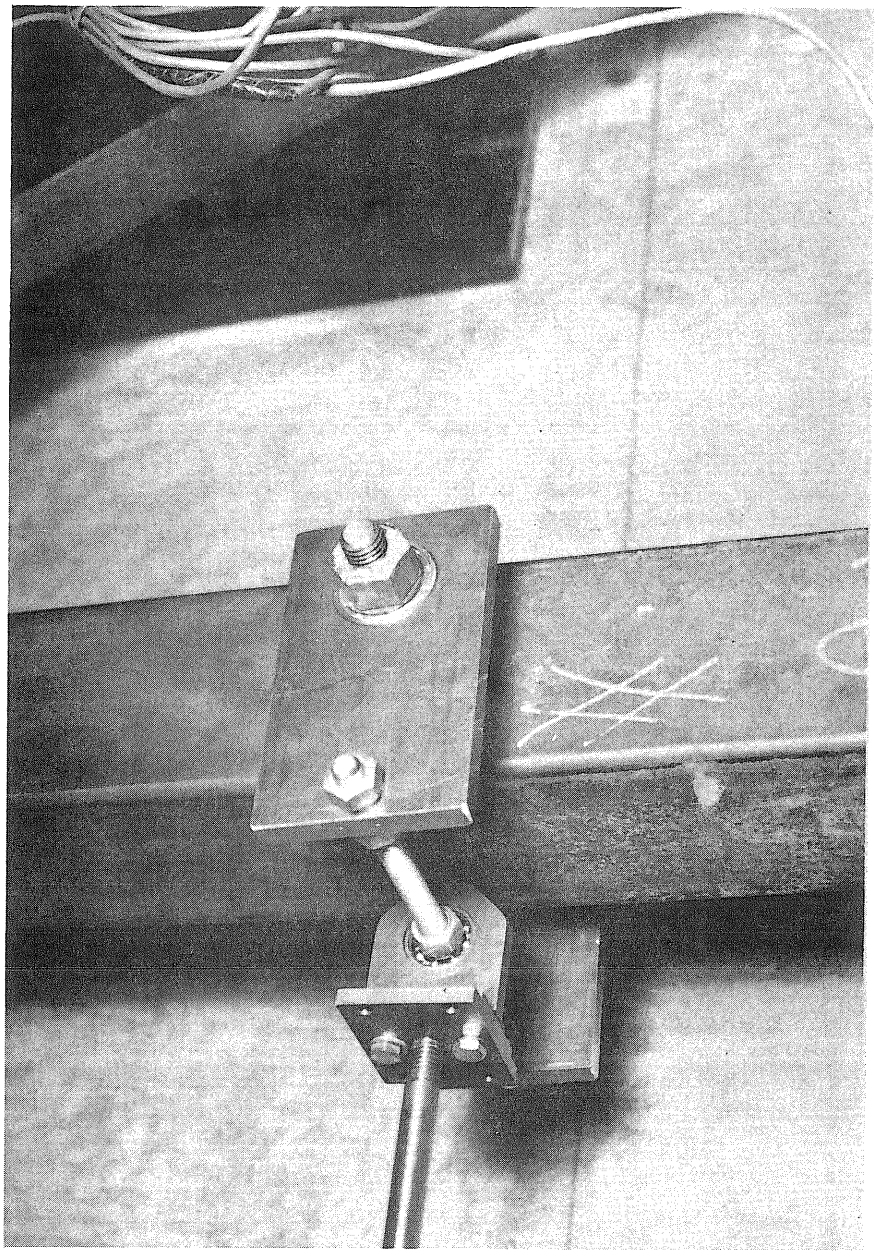

Fig. 2.12 Contd. Loading Frame-Ram Connection: Type B

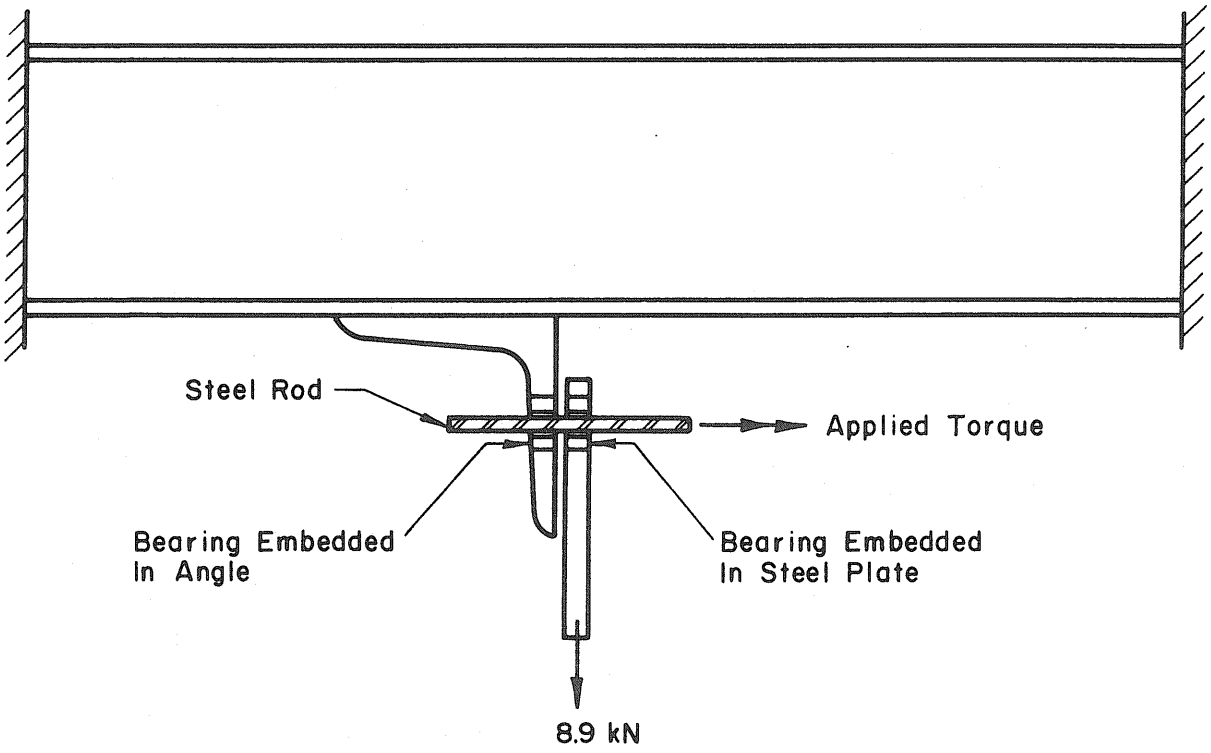


Fig. 2.13 Bearing Connection Test Setup

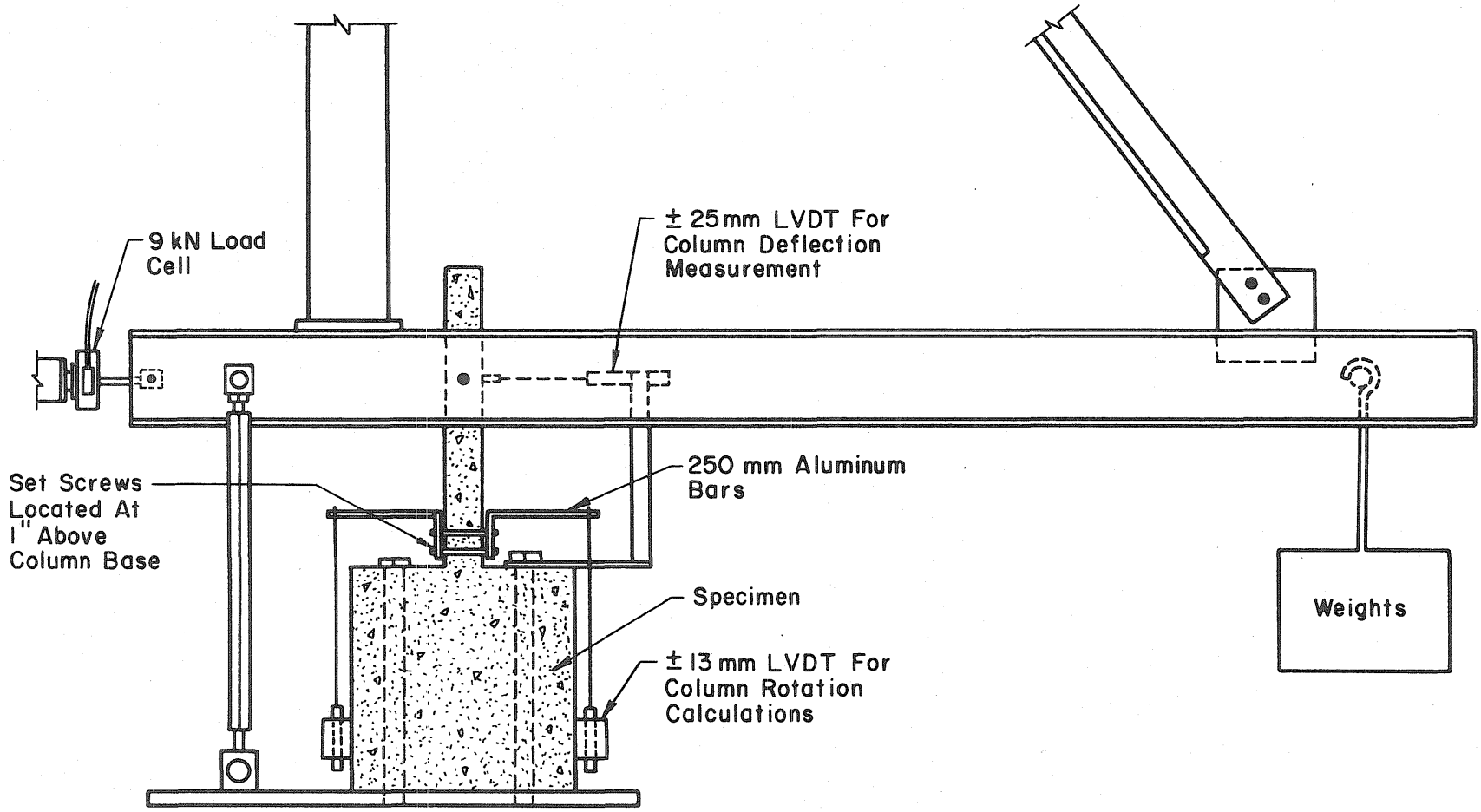


Fig. 2.14 Instrumentation

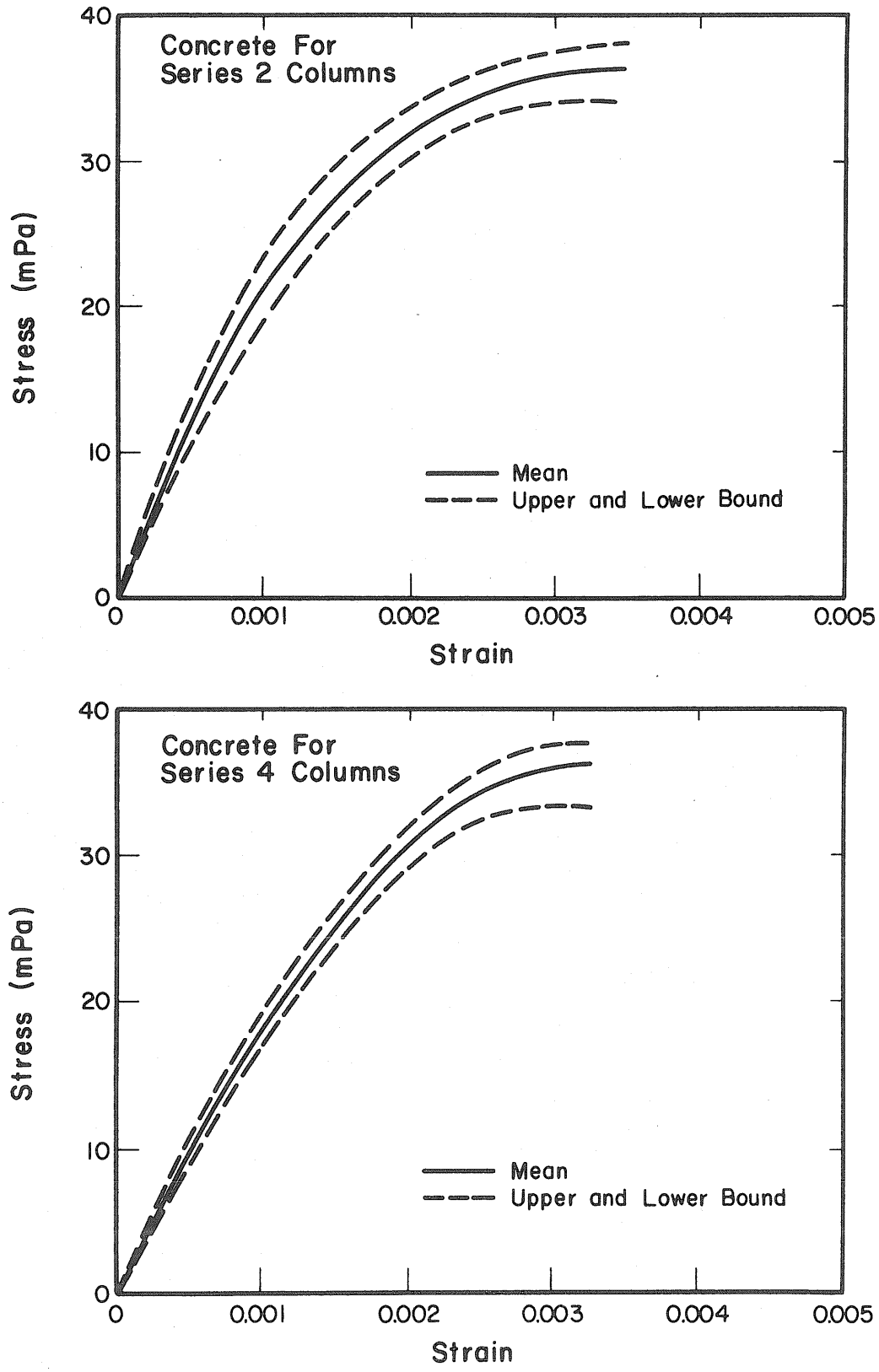


Fig. 2.15 Measured Concrete Stress-Strain Relationships

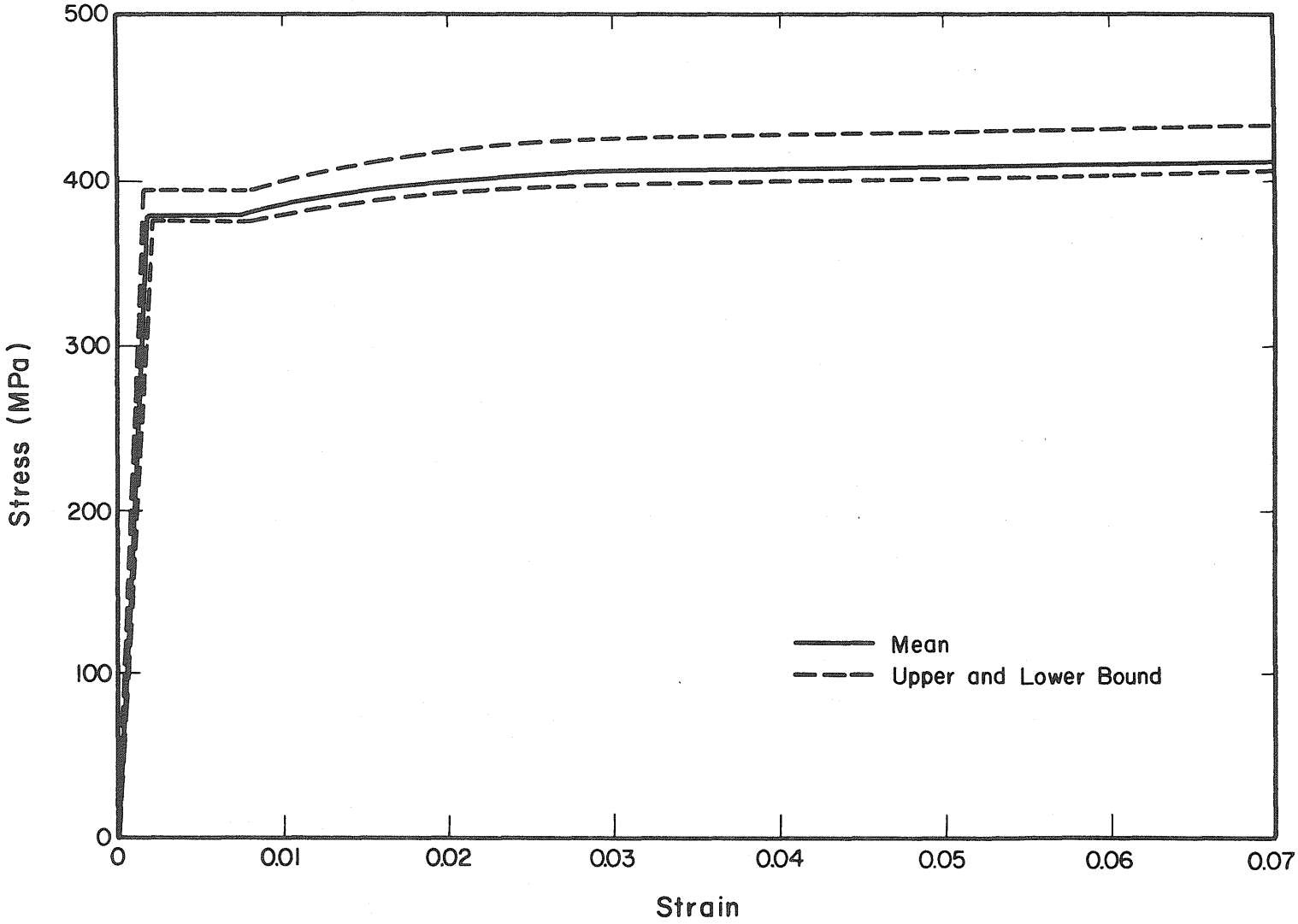


Fig. 2.16 Measured Steel Stress-Strain Relationship

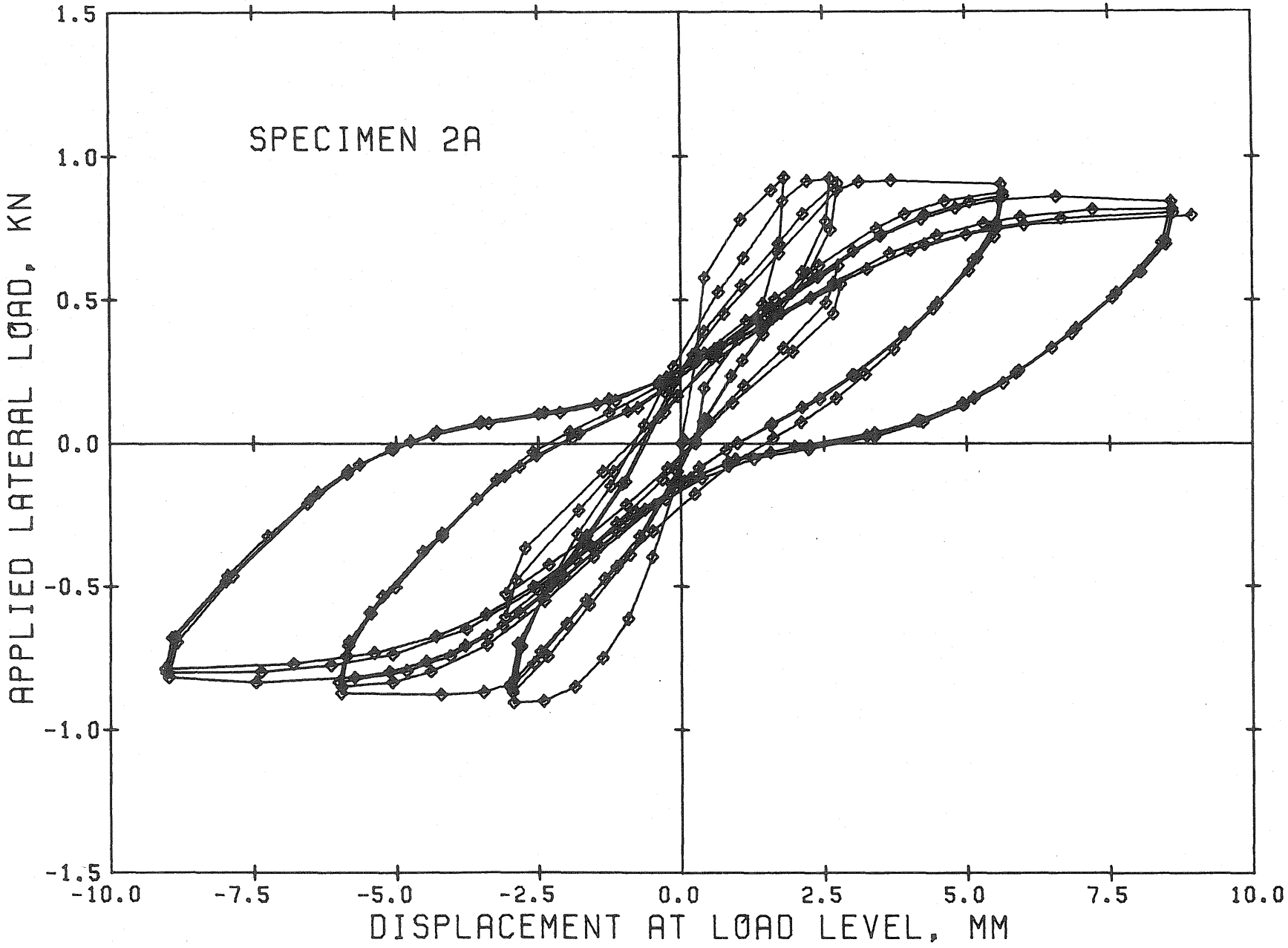


Fig. 3.1 Measured Hysteresis Relationships for Specimen 2A

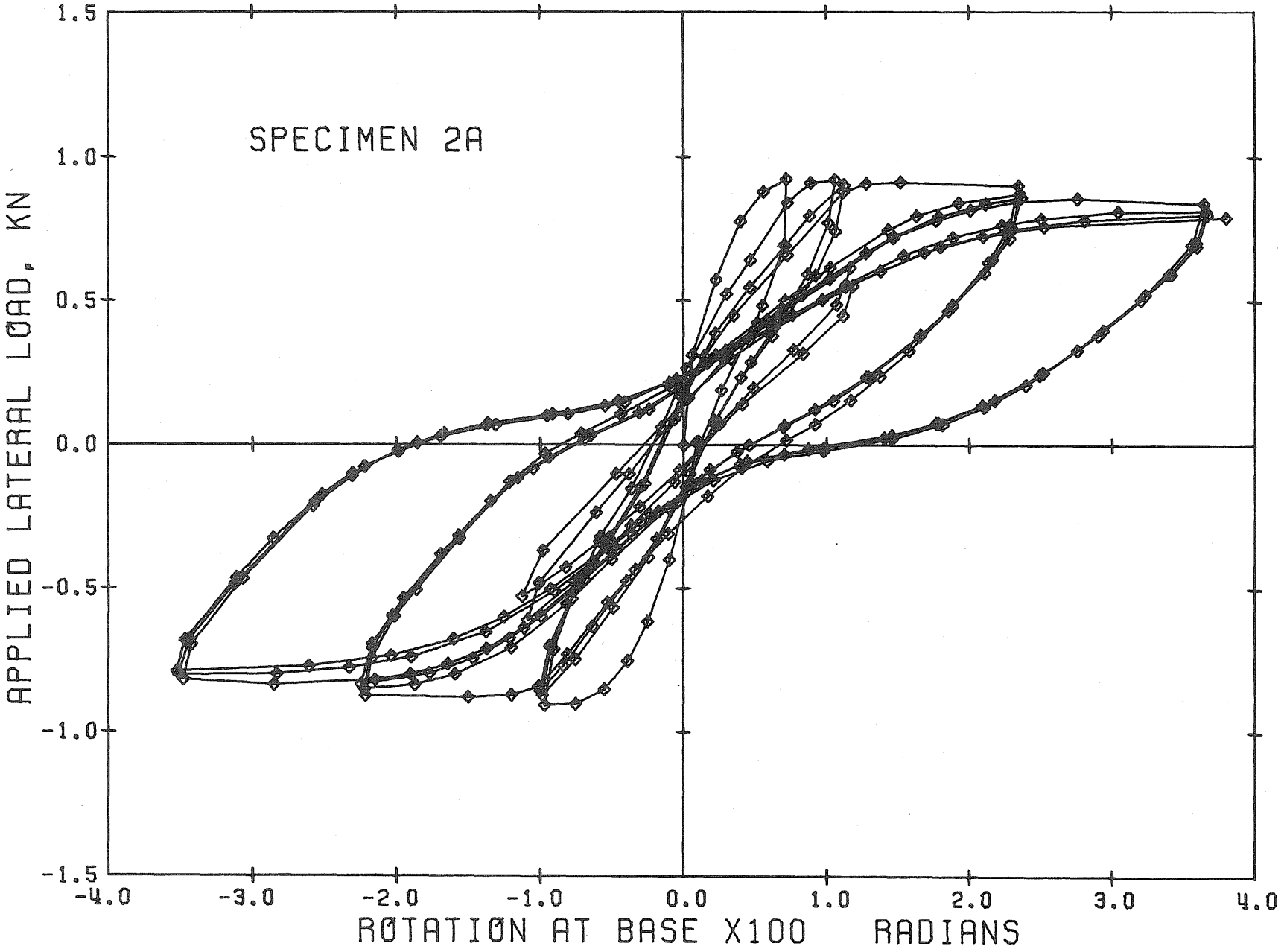


Fig. 3.1 Contd. Measured Hysteresis Relationships for Specimen 2A

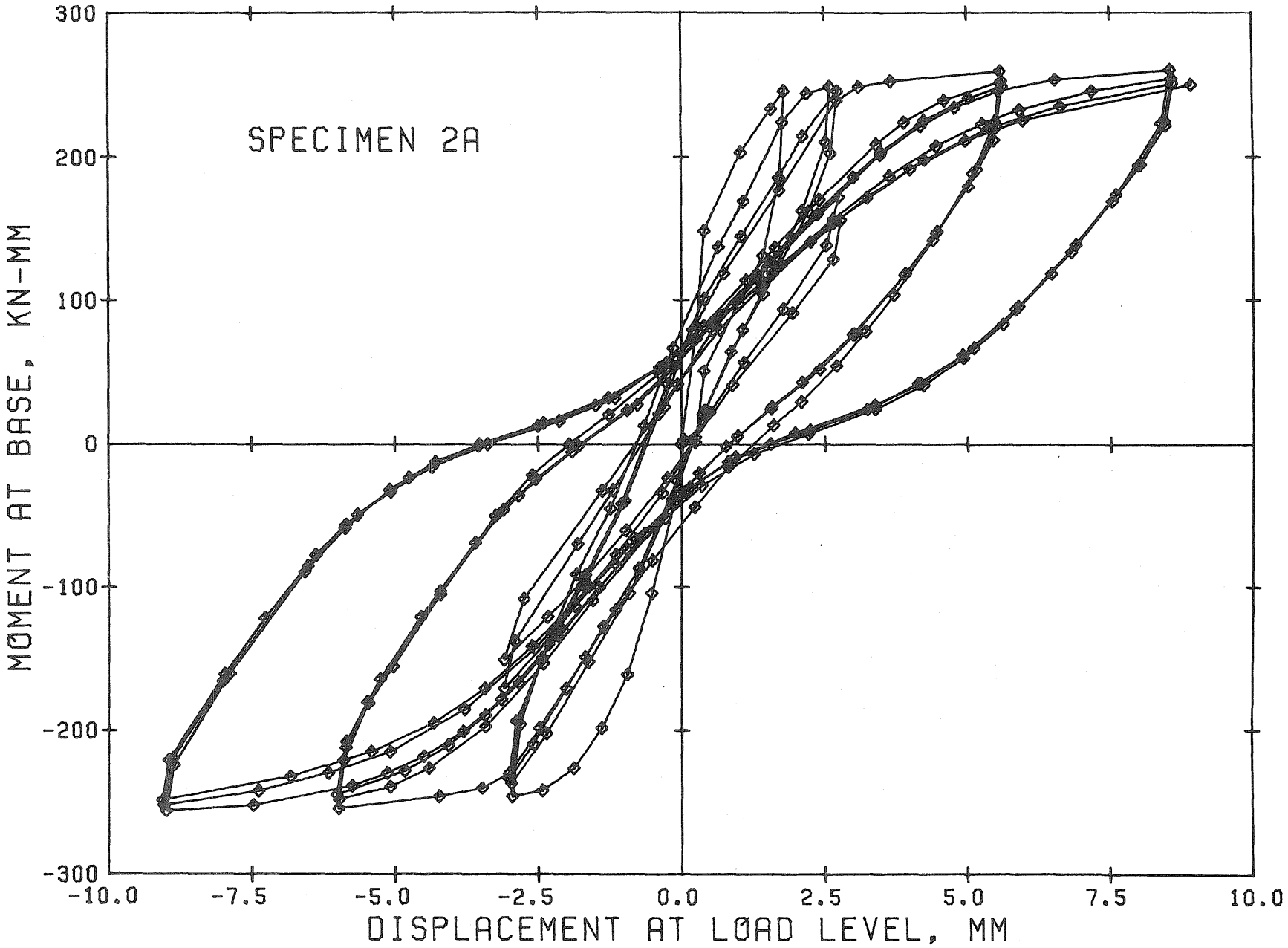


Fig. 3.1 Contd. Measured Hysteresis Relationships for Specimen 2A

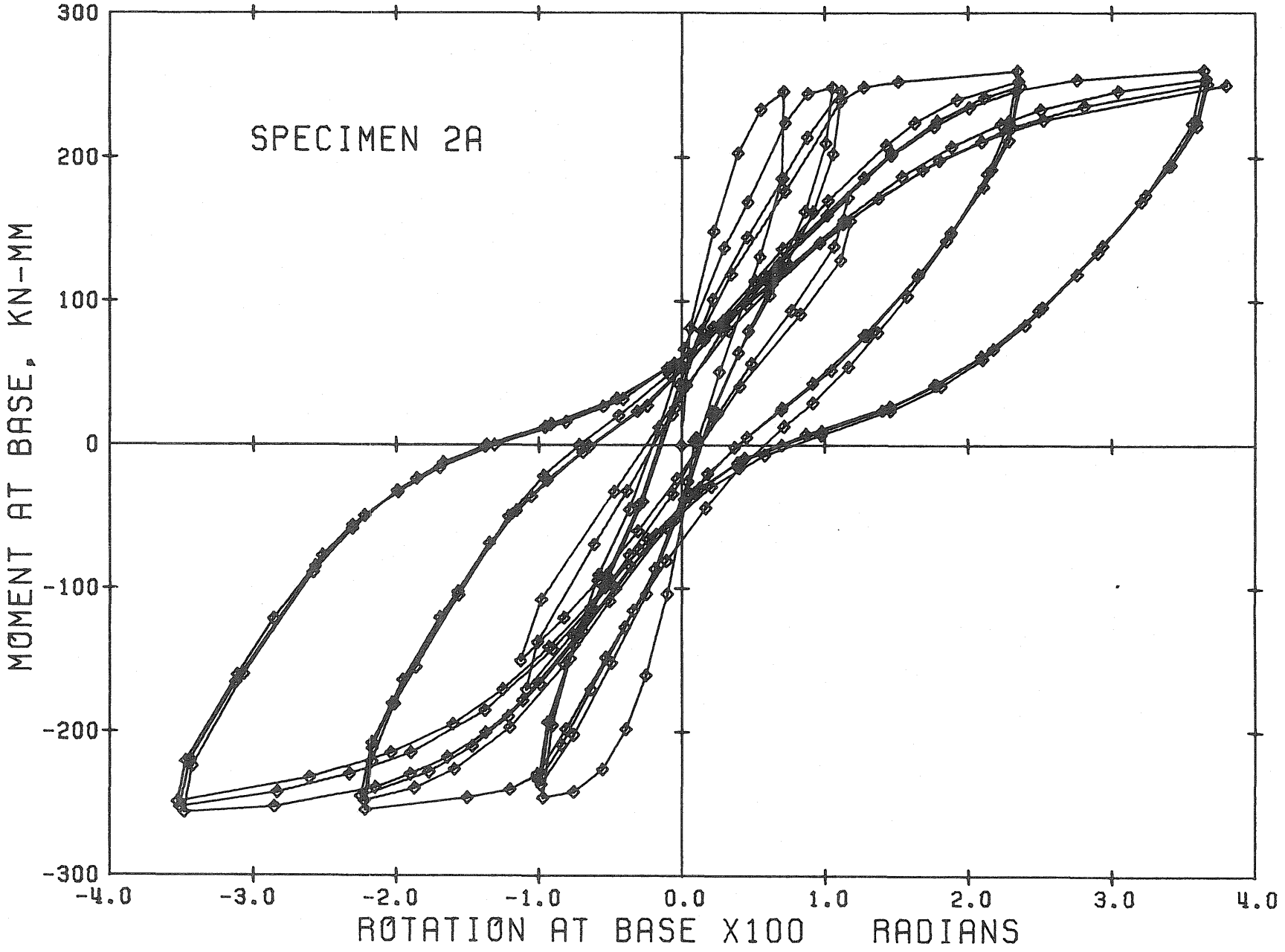


Fig. 3.1 Contd. Measured Hysteresis Relationships for Specimen 2A

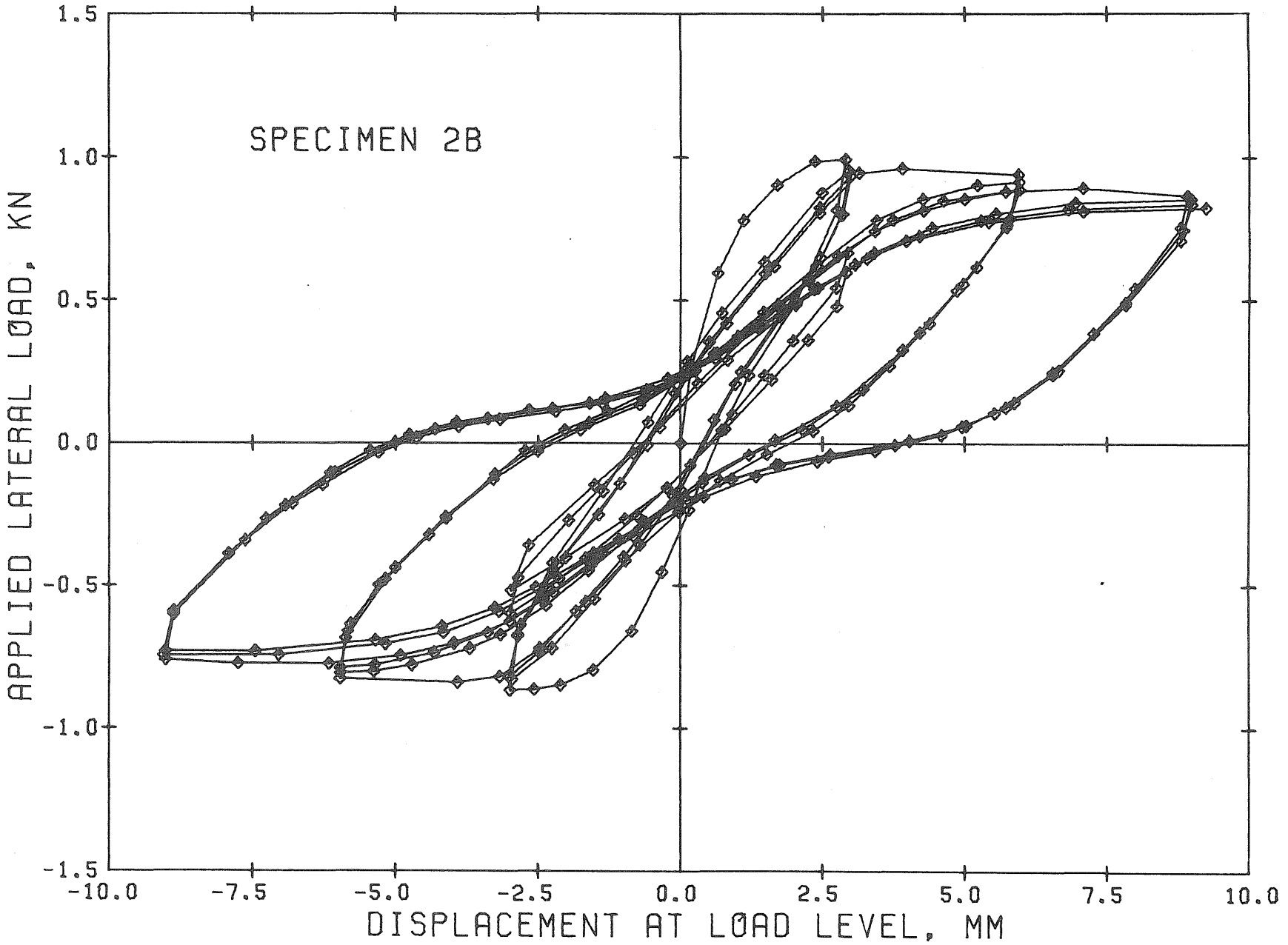


Fig. 3.2 Measured Hysteresis Relationships for Specimen 2B

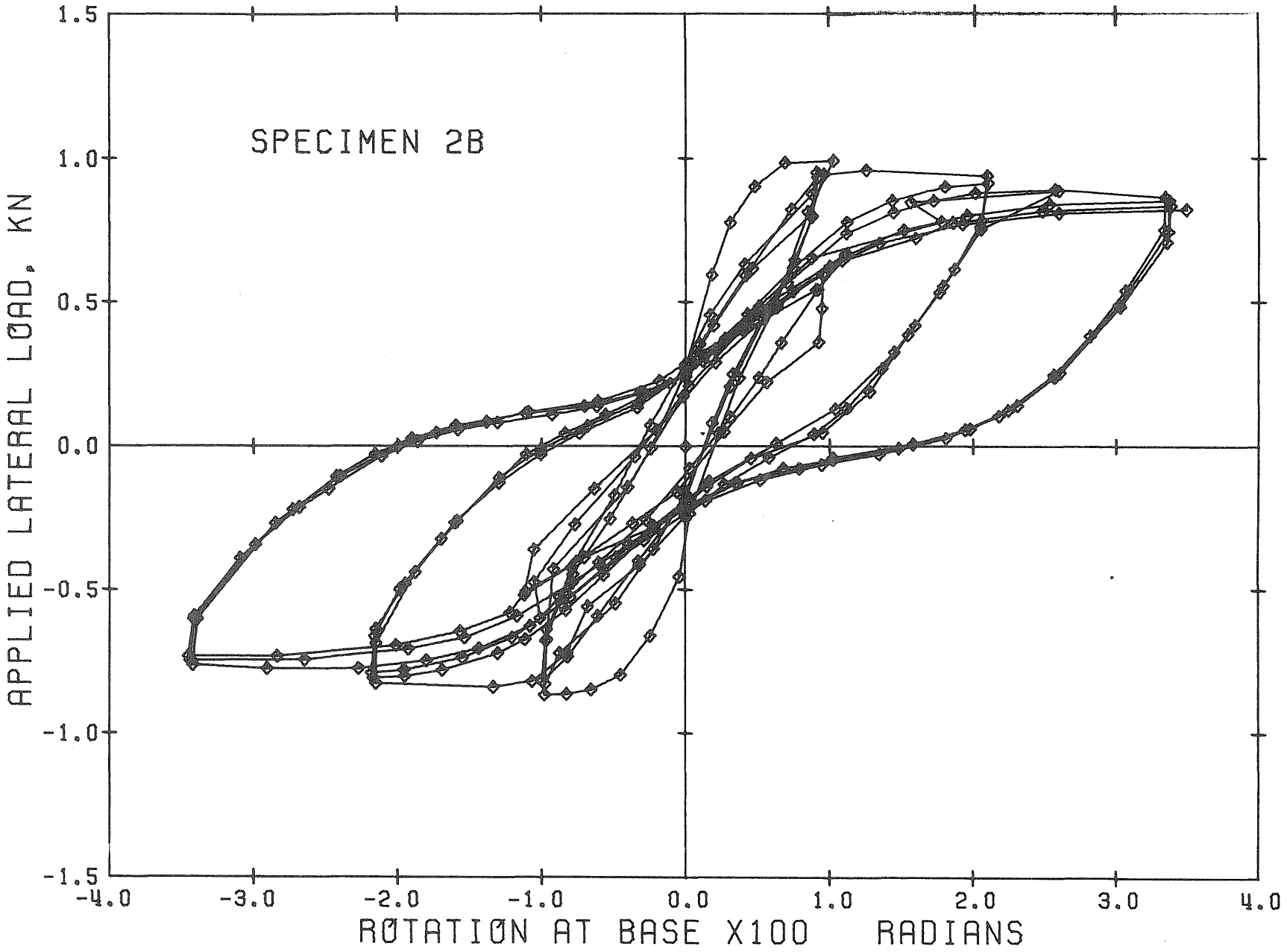


Fig. 3.2 Contd. Measured Hysteresis Relationships for Specimen 2B

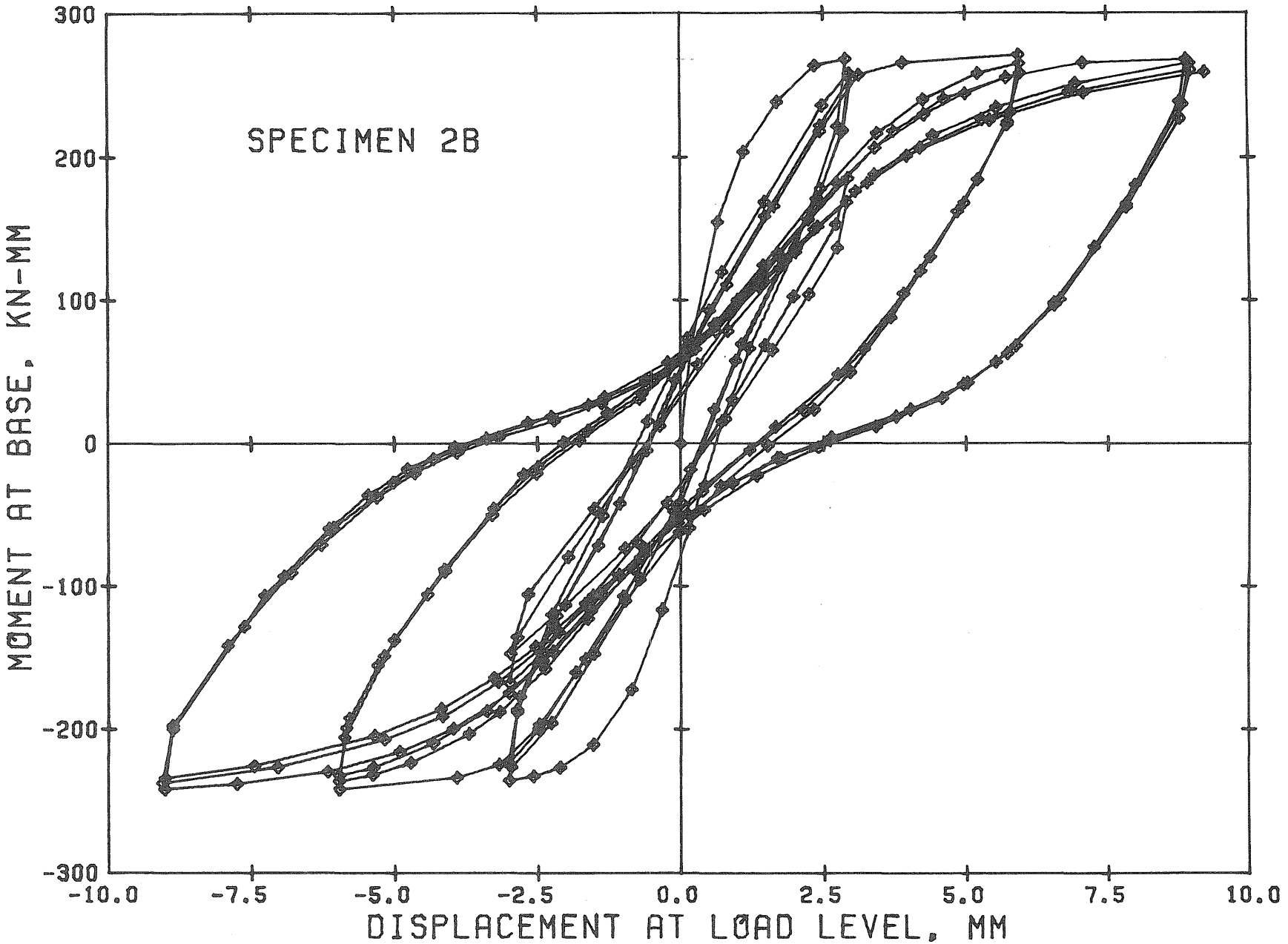


Fig. 3.2 Contd. Measured Hysteresis Relationships for Specimen 2B

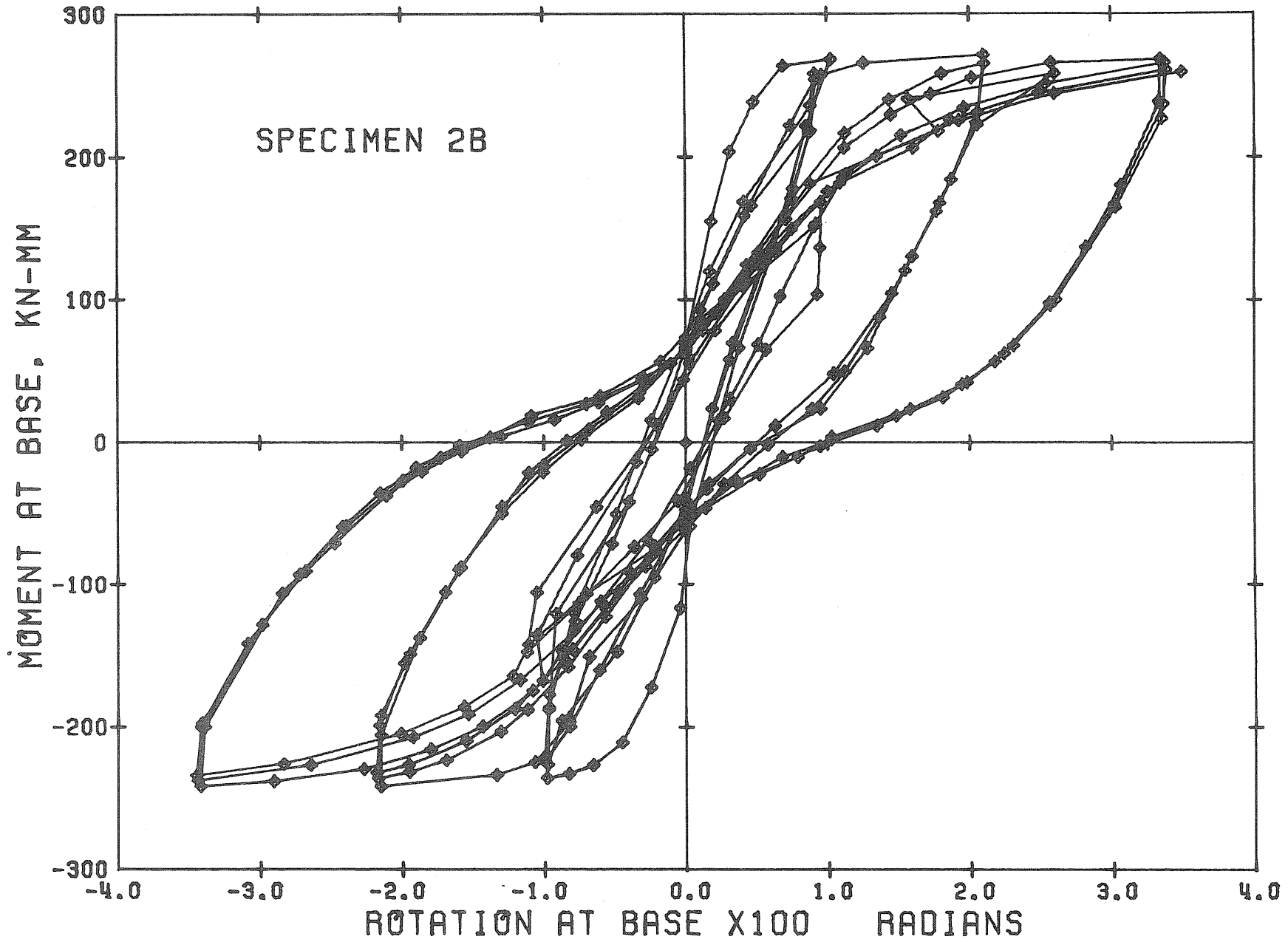


Fig. 3.2 Contd. Measured Hysteresis Relationships for Specimen 2B

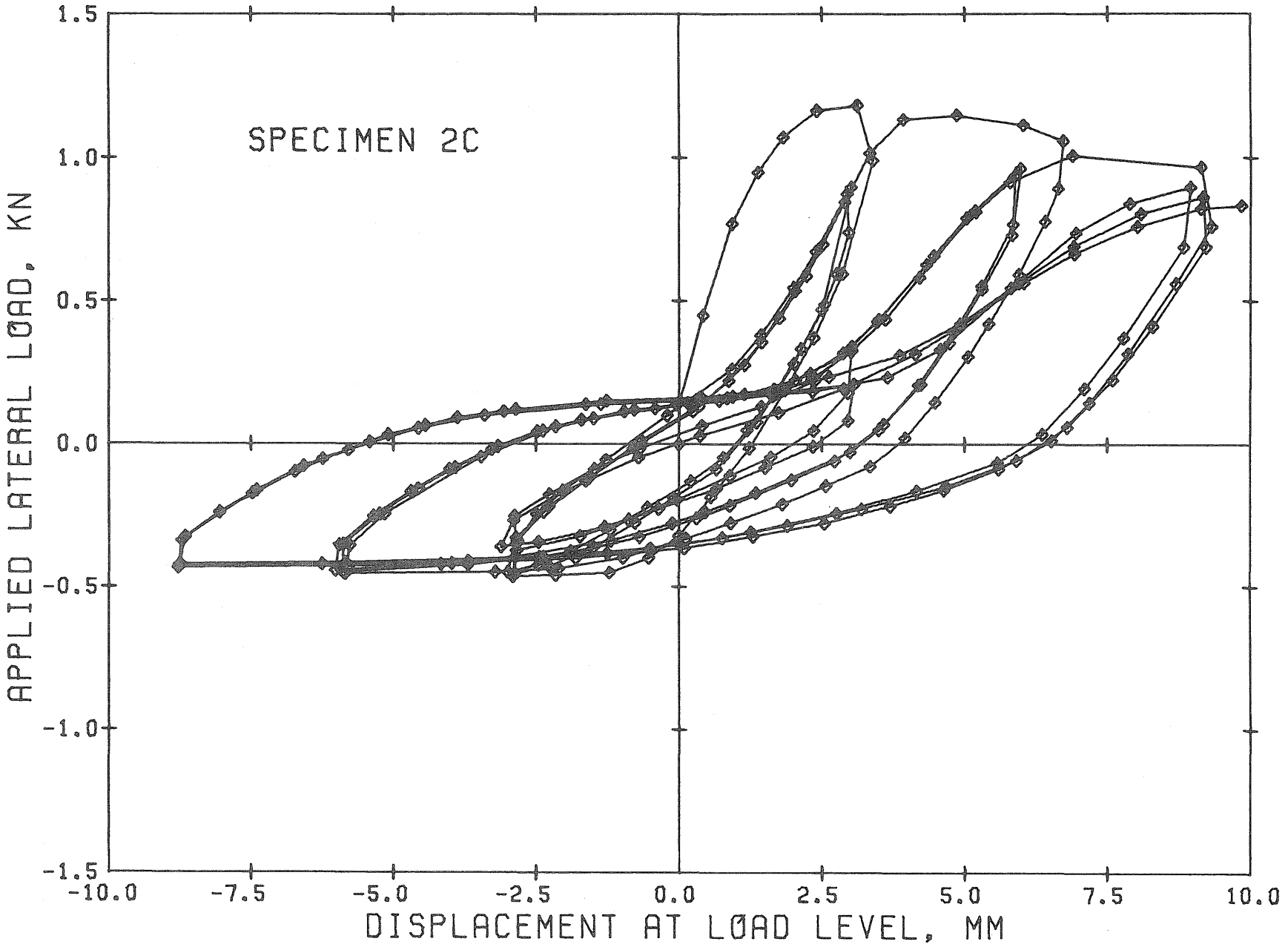


Fig. 3.3 Measured Hysteresis Relationships for Specimen 2C

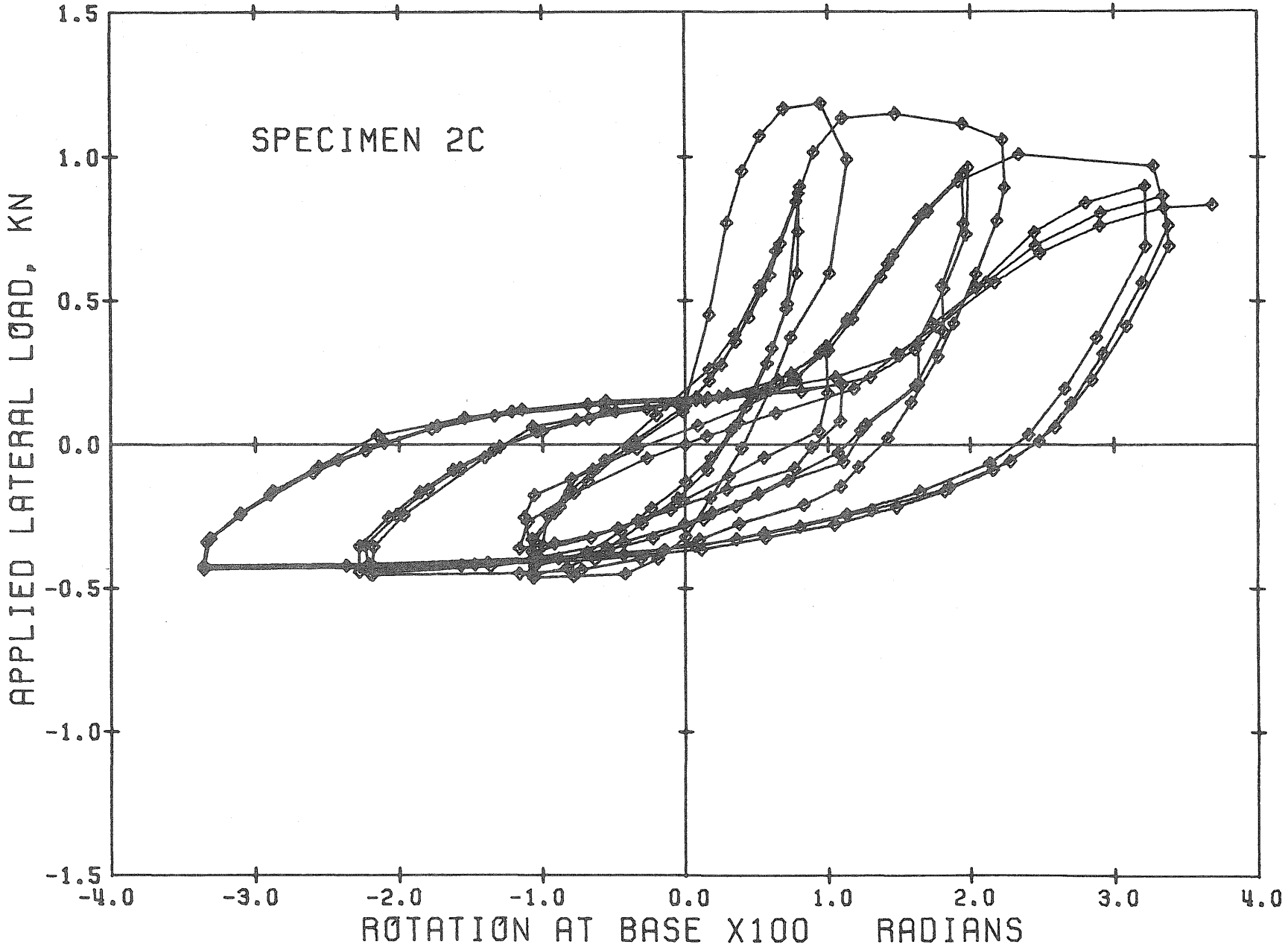


Fig. 3.3 Contd. Measured Hysteresis Relationships for Specimen 2C

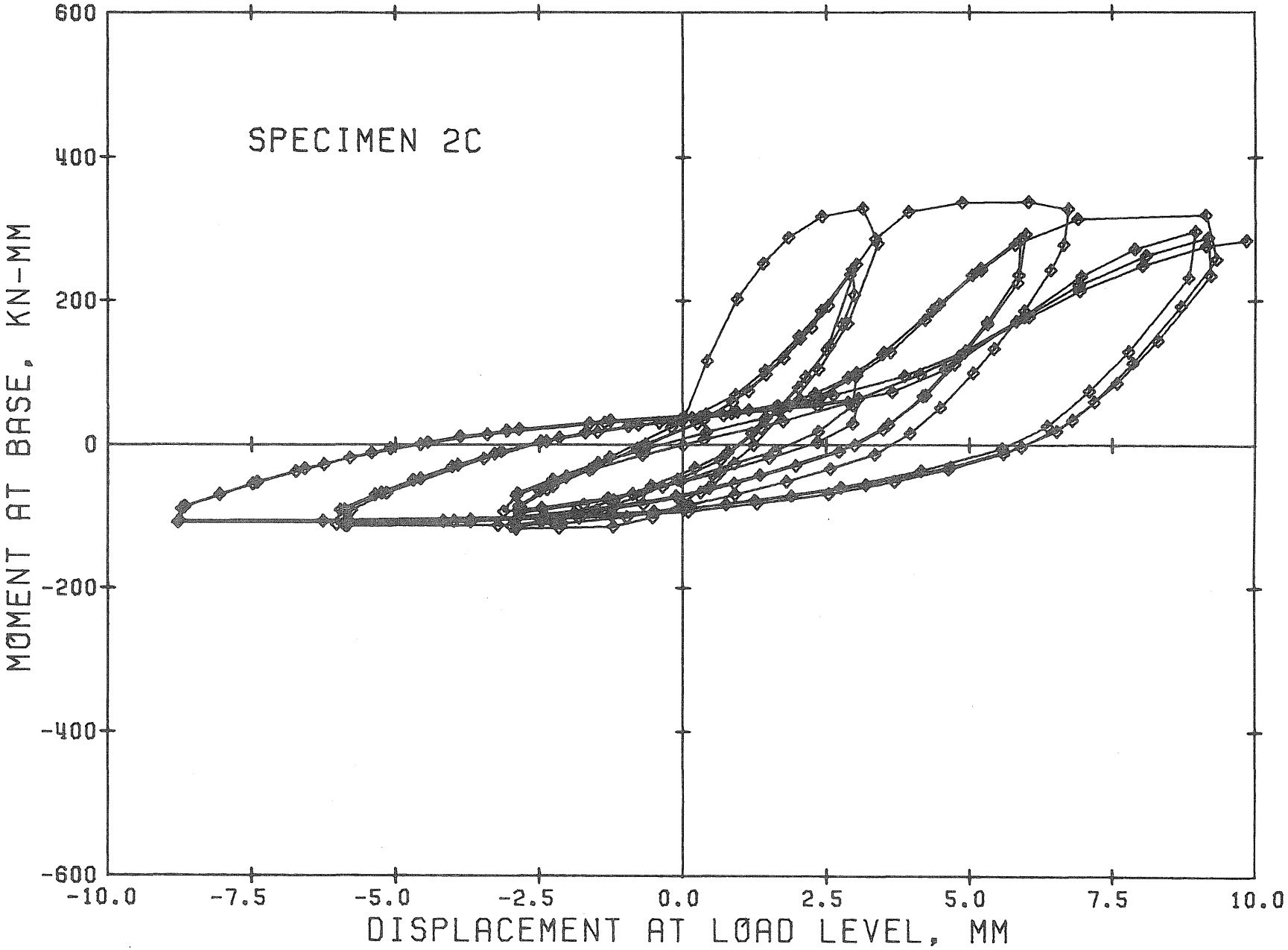


Fig. 3.3 Contd. Measured Hysteresis Relationships for Specimen 2C

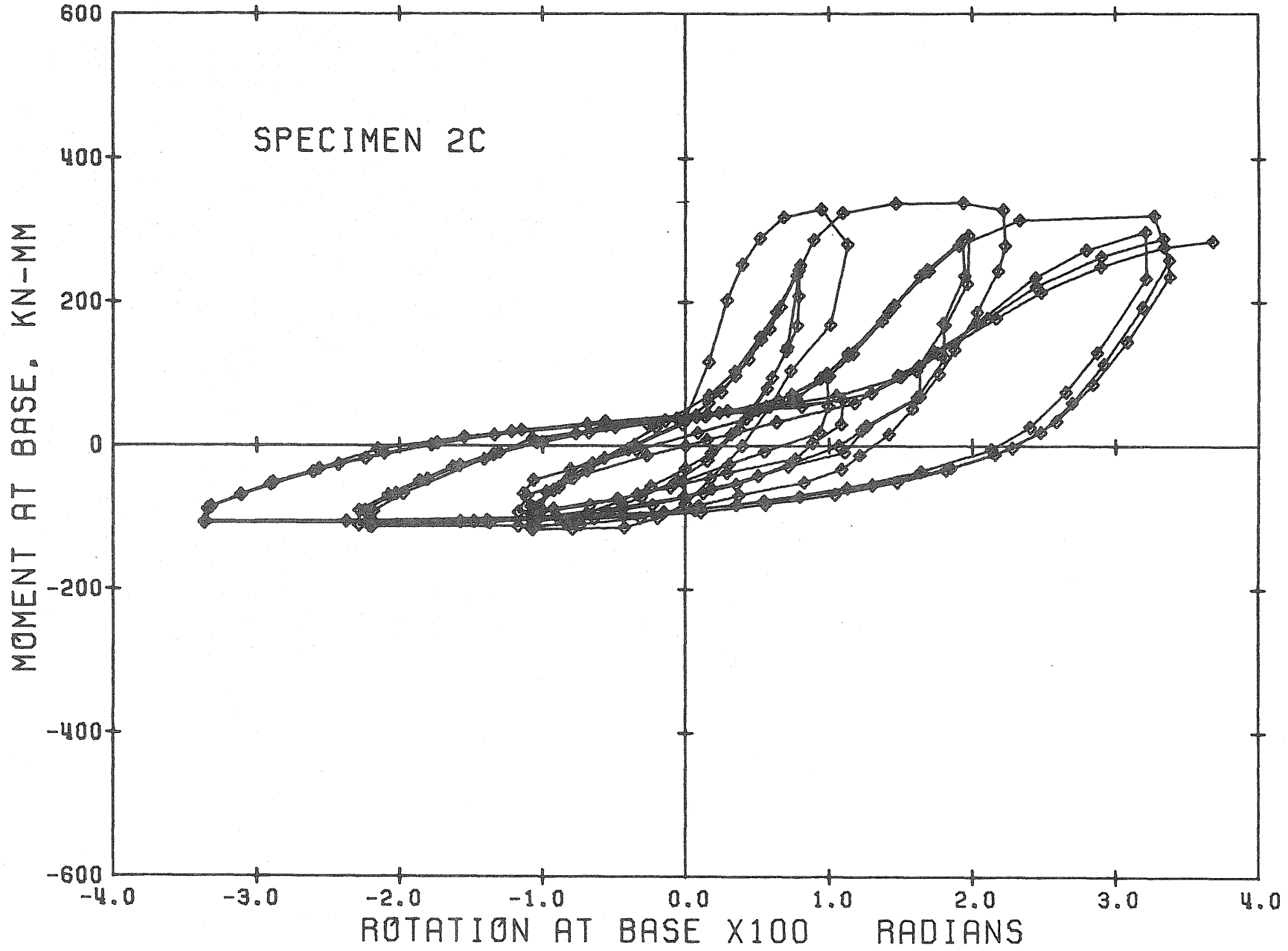


Fig. 3.3 Contd. Measured Hysteresis Relationships for Specimen 2C

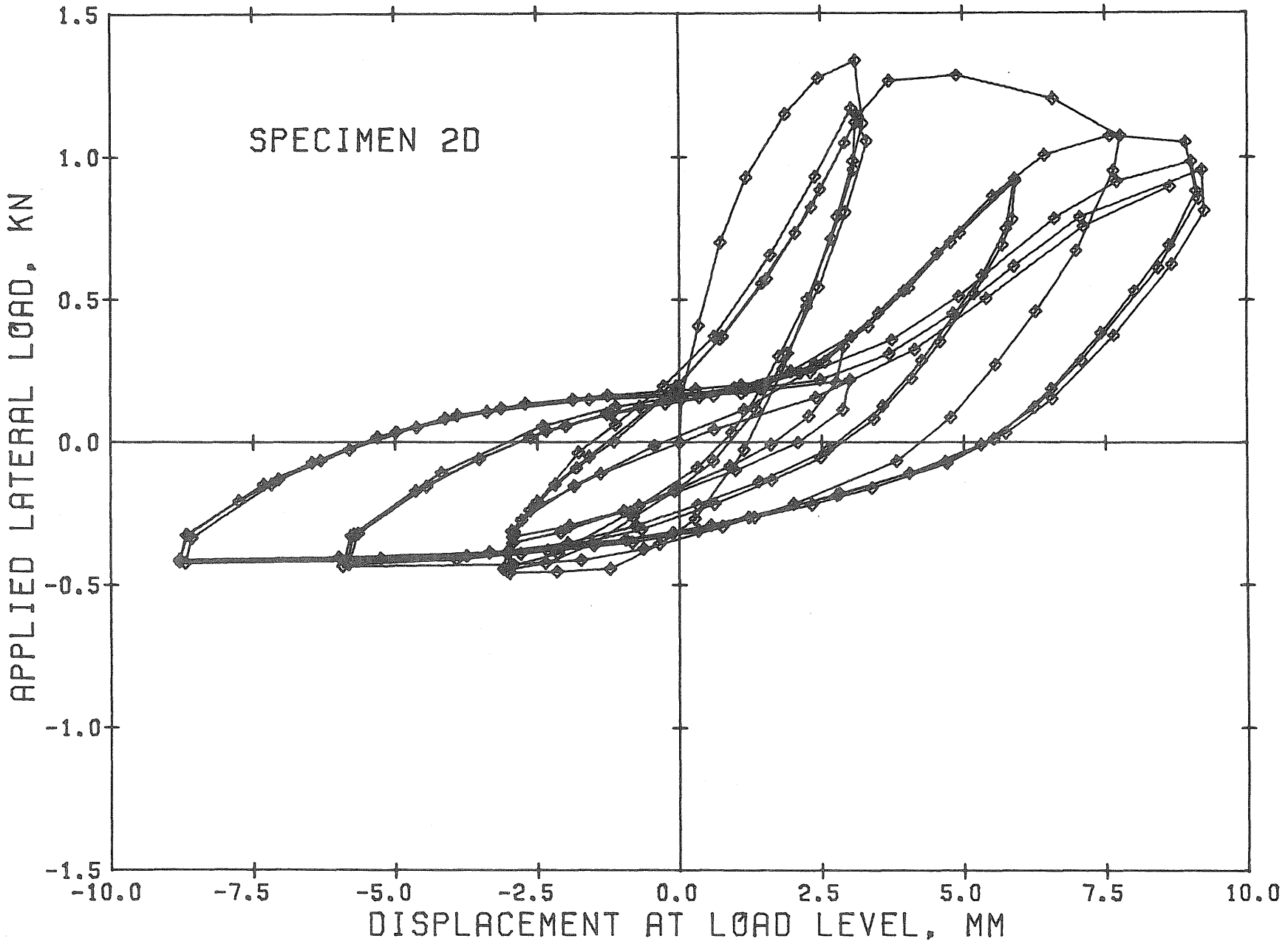


Fig. 3.4 Measured Hysteresis Relationships for Specimen 2D

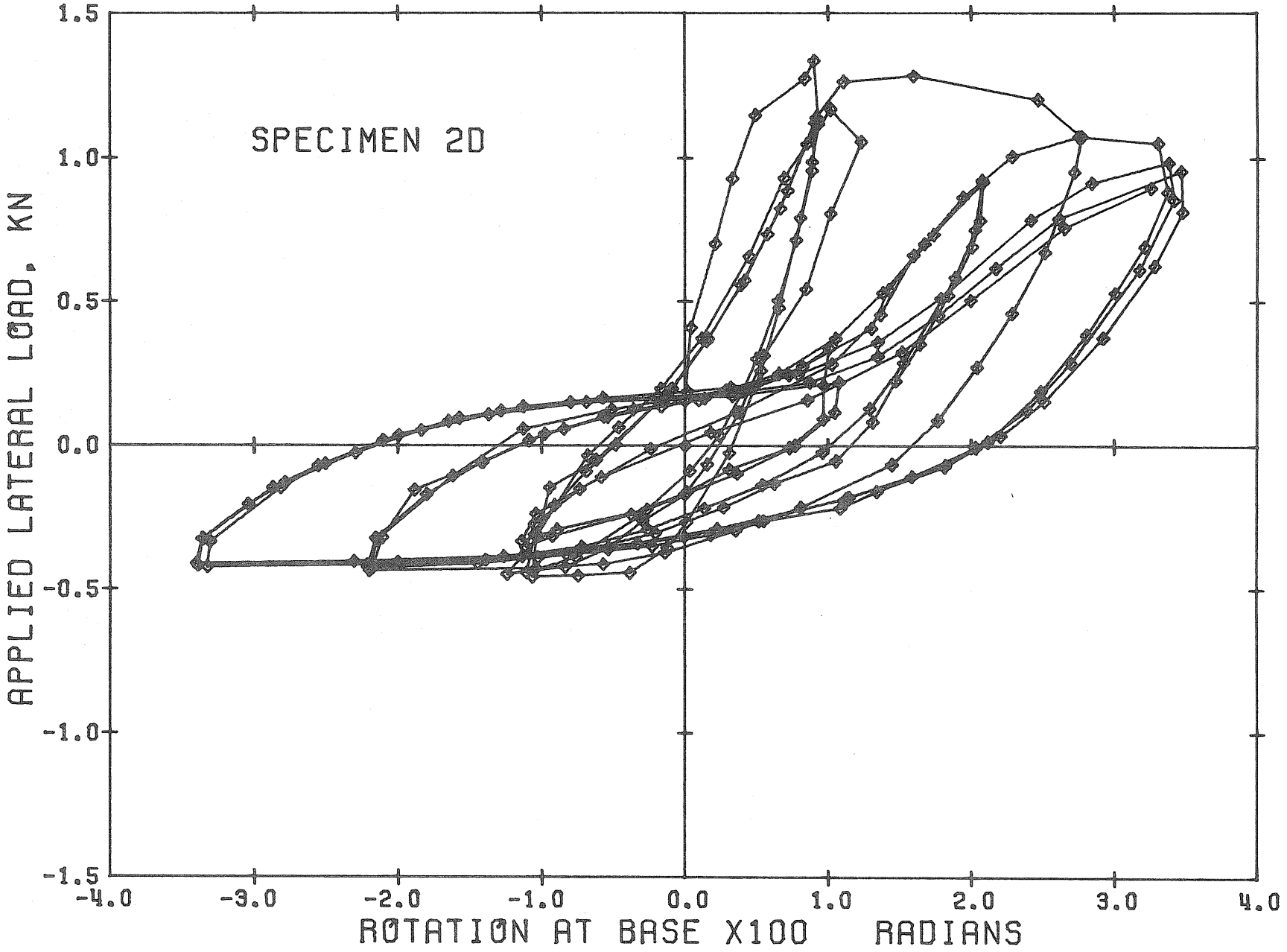


Fig. 3.4 Contd. Measured Hysteresis Relationships for Specimen 2D

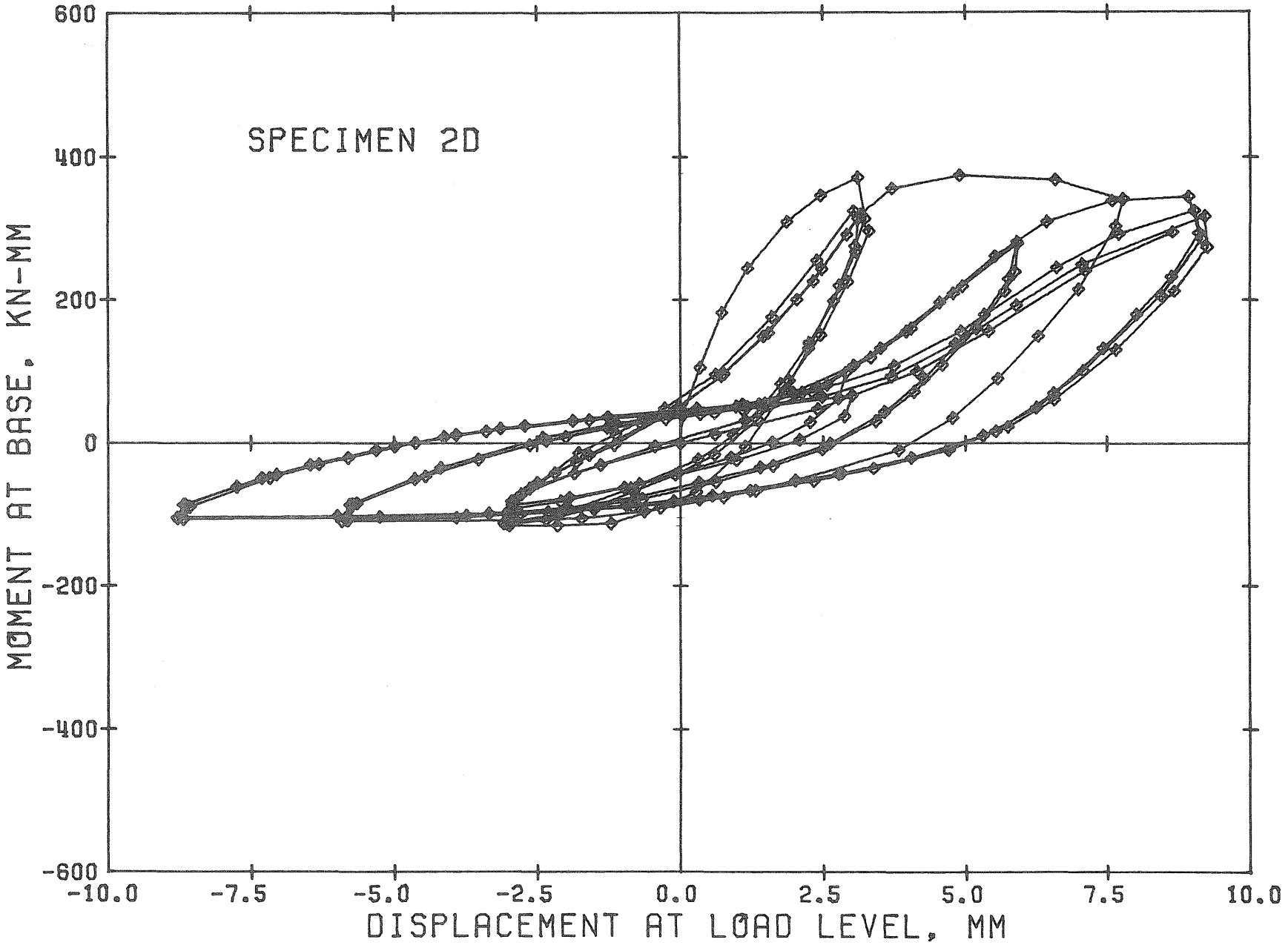


Fig. 3.4 Contd. Measured Hysteresis Relationships for Specimen 2D

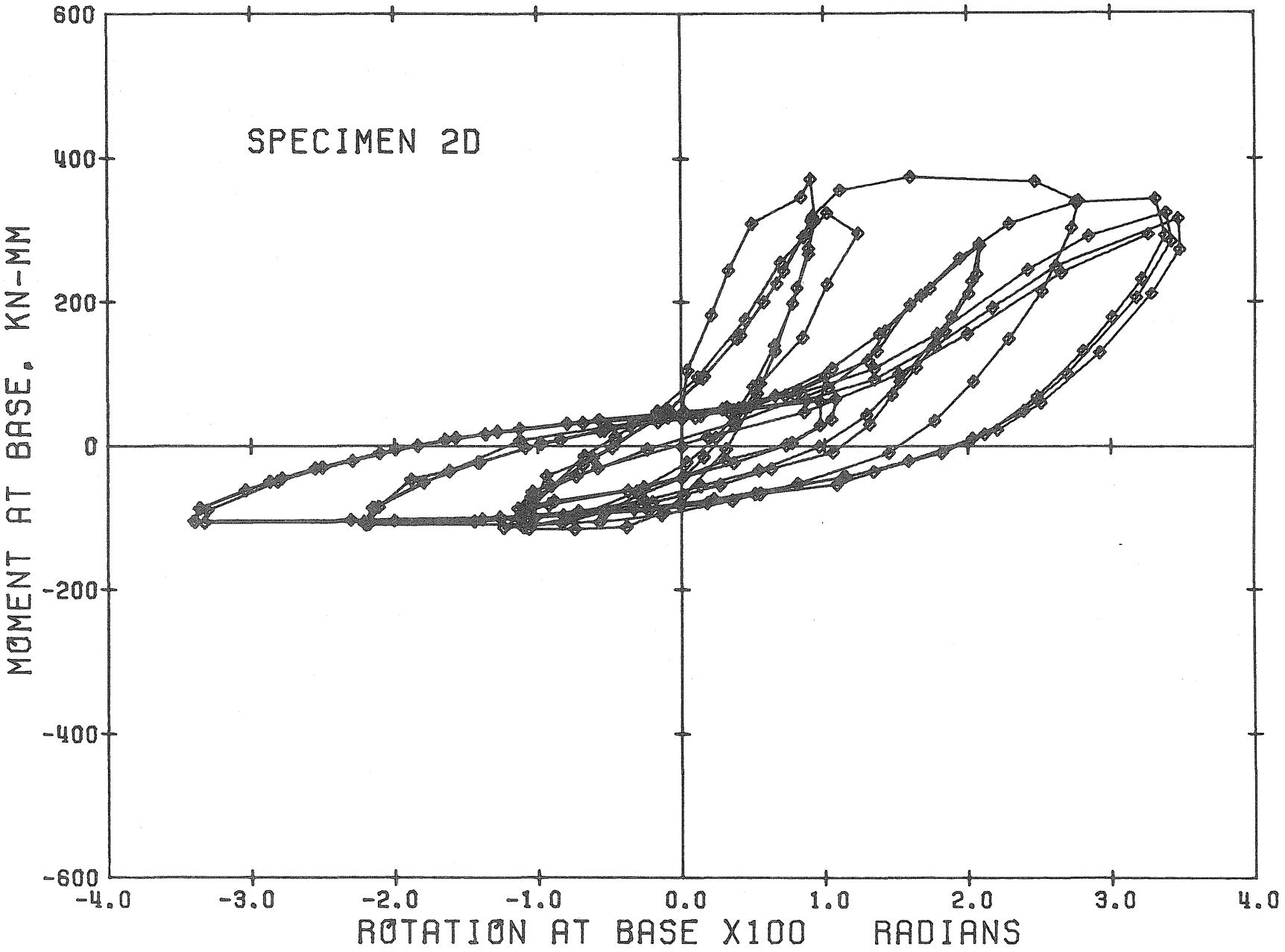


Fig. 3.4 Contd. Measured Hysteresis Relationships for Specimen 2D

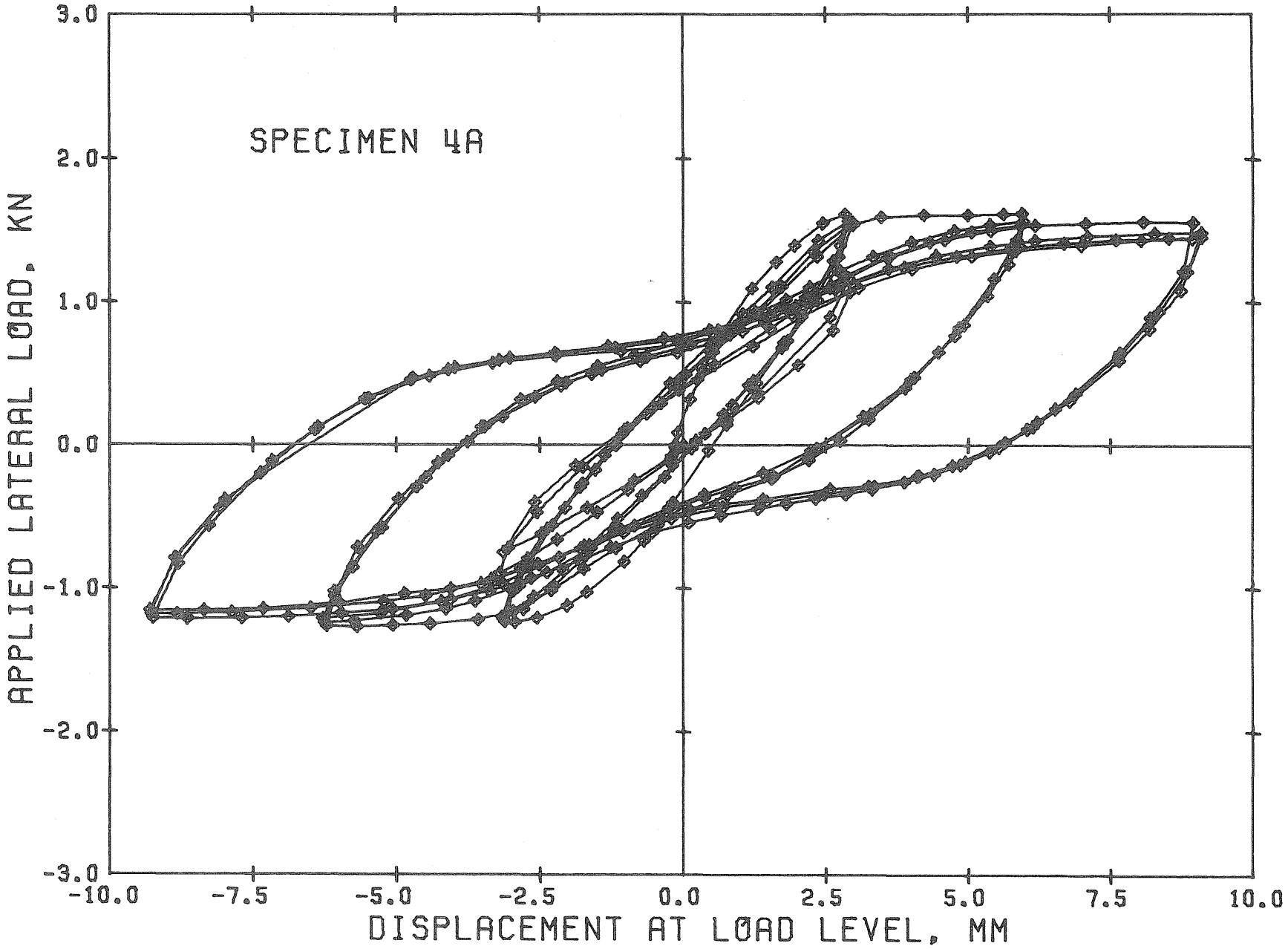


Fig. 3.5 Measured Hysteresis Relationships for Specimen 4A

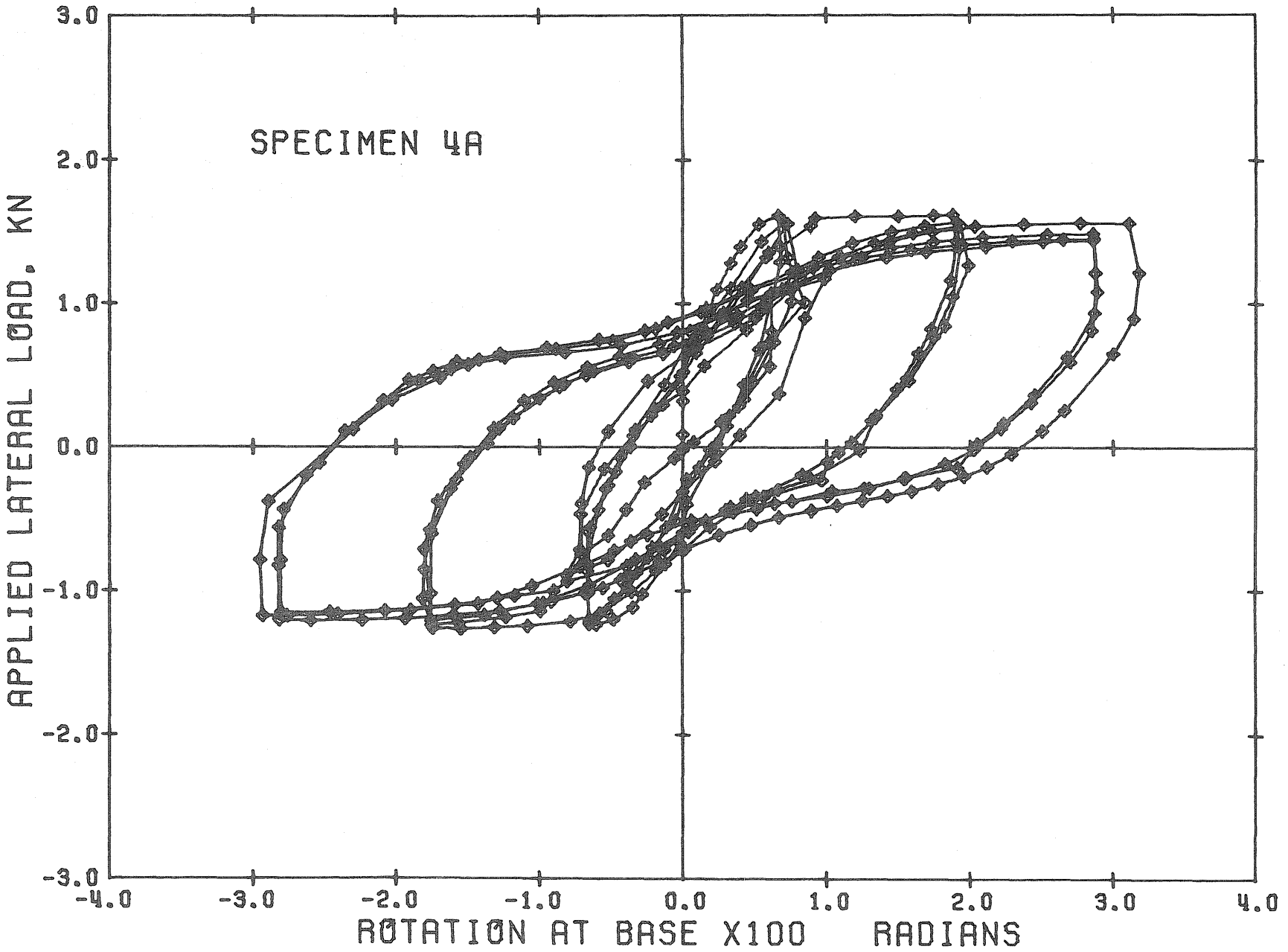


Fig. 3.5 Contd. Measured Hysteresis Relationships for Specimen 4A

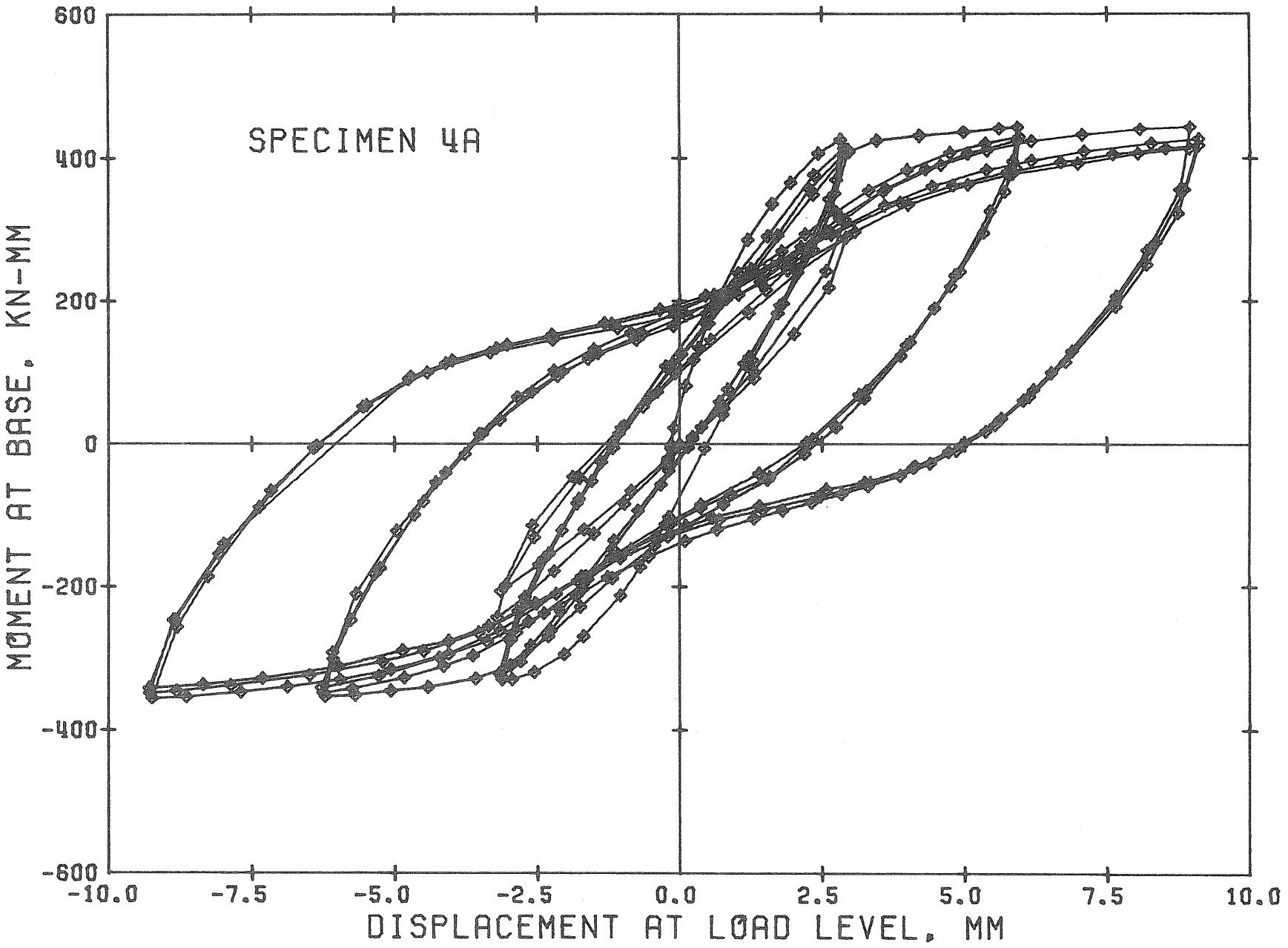


Fig. 3.5 Contd. Measured Hysteresis Relationships for Specimen 4A

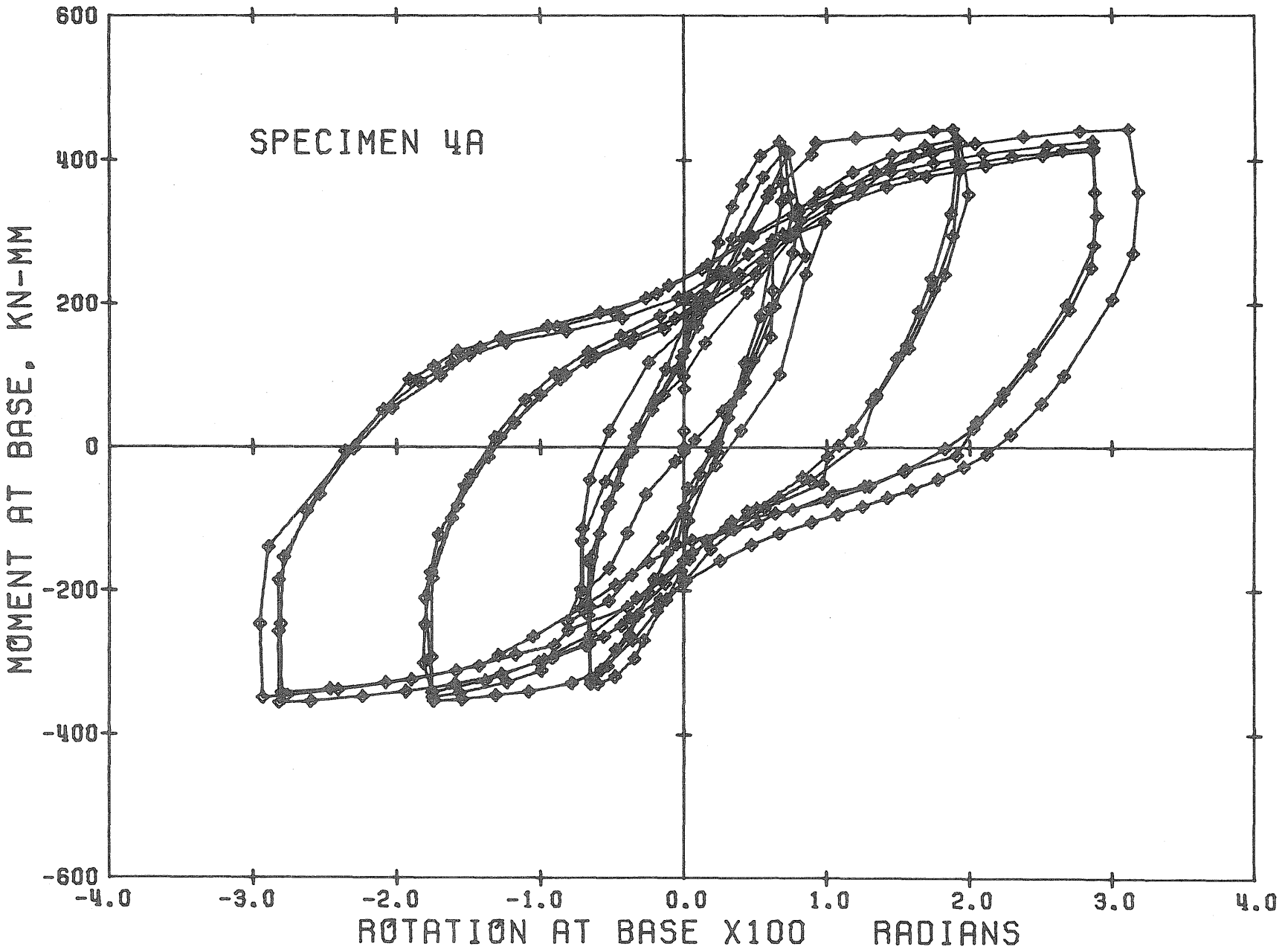


Fig. 3.5 Contd. Measured Hysteresis Relationships for Specimen 4A

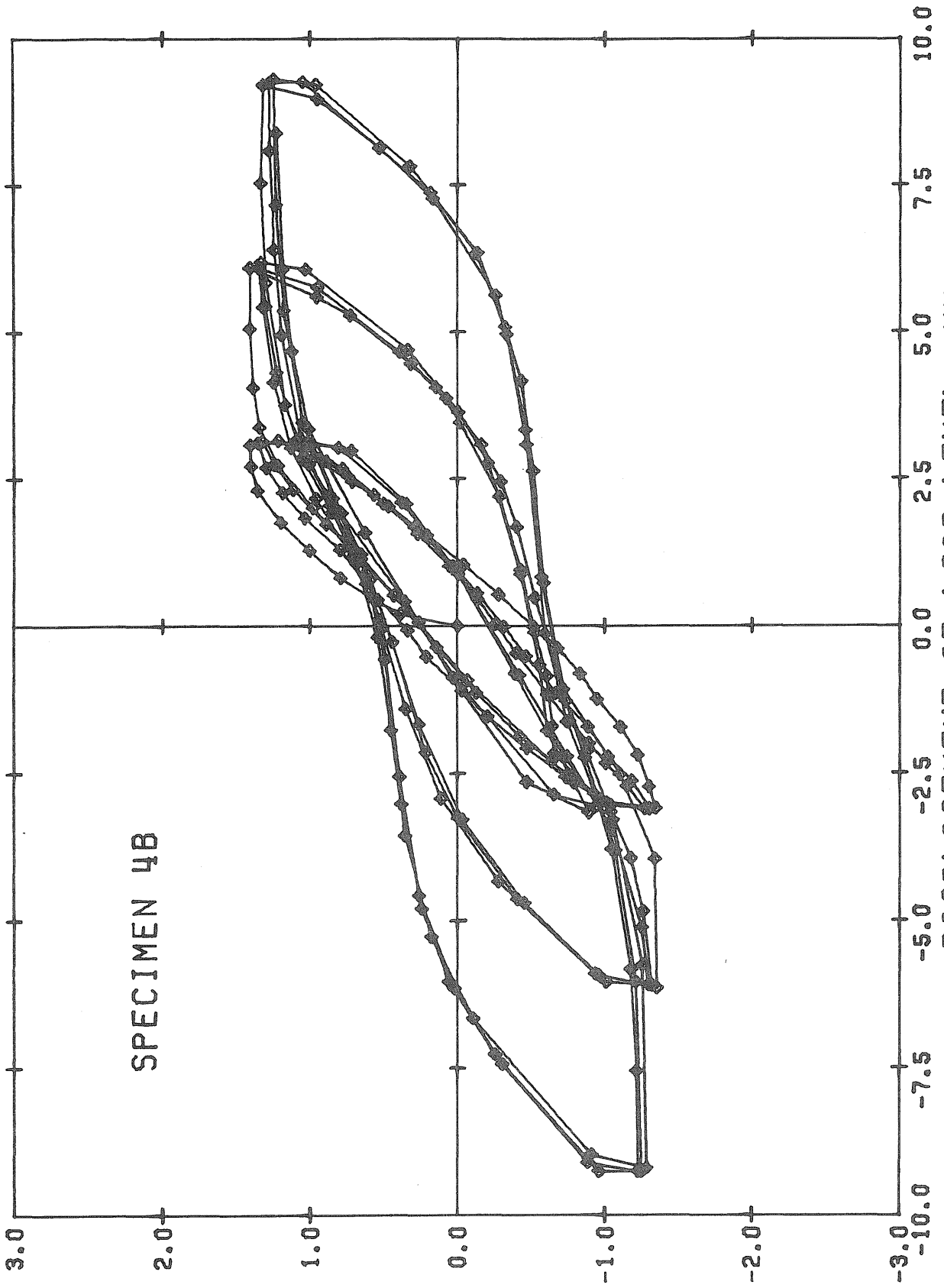


Fig. 3.6 Measured Hysteresis Relationships for Specimen 4B

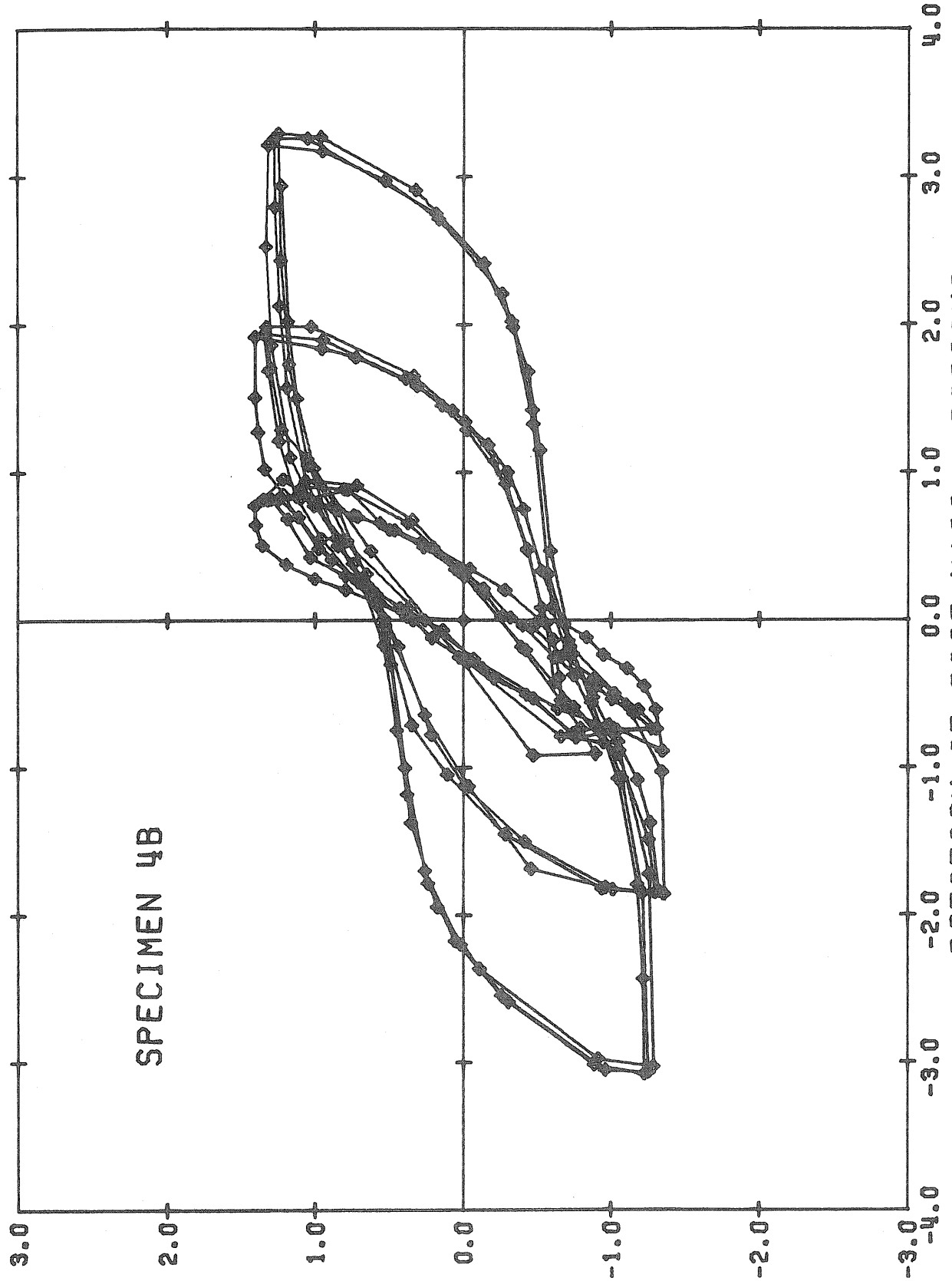


Fig. 3.6 Contd. Measured Hysteresis Relationships for Specimen 4B

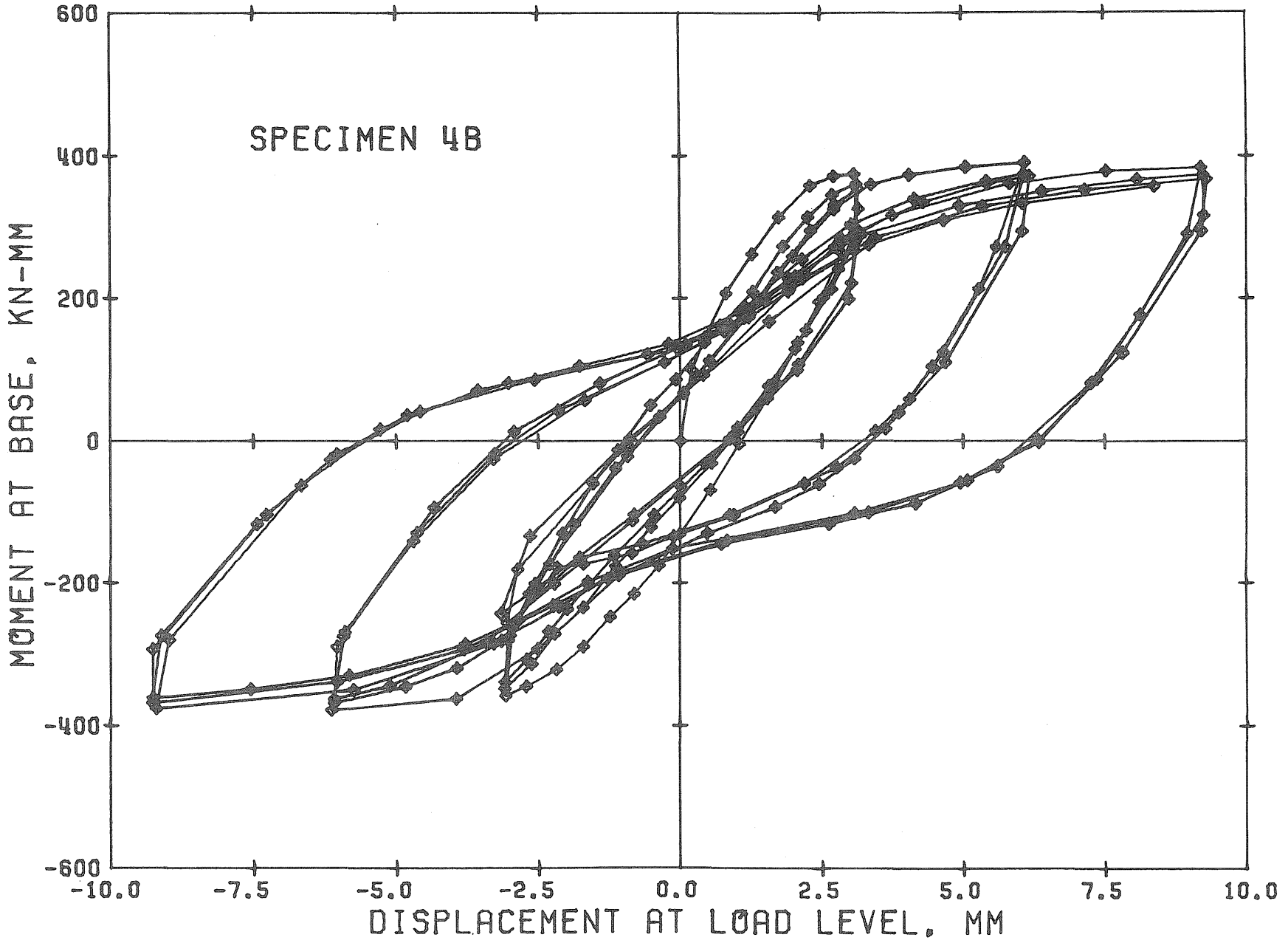


Fig. 3.6 Contd. Measured Hysteresis Relationships for Specimen 4B

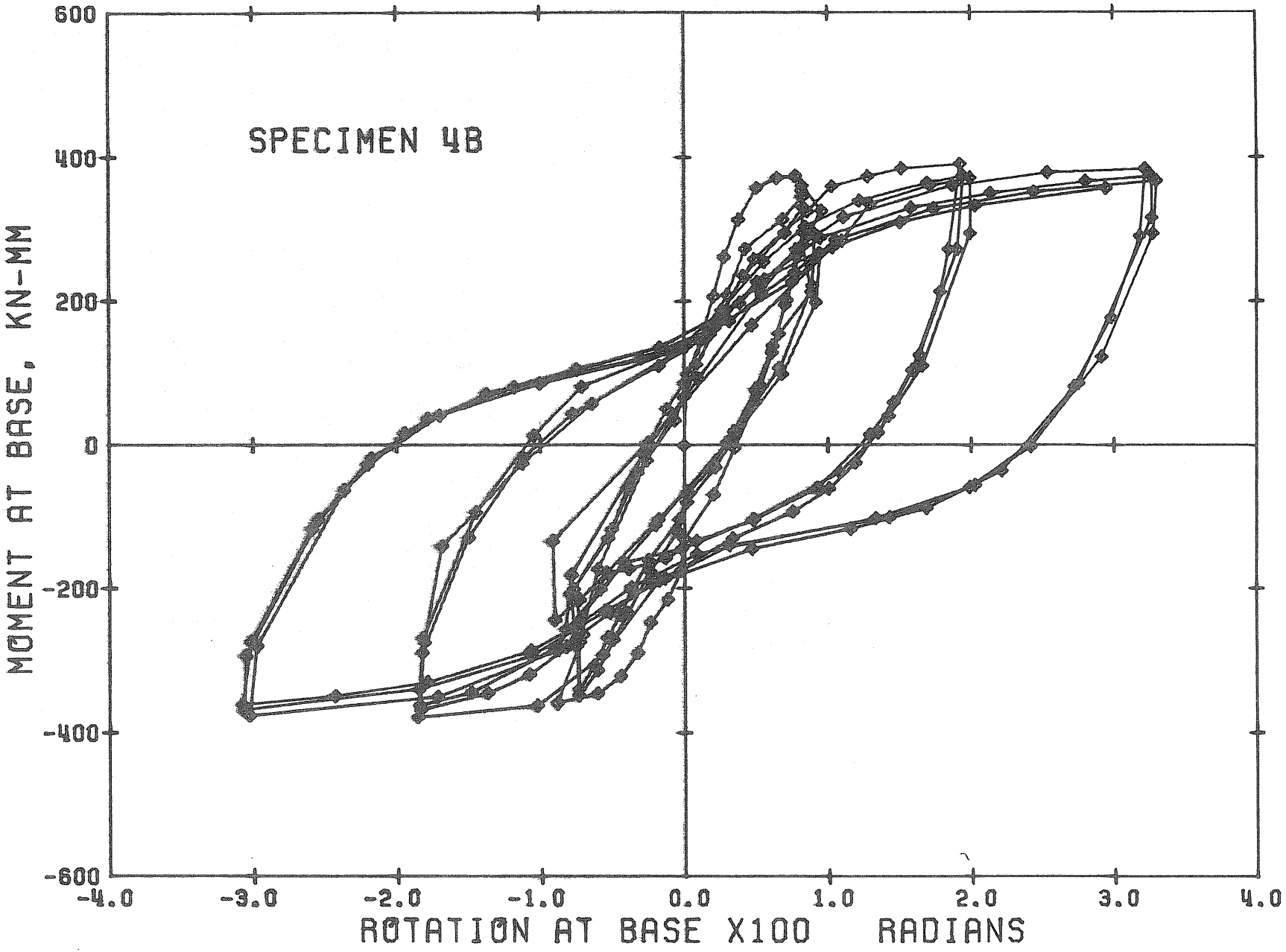


Fig. 3.6 Contd. Measured Hysteresis Relationships for Specimen 4B

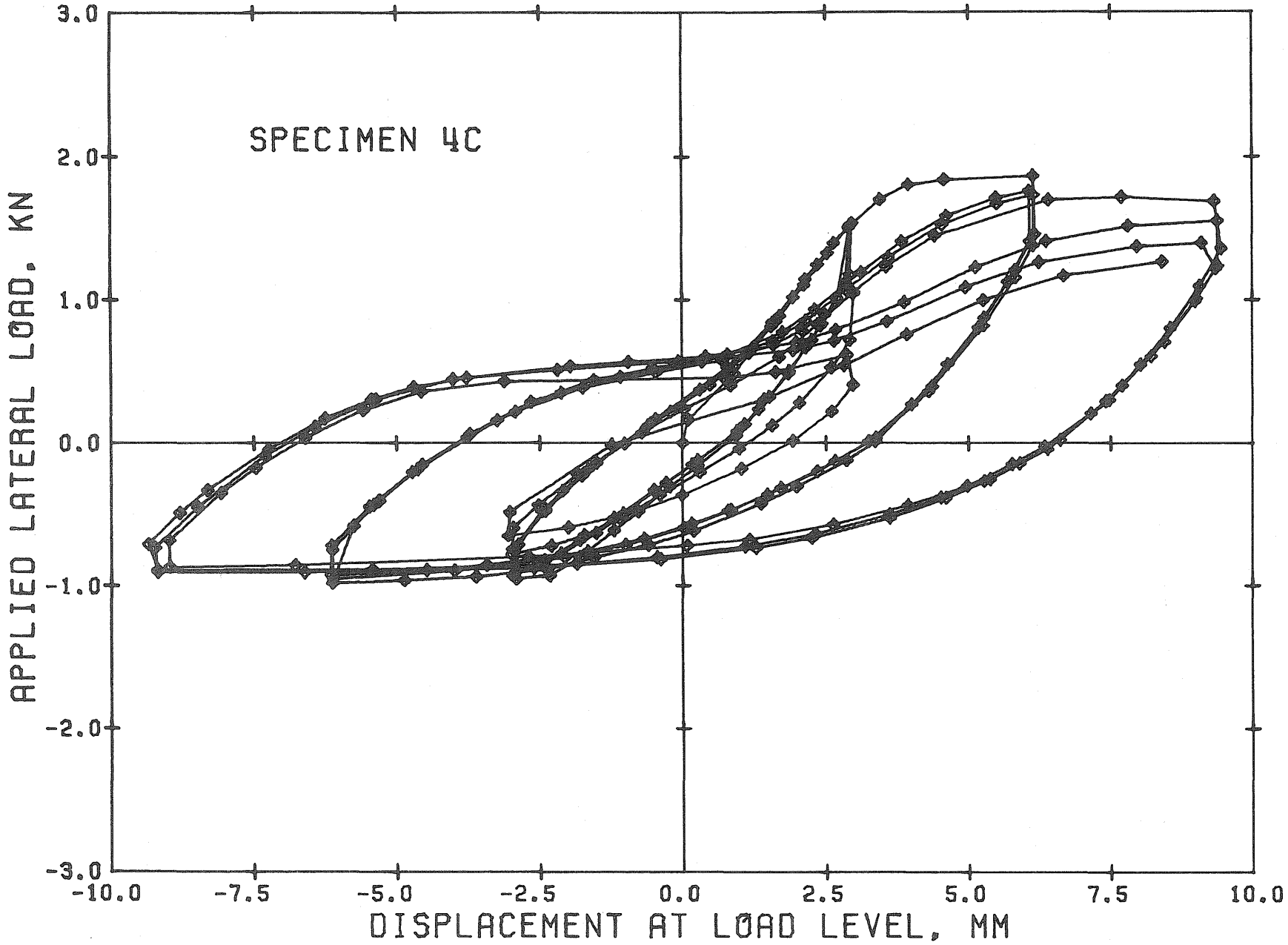


Fig. 3.7 Measured Hysteresis Relationships for Specimen 4C

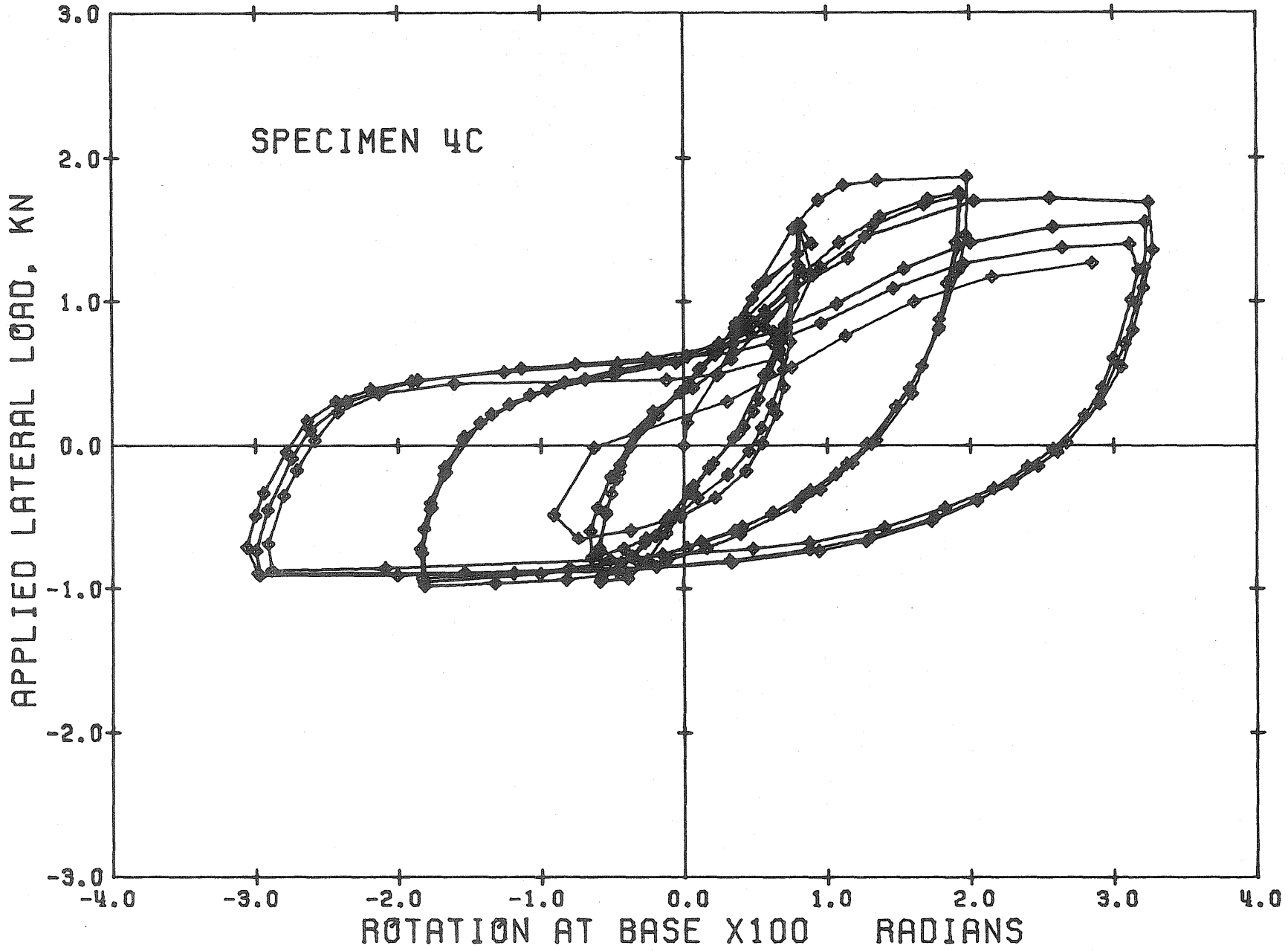


Fig. 3.7 Contd. Measured Hysteresis Relationships for Specimen 4C

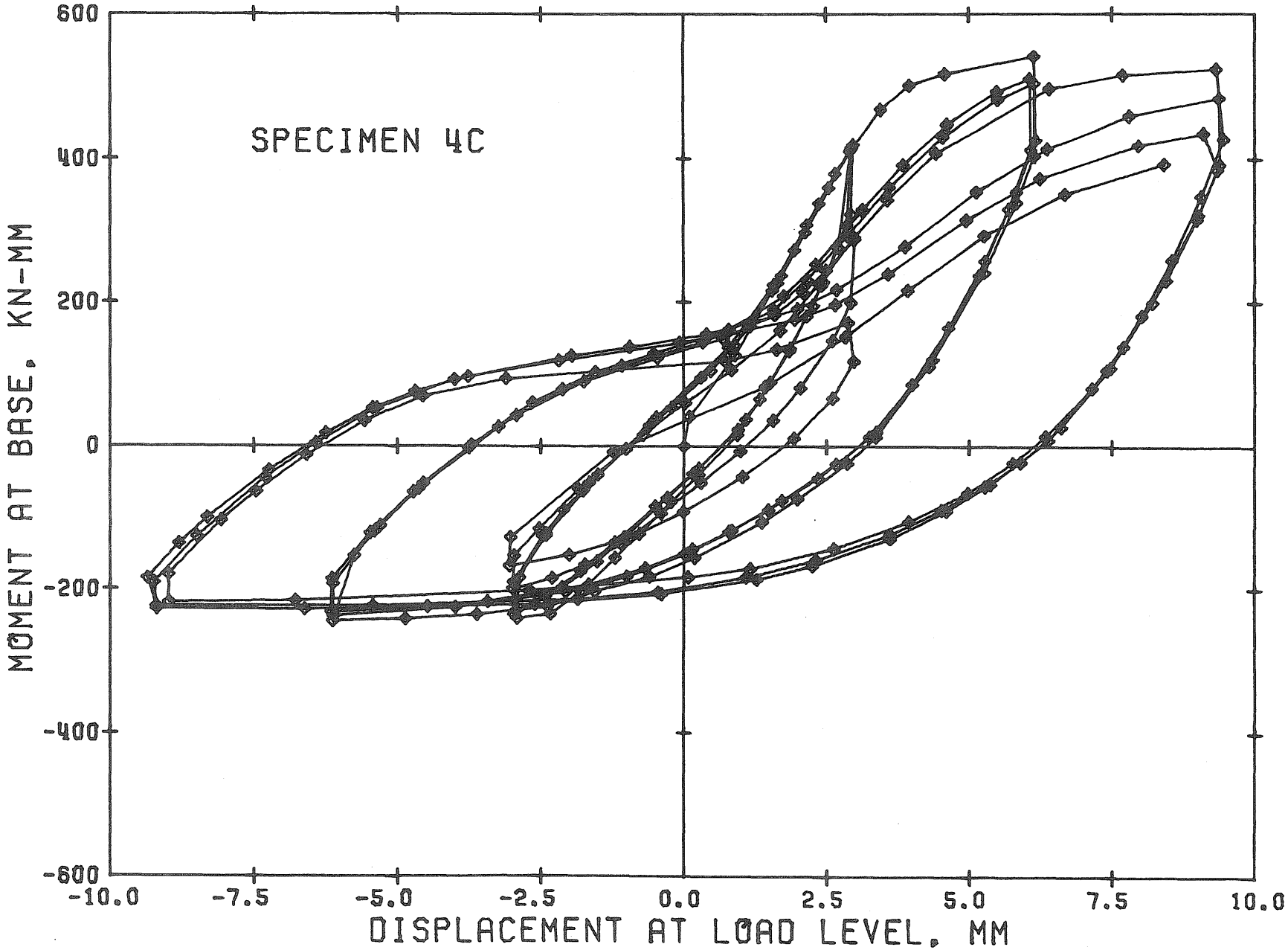


Fig. 3.7 Contd. Measured Hysteresis Relationships for Specimen 4C

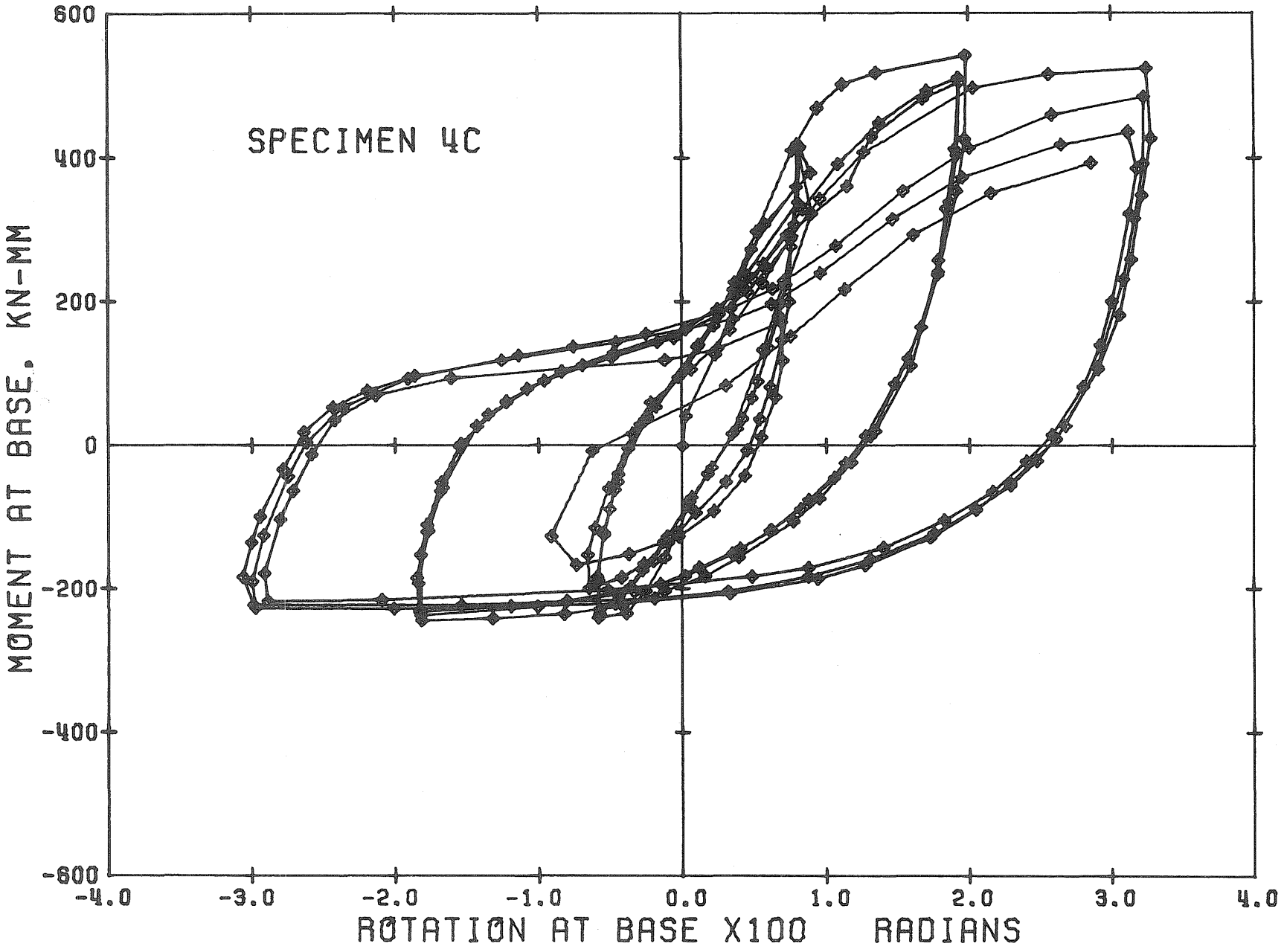


Fig. 3.7 Contd. Measured Hysteresis Relationships for Specimen 4C

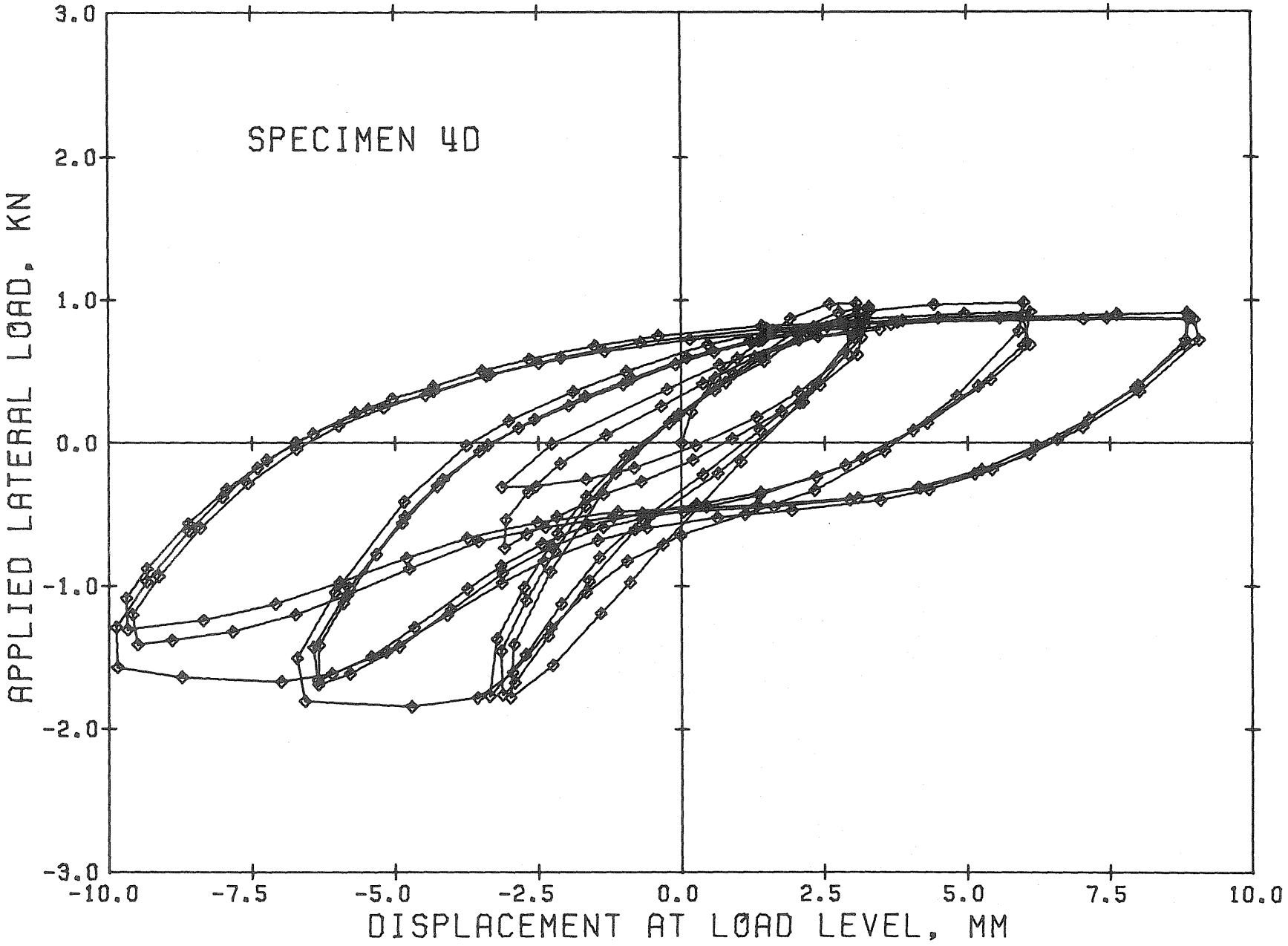


Fig. 3.8 Measured Hysteresis Relationships for Specimen 4D

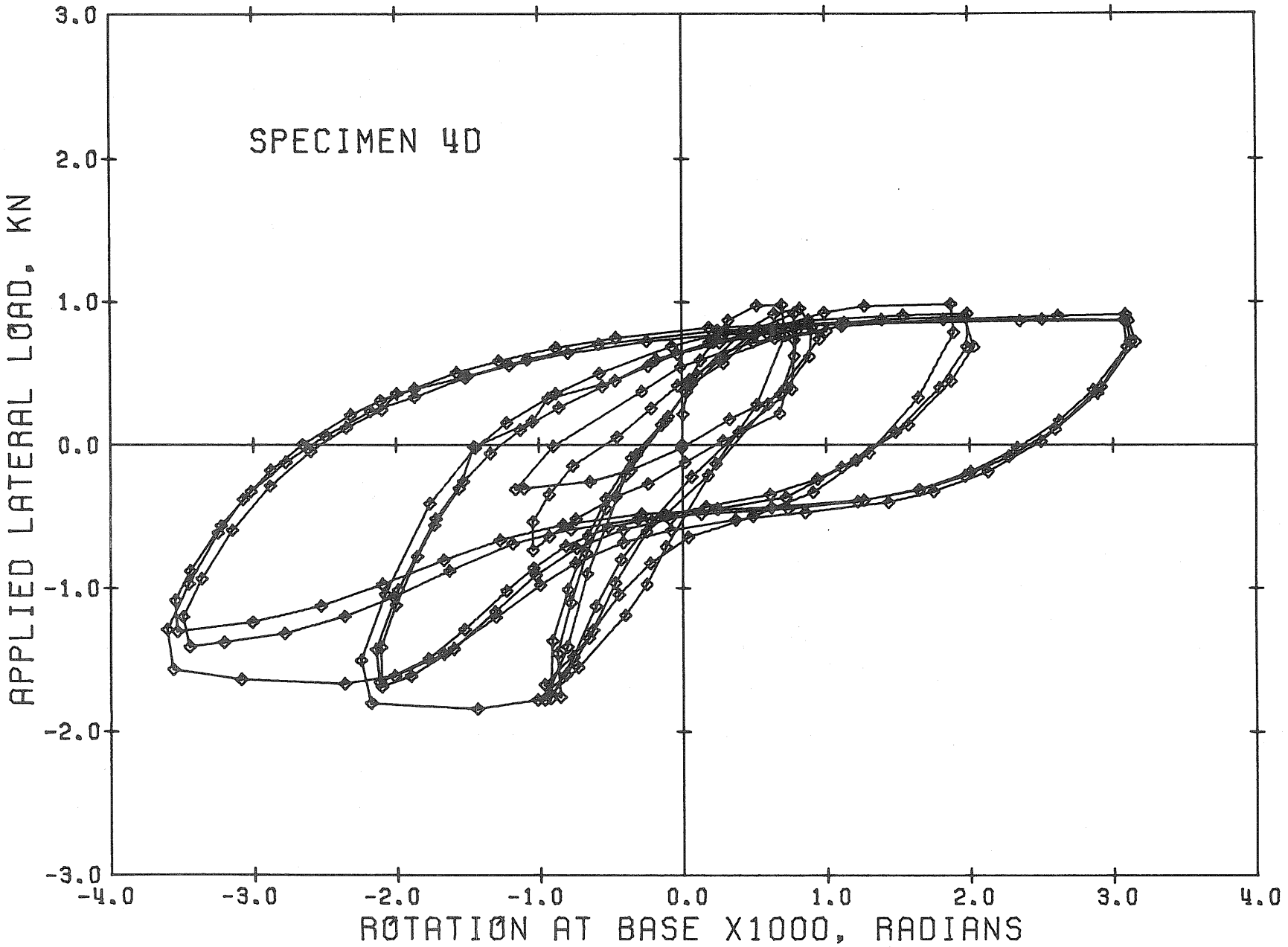


Fig. 3.8 Contd. Measured Hysteresis Relationships for Specimen 4D

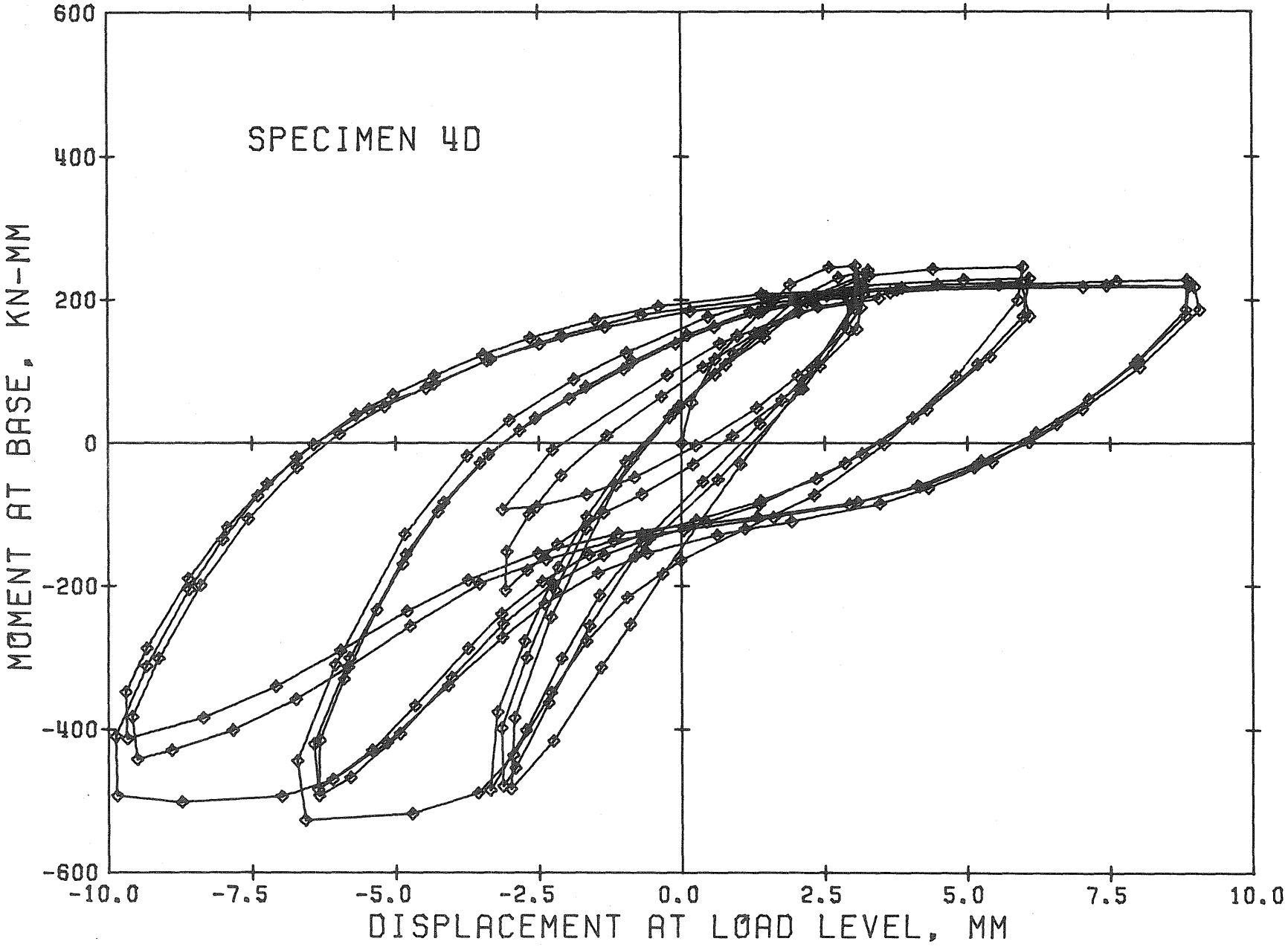


Fig. 3.8 Contd. Measured Hysteresis Relationships for Specimen 4D

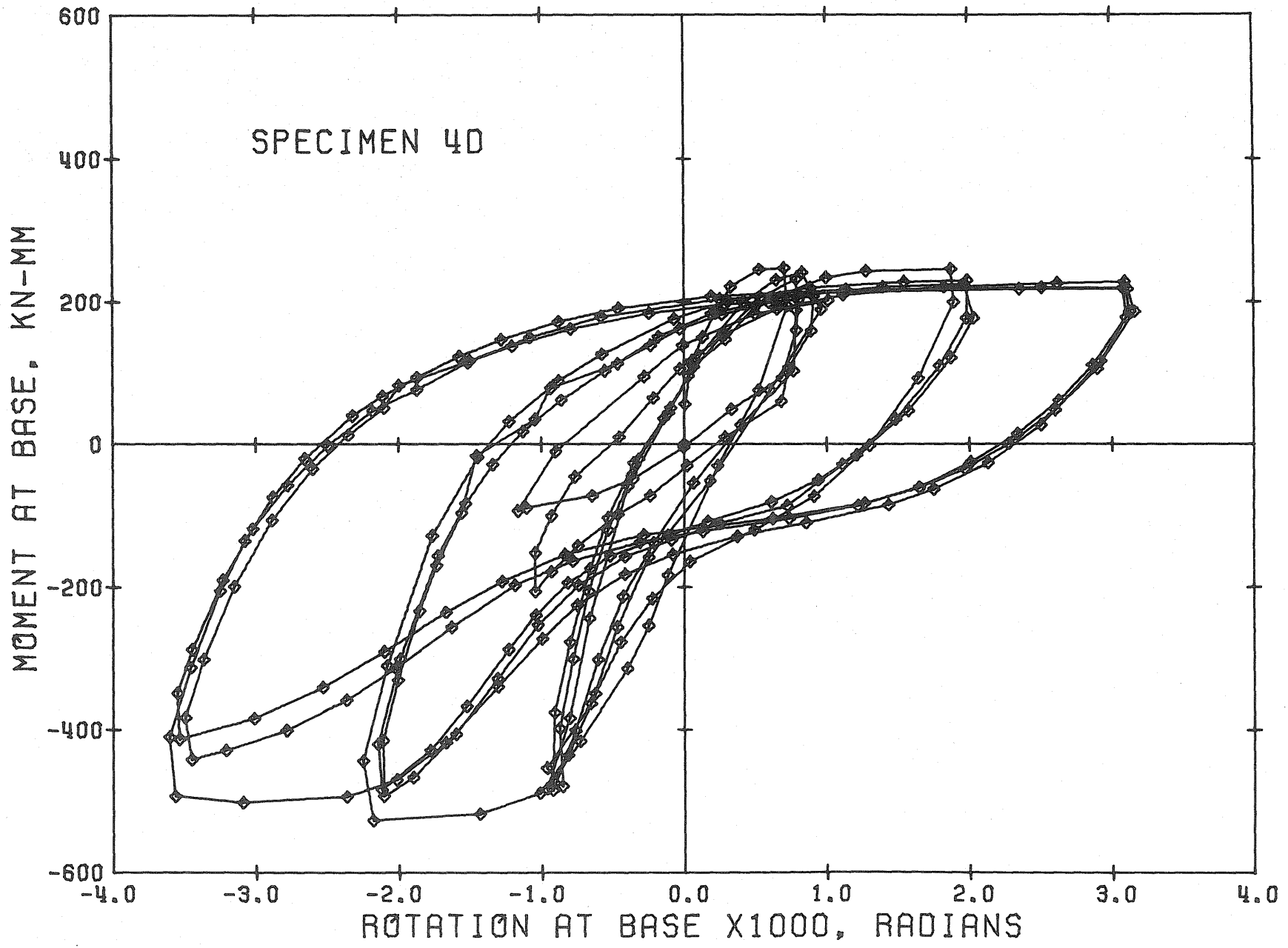


Fig. 3.8 Contd. Measured Hysteresis Relationships for Specimen 4D

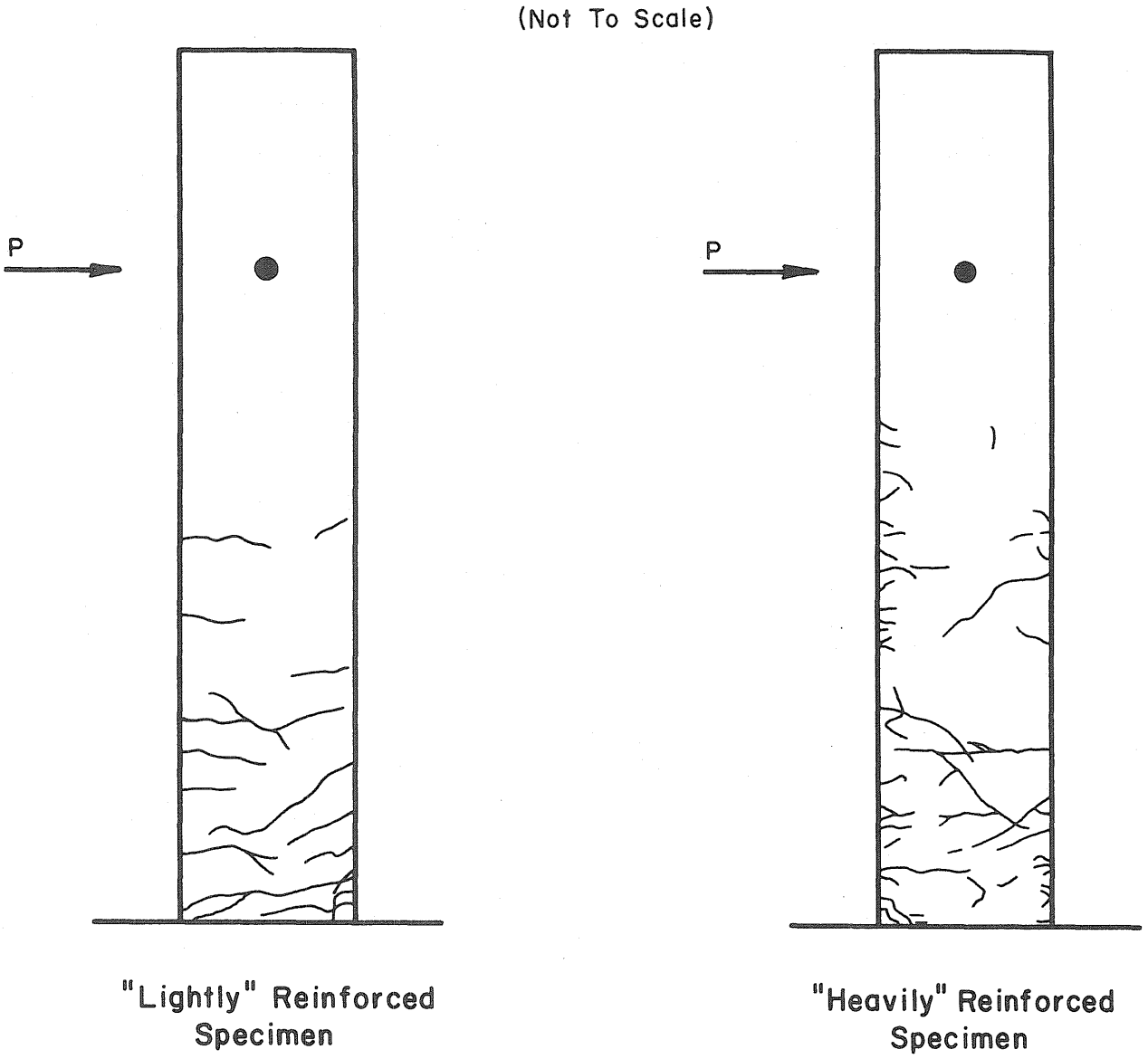


Fig. 3.9 Crack Patterns at 9 mm

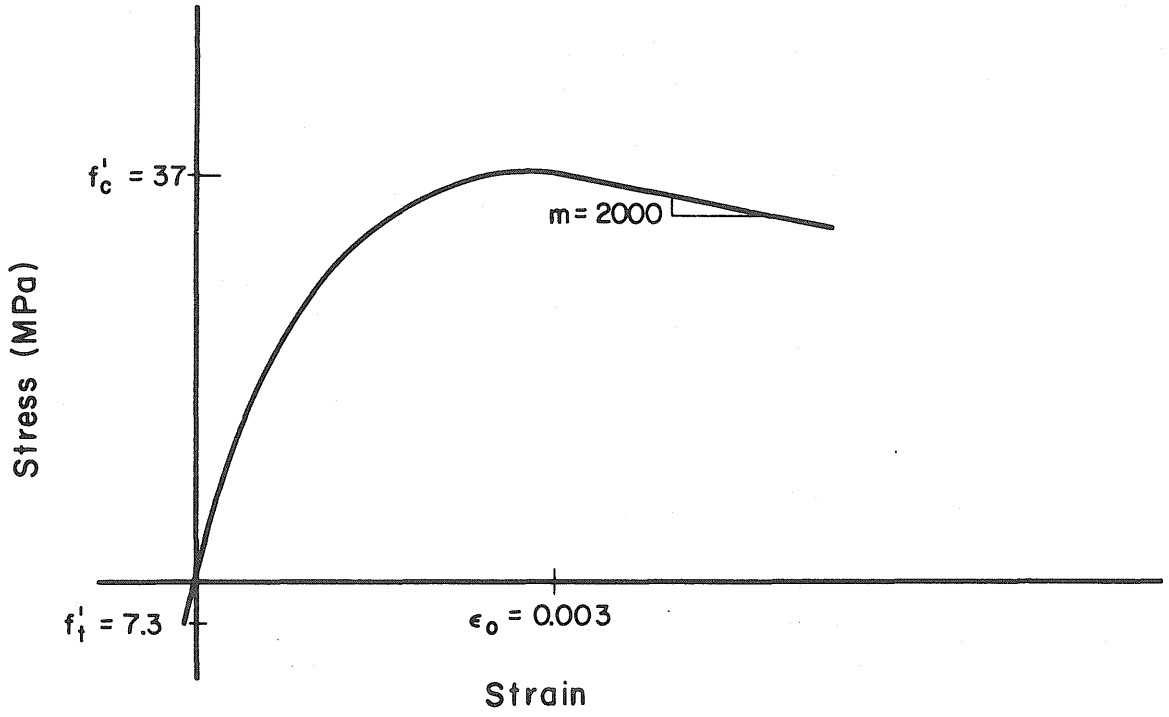


Fig. 4.1 Idealized Stress-Strain Curve for Concrete

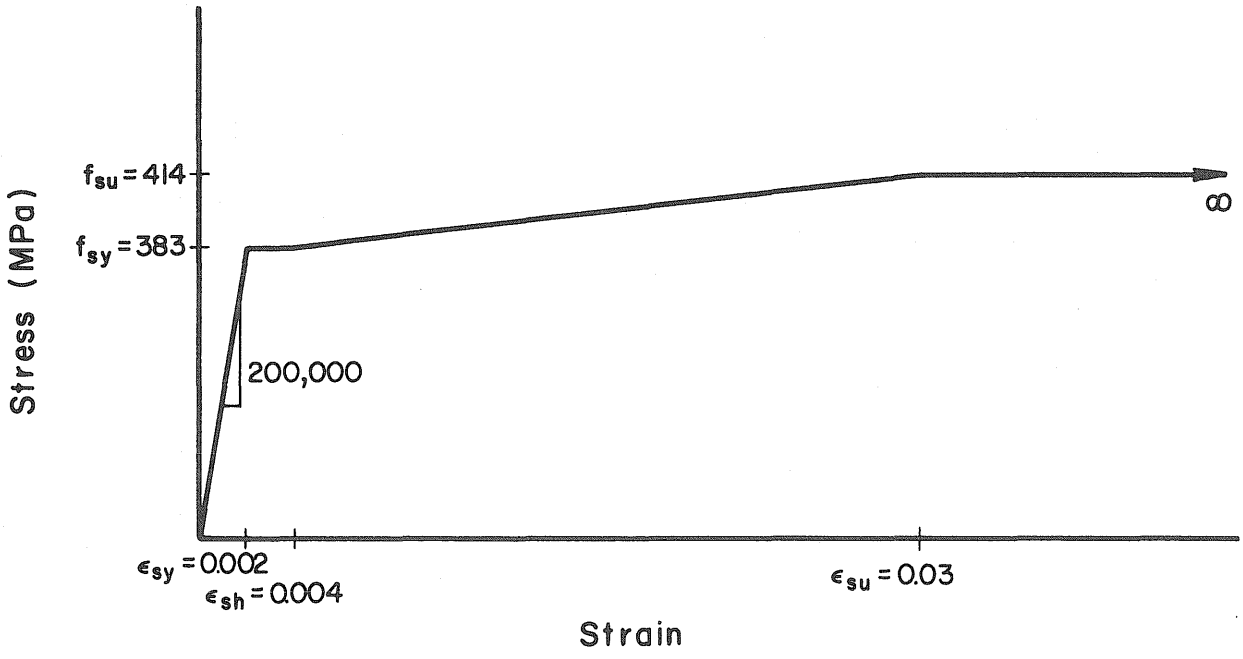


Fig. 4.2 Idealized Stress-Strain Curve for Steel

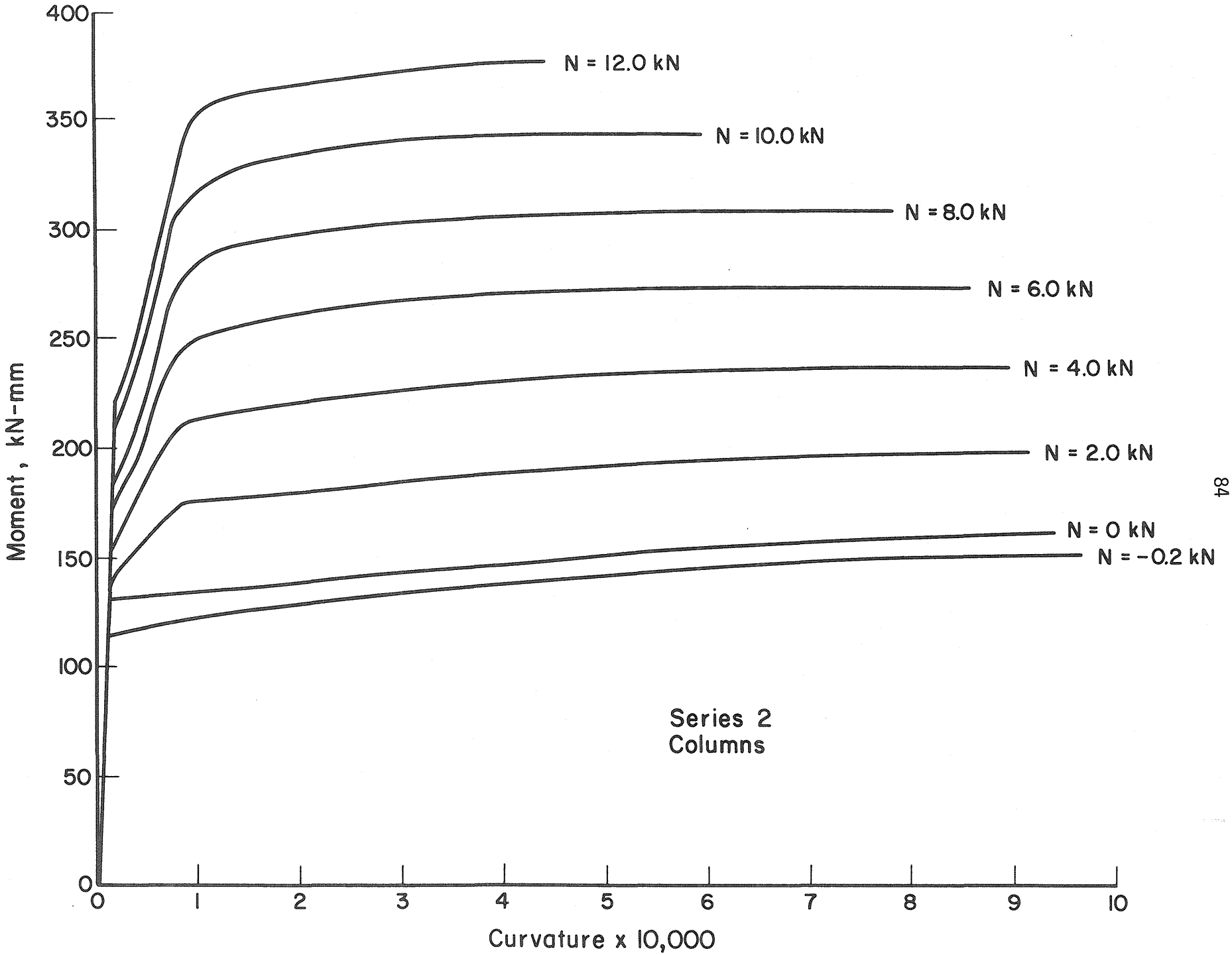


Fig. 4.3 Moment-Curvature Relationships for Series 2 Specimens

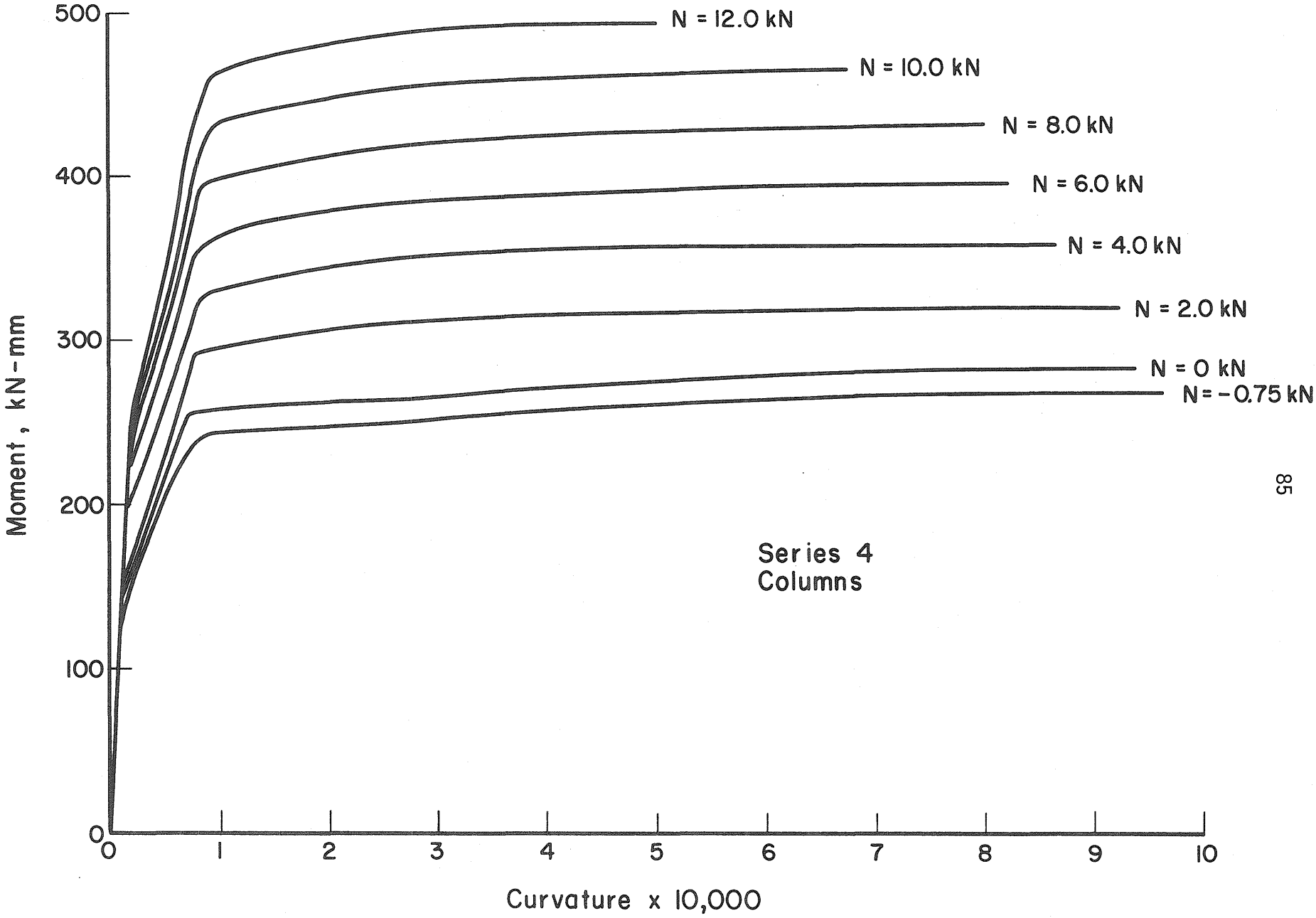


Fig. 4.4 Moment-Curvature Relationships for Series 4 Specimens

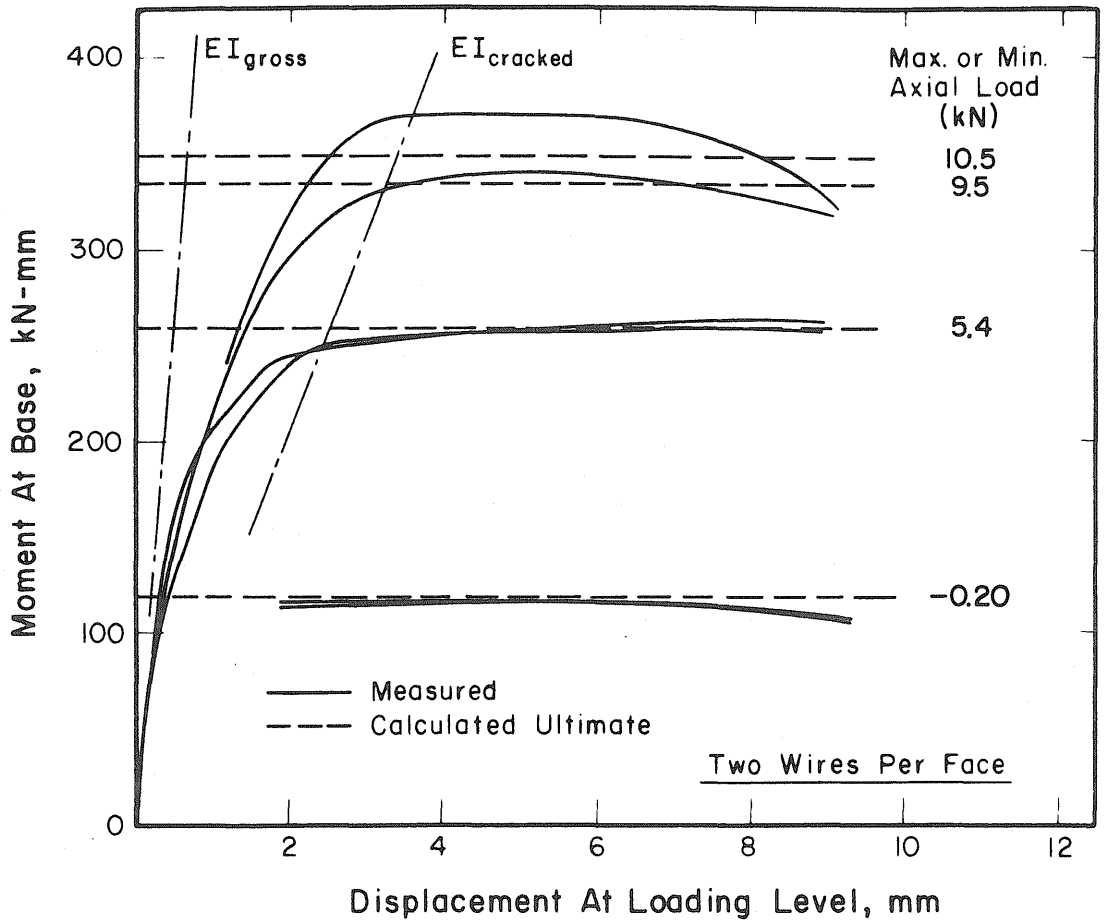


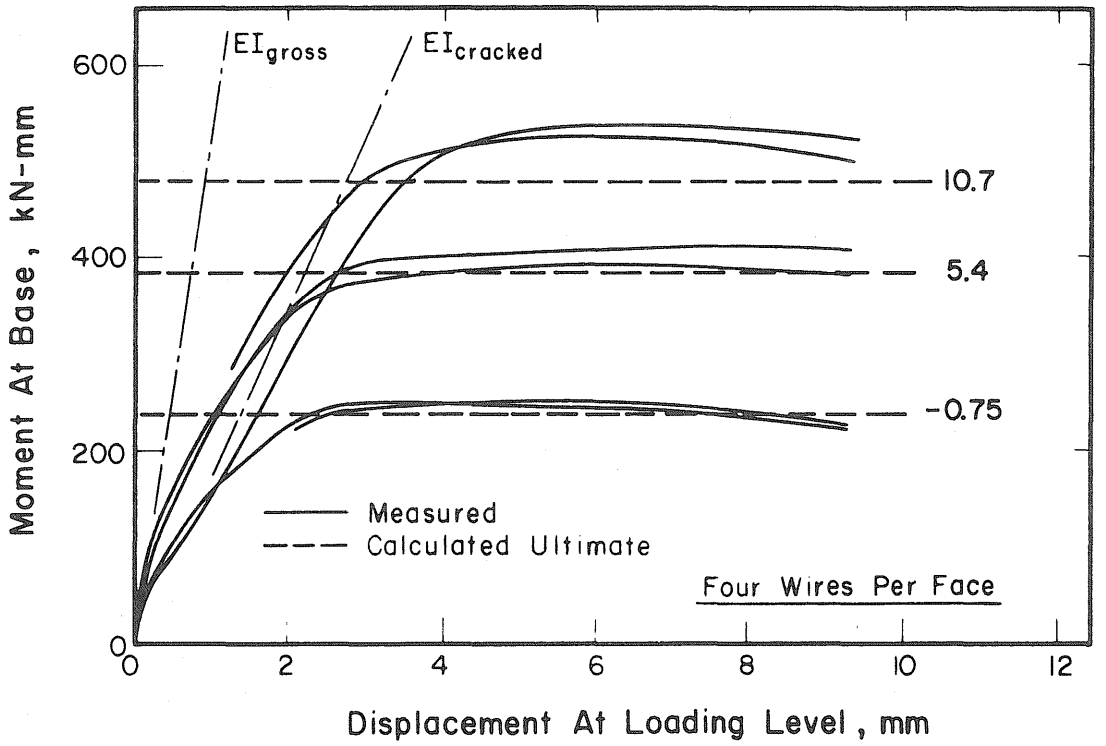


Fig. 4.5 Comparison of Measured and Calculated Strengths

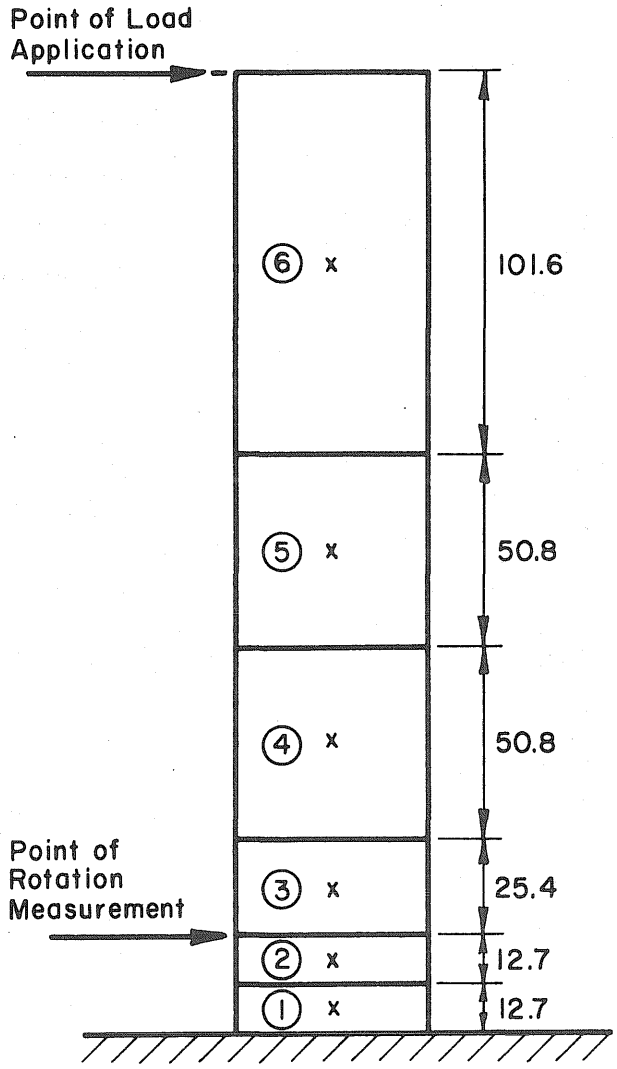


Fig. 4.6 Idealized Model of Column Specimen

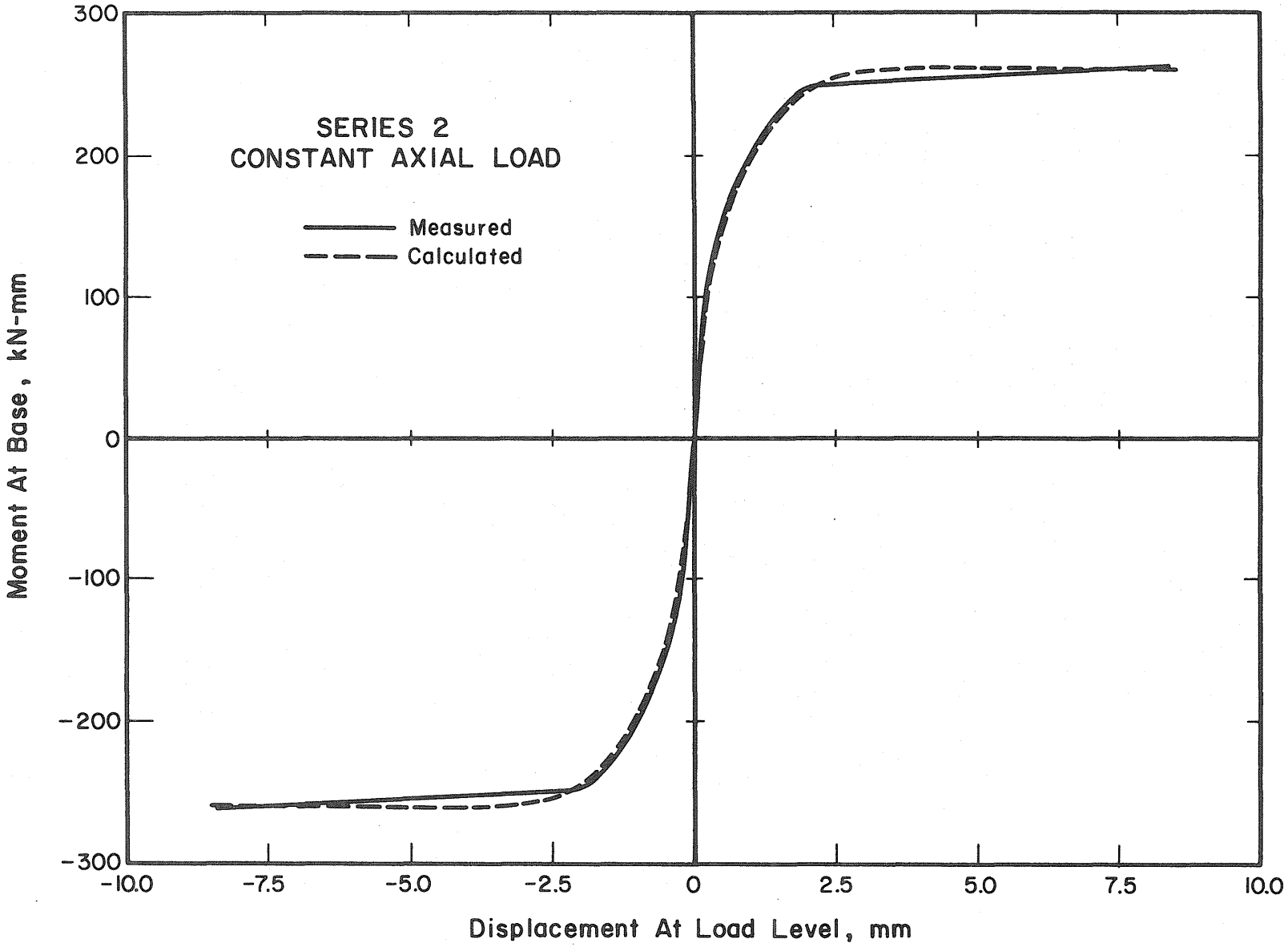


Fig. 4.7 Comparison of Measured and Calculated Moment-Deflection Relationships

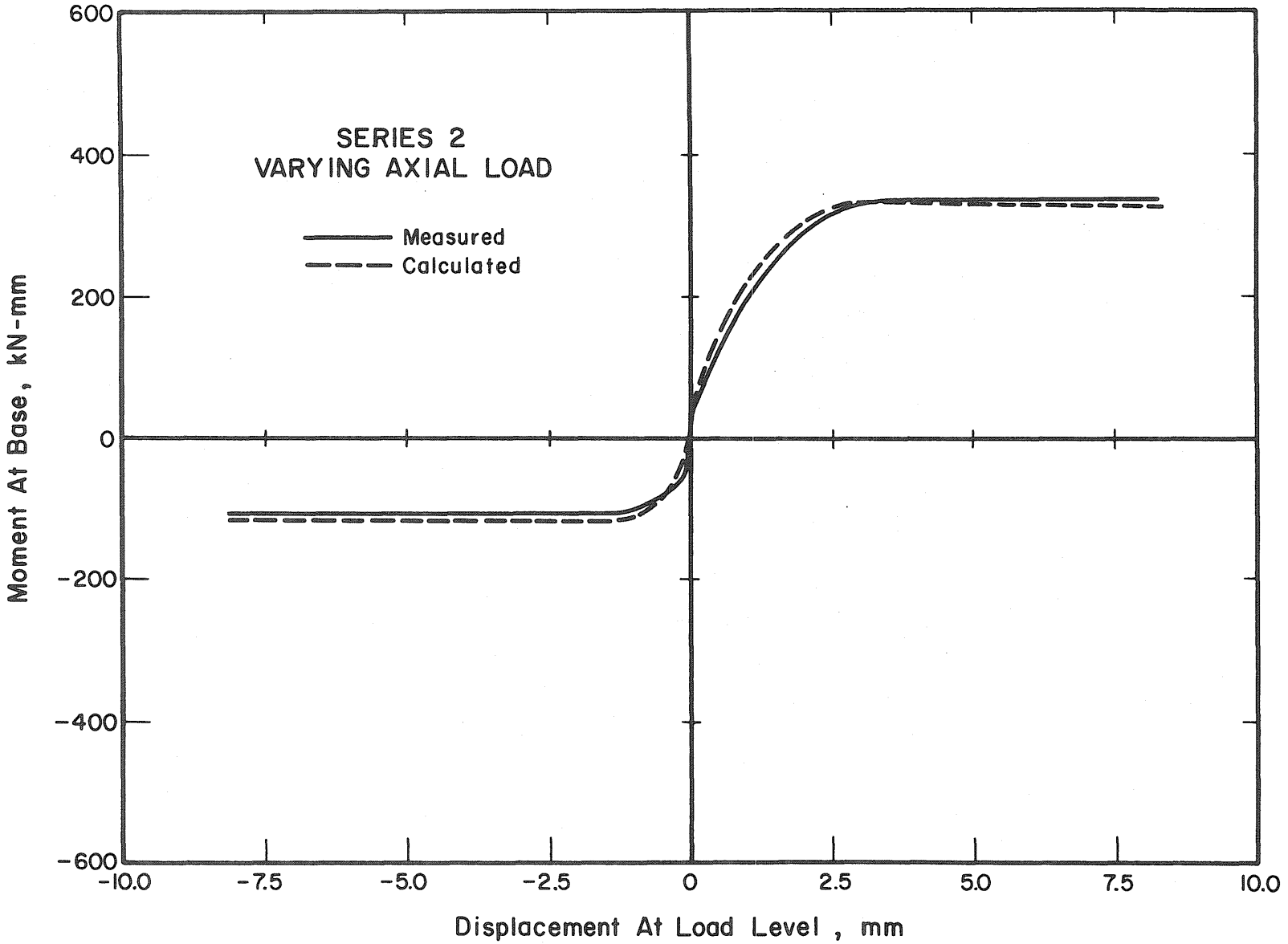


Fig. 4.7 Contd. Comparison of Measured and Calculated Moment-Deflection Relationships

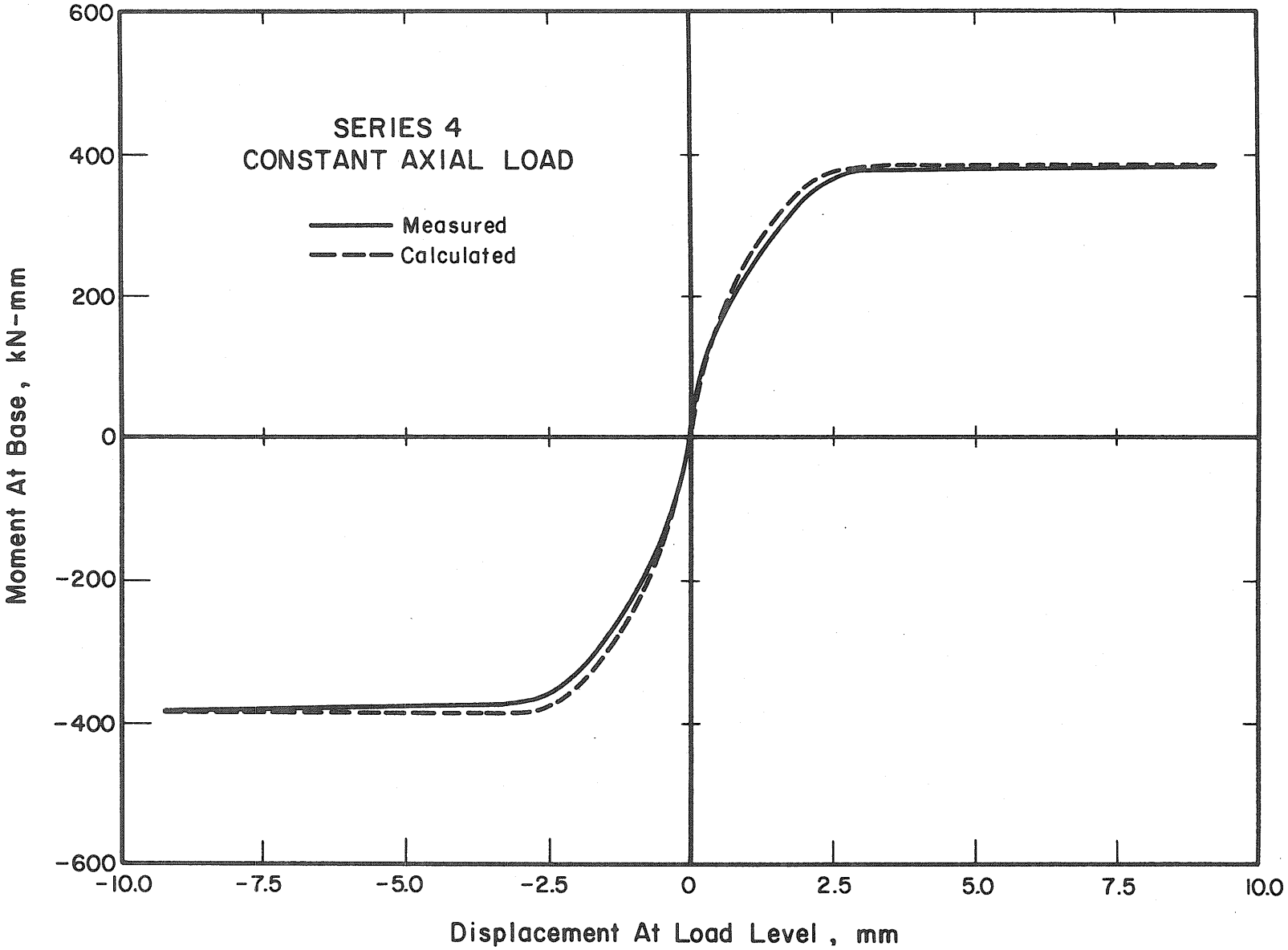


Fig. 4.7 Contd. Comparison of Measured and Calculated Moment-Deflection Relationships

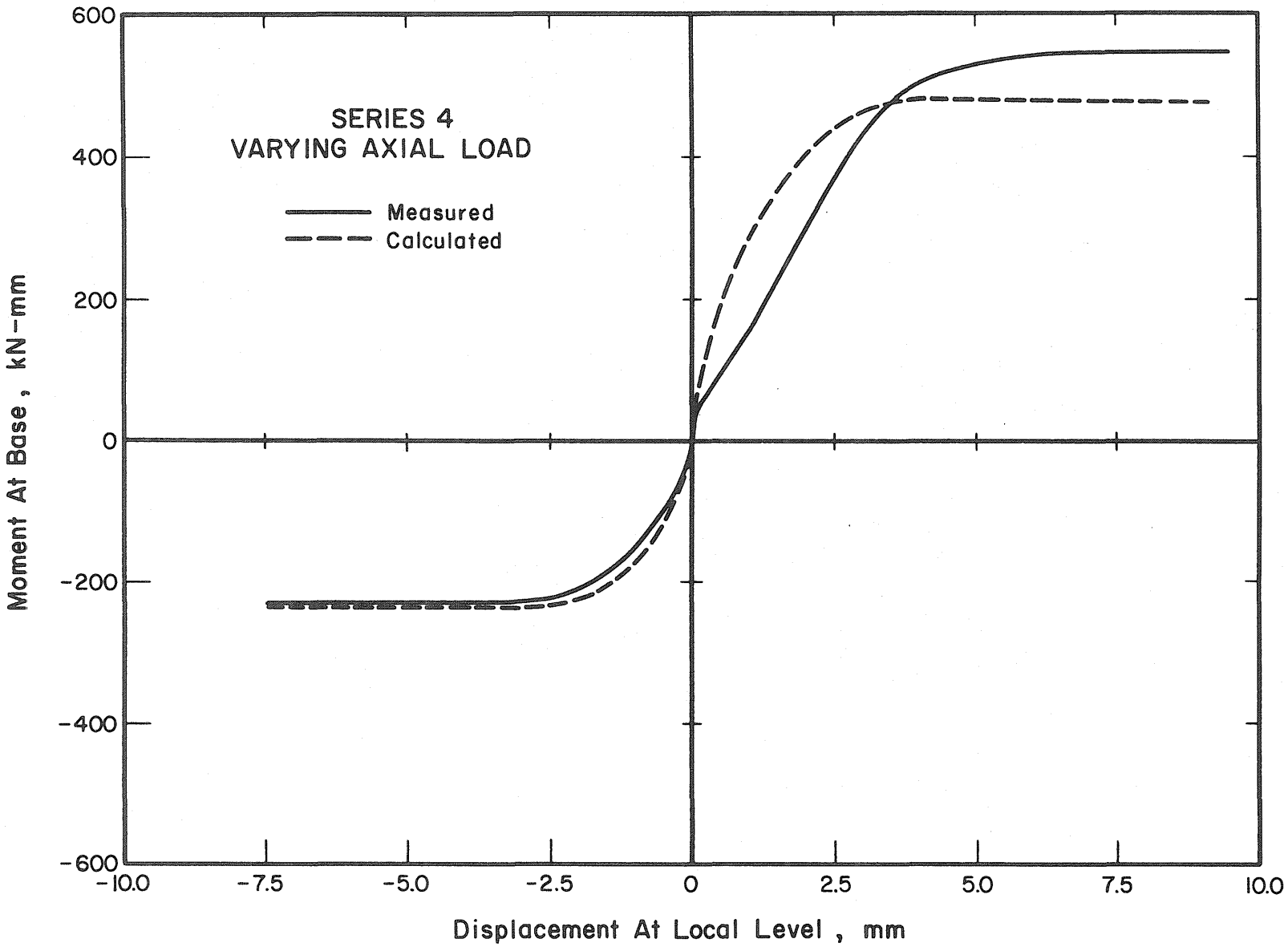


Fig. 4.7 Contd. Comparison of Measured and Calculated Moment-Deflection Relationships

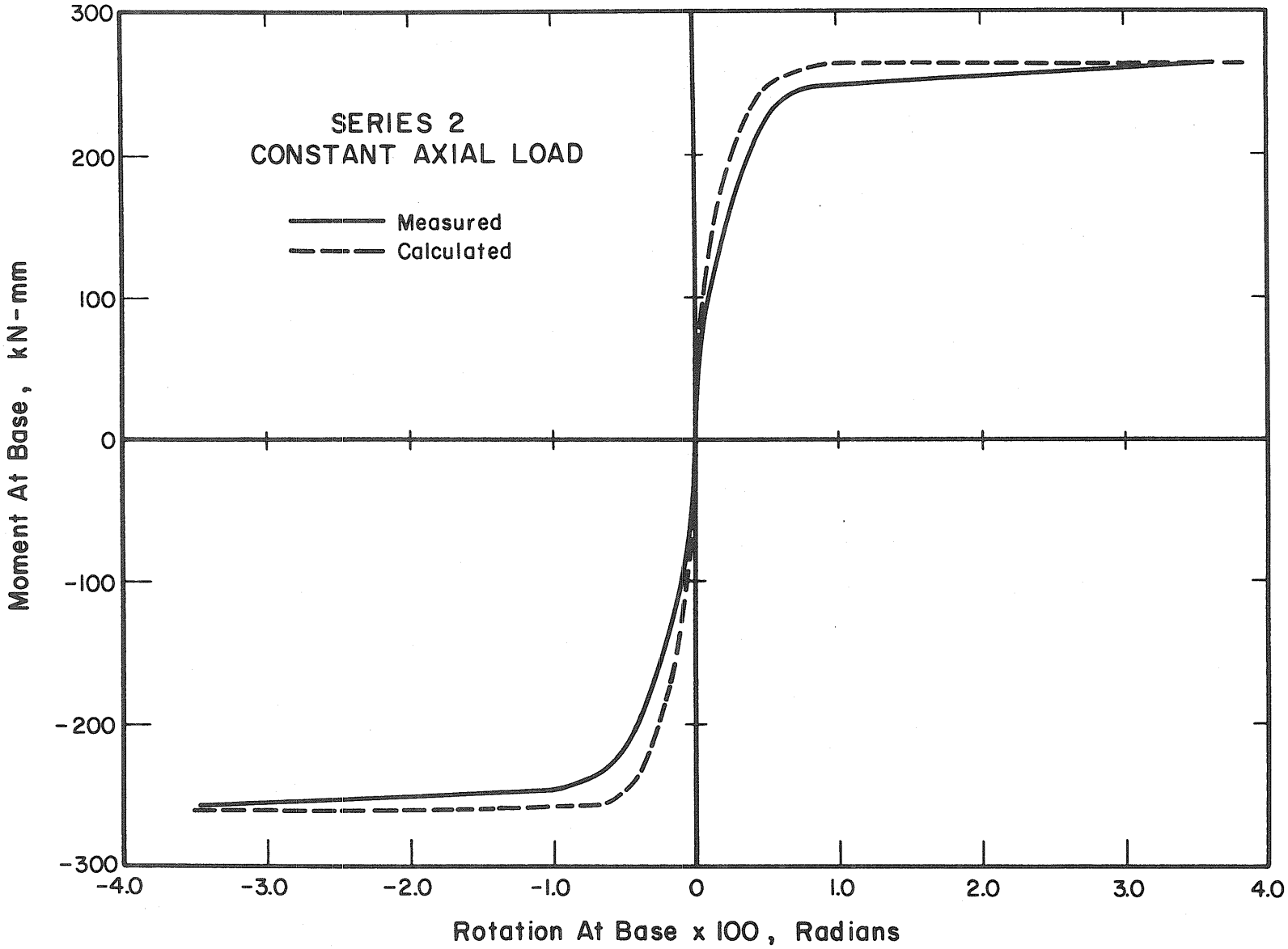


Fig. 4.8 Comparison of Measured and Calculated Moment-Rotation Relationships

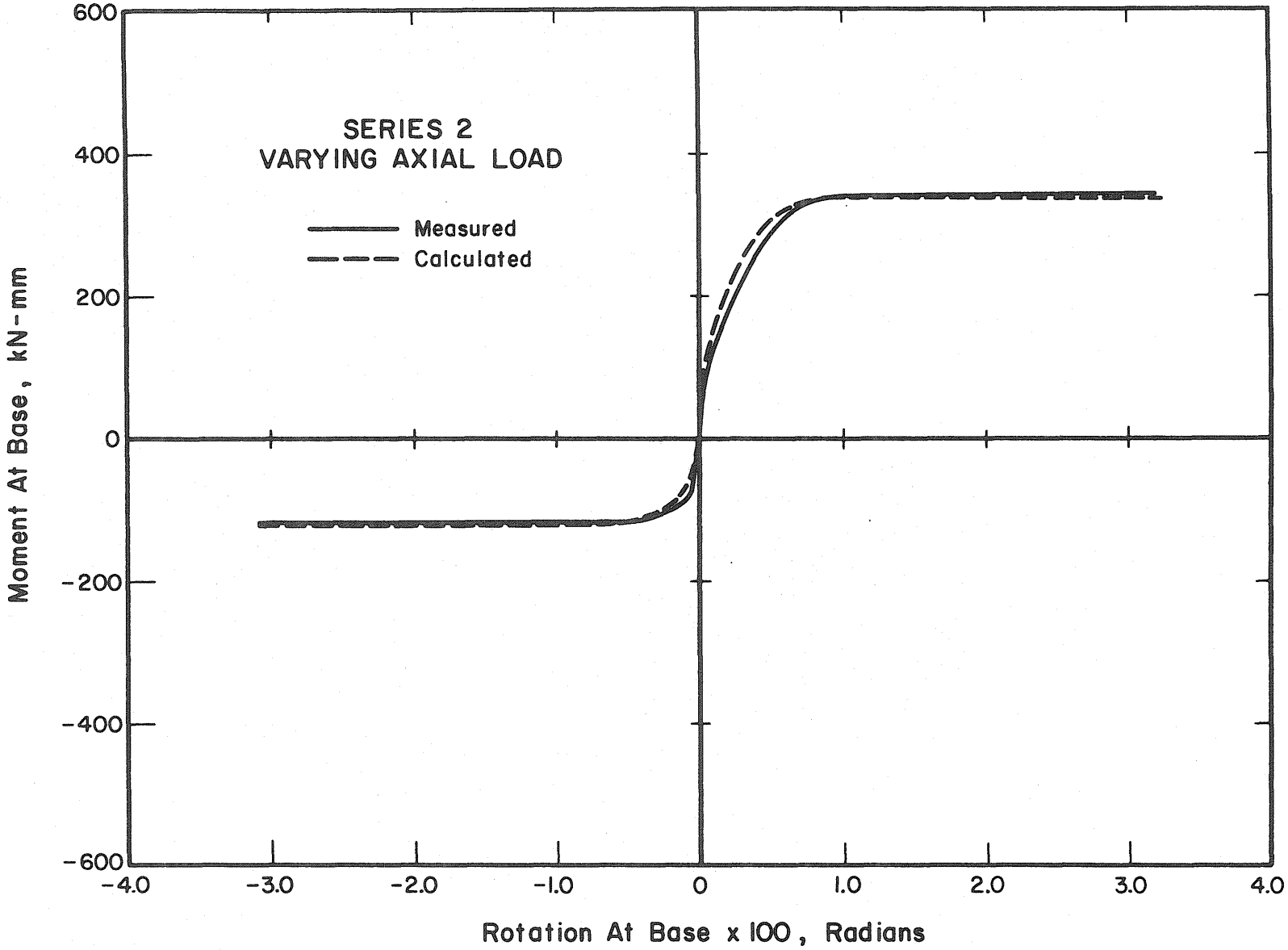


Fig. 4.8 Contd. Comparison of Measured and Calculated Moment-Rotation Relationships

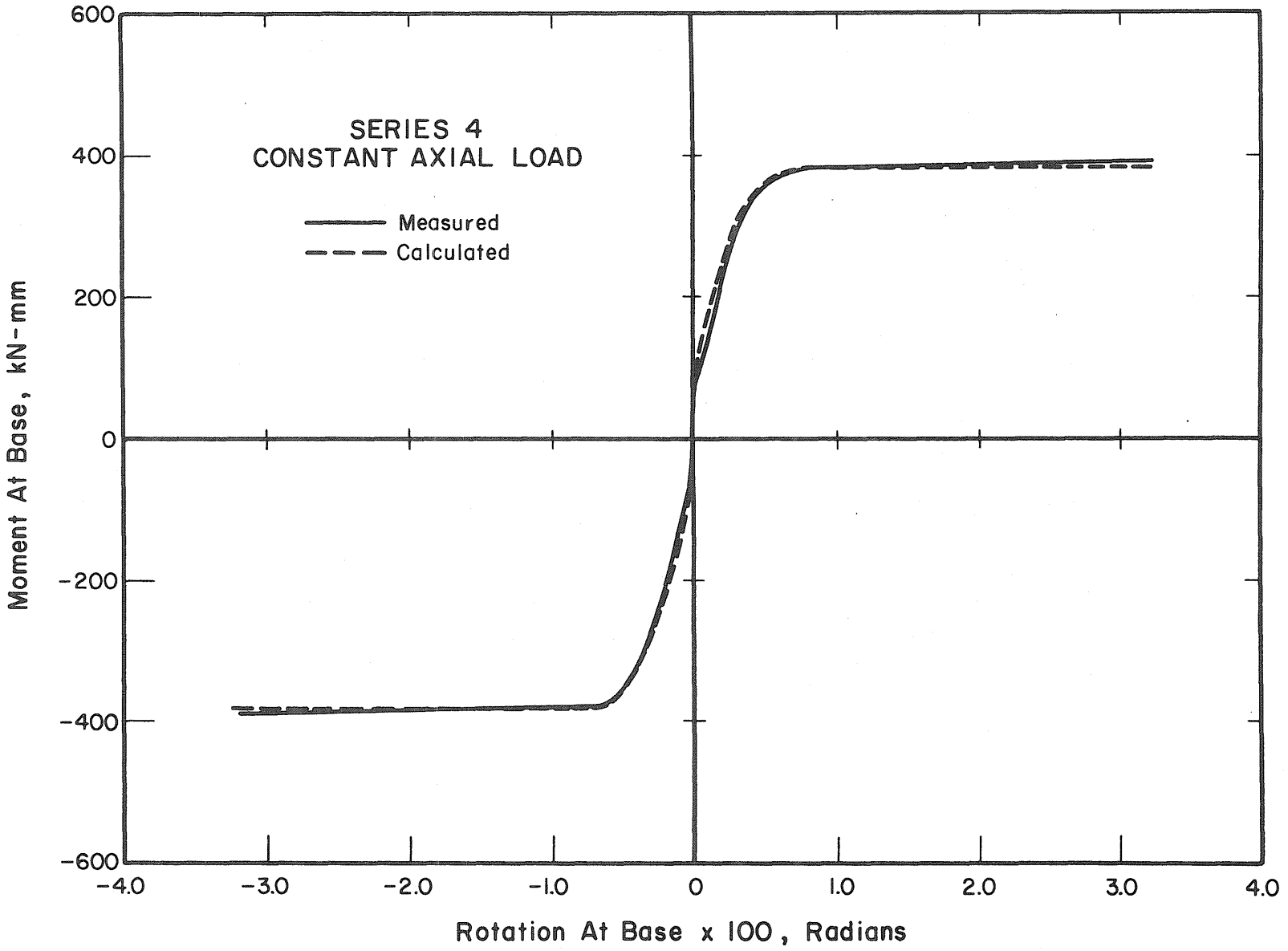


Fig. 4.8 Contd. Comparison of Measured and Calculated Moment-Rotation Relationships

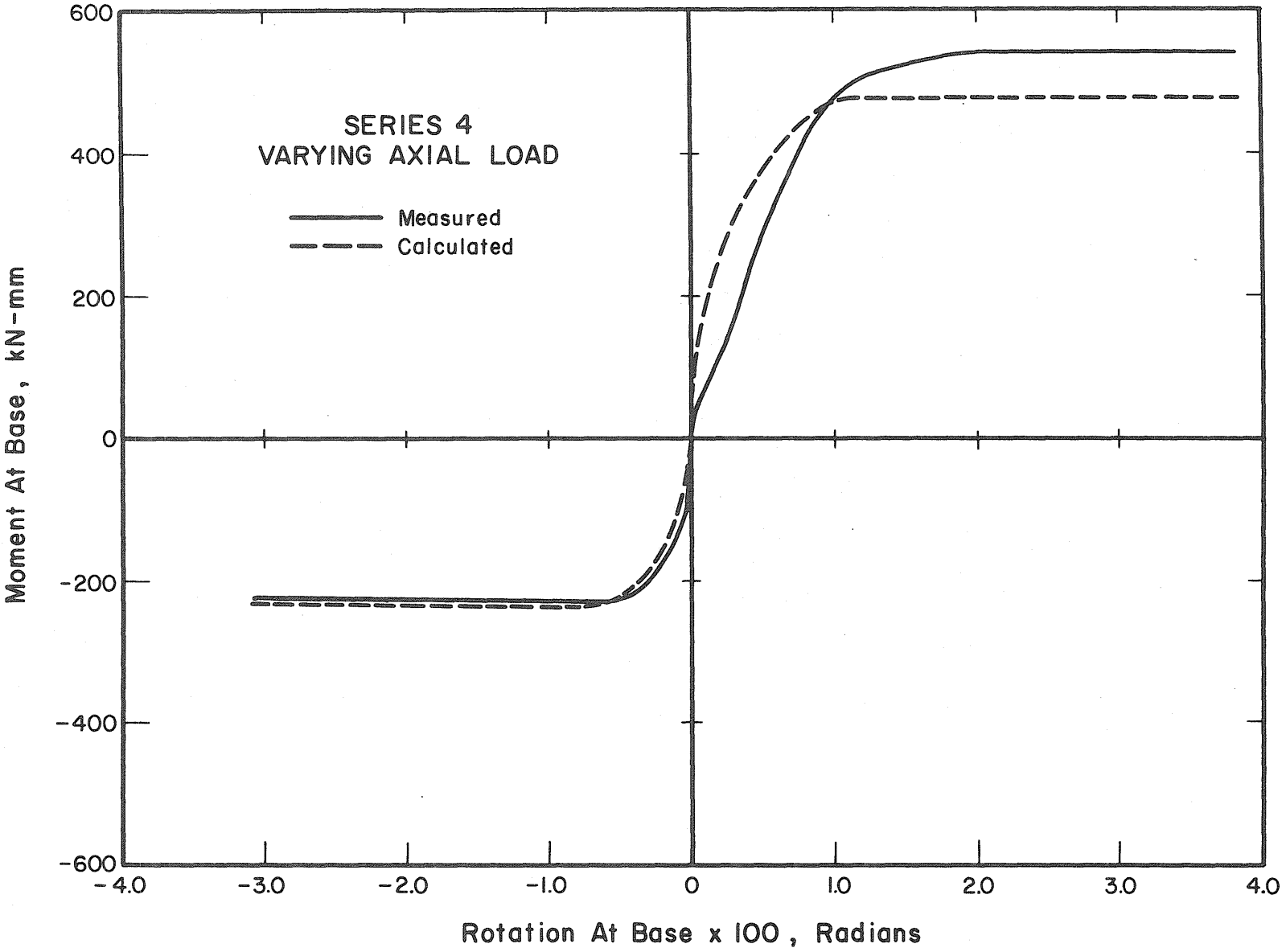


Fig. 4.8 Contd. Comparison of Measured and Calculated Moment-Rotation Relationships